The Design of Antimicrobial Detachable Thin Films for the Study of Hepatic Infections

Margaret E. Cassin

Thesis submitted to the faculty of Virginia Polytechnic Institute and State University in fulfillment of the requirements for the degree of

Master of Science in
Chemical Engineering

Padmavathy Rajagopalan, Chair
Richey Davis
Biswarup Mukhopadhyay

September 22, 2015
Blacksburg, VA

Keywords: Antimicrobial, polyelectrolyte multilayer, hepatocyte

The Design of Antimicrobial Detachable Thin Films for the Study of Hepatic Infections

Margaret E. Cassin

ABSTRACT

Microbial infections are a global problem. Due to the over and misuse of antibiotics, drug-resistant pathogens are becoming more common. It is imperative to explore broad spectrum antimicrobial approaches. In this work, we modified collagen/hyaluronic acid polyelectrolyte multilayers (PEMs) with the natural antimicrobial peptide, LL-37 to study hepatic infections. LL-37 was physisorbed and covalently linked to the surface of the PEMs. *Escherichia coli* DH10B were cultured in the presence of LL-37modified PEMs in bacterial adhesion and contact killing models. Physisorbed LL-37 PEMs prevented bacterial adhesion and could also kill pathogens in the surrounding environment due to the release of LL-37 from the film. Immobilized LL-37 PEMs resulted in less bacterial adhesion on the surface due to the presence of the peptide. Films were then placed in contact with primary rat hepatocytes as well as in hepatocyte/bacteria co-cultures. LL-37 input concentrations up to of 16μM did not exhibit cytotoxic effects on hepatocytes. The LL-37 modified PEMs exhibited a hepatoprotective effect on albumin and urea secretion functions in co-cultures. The hepatoprotective effects were dependent on the ratio of hepatocytes and bacteria as well as the concentration of LL-37. These findings are encouraging and demonstrate that LL-37 modified PEMs can be used to investigate hepatic infections caused by bacteria.

Acknowledgements

First, I would like to thank my family and friends for all their love and support during my time at Virginia Tech. From the late night phone calls to the encouraging letters, I would not have succeeded without you.

I would like to express my appreciation to my advisor Dr. Padma Rajagopalan for her endless patience and support toward me and my project. I thank you for always pushing me onward, getting me to ask the hard questions, and for making me question what I think I know. While I still have a lot to learn, I know I've moved forward academically and as a person.

I would like to thank the rest of my thesis committee: Dr. Richey Davis and Dr. Biswarup Mukhopadhyay for their feedback and excellent insight toward this thesis. My thanks also to Dr. Dwi Susanti for all her help in learning bacterial culture skills. You were a wonderful teacher.

To the chemical engineering department at Virginia Tech for giving me this opportunity to further my education, learn new skills, dive into exciting research, and meet amazing people – I thank you. Thank you to the Institute for Critical Technology and Applied Sciences for the use of their facilities and the National Science Foundation (DBI-1062380) for funding.

Lastly, I would like to thank my labmates – Sophia Orbach, Rebekah Less, Lucas Vu, Andrew Ford, and Gaurav Jain. You five have been through it all with me and I'm so grateful for your constant support, your training, your insight, and the joy you've brought to my last 3 years. From research to classes, from coffee breaks to tailgates, I know I found true friends here.

Table of Contents

Table of Figures

Table of Tables

List of Abbreviations

2D – Two-dimensional
3D – Three-dimensional
AFM – Atomic force microscope
AMP – Antimicrobial peptide
BL – Bilayer
BSA – Bovine serum albumin
COL – Collagen
CS – Collagen sandwich
CYP – Cytochrome
DMEM – Dulbecco's modified Eagle medium
E. coli – *Escherichia coli*
ECM – Extracellular matrix
EDC – 1-ethyl-3-[3-dimethylaminopropyl]carbodiimide
ELISA - Enzyme-linked immunosorbent assay
FPRL1 – Formyl peptide receptor-like 1
HA – Hyaluronic acid
hCAP18 – Human cationic antimicrobial protein
HM – Hepatocyte monolayer
HSC – Hepatic stellate cell
K. pneumoniae – *Klebsiella pneumoniae*
KC – Kupffer cell
LB – Lysogeny broth
LbL – Layer-by-layer
LPS – Lipopolysaccharide
LSEC – Liver sinusoidal endothelial cell
MES – 2-[morpholino]ethanesulfonic acid
MIC – Minimum inhibitory concentration
MRSA – Methicillin-resistant *Staphylococcus aureus*
NHS – N-hydroxysuccinimide
NPC – Nonparenchymal cell
OD – Optical density
PAA – Poly(acrylic acid)
PAH – Poly(allylamine hydrochloride)
PBS – Phosphate buffered saline
PC – Parenchymal cell
PCL – Poly(caprolactone)
PDAC – Poly(diallyldimethylammonium)
PE – Polyelectrolyte
PEG – Poly(ethylene glycol)
PEI – Poly(ethylenimine)
PEO – Poly(ethylene oxide)
PEM – Polyelectrolyte multilayer
PGA – Poly(glycolic acid)
PHB – Poly-β-hydroxybutyrate
PLA – Poly(lactic acid)
PLGA – Poly(lactic-glycolic acid)
PTFE – Poly(tetrafluoroethylene)
PVS – Poly(vinyl sulfate)
RGD – Arginine-Glycine-Aspartic acid
SDS – Sodium dodecyl sulfate
SE-1 – Sinusoidal endothelial-1
SPS – Sulfonated polystyrene
TCPS – Tissue culture polystyrene
VRE – Vancomycin-resistant *Enterococcus*
YM – Young's modulus

1 Literature Review

1.1 Polyelectrolyte Multilayers

Polyelectrolytes (PEs) are polymers with ionic groups along the chain backbone [1, 2]. The degree of ionization of a PE can be modified through dissolution in different solvents and the use of salts. Changes in ionization, and therefore chain conformations of a PE, can affect its viscosity and optical properties in solution [3, 4]. Polyelectrolyte multilayers (PEMs) are assembled through the layer-by-layer (LbL) deposition of alternatively charged PEs [5-7] wherein the electrostatic interactions between PEs directs their self-assembly. Typically, the first step in assembling PEMs is to start with a charged substrate. The first PE deposited exhibits an opposing charge to that of the underlying charged substrate [8]. The overcompensation of charge permits the successive deposition of alternately charged PEs [5, 7, 9-11] (**Figure 1**). The irreversibility of this process enables the assembly of a stable multilayer [8, 12]. A significant advantage of this process is that substrate size and topography do not affect PEM assembly [13]. PEMs are widely used in separations, water treatment, coatings, microfluidics, fuel cells, as well as pH and electrochemical sensors [7, 14-18].

The use of PEMs in biological applications continues to gain popularity [19-33]. The ease of fabrication, ability to tune their chemical and mechanical properties, the introduction of functional moieties, proteins or peptides [19, 34-38], and the availability of different PE combinations make such multilayers ideal for biocompatible substrates [39-43], basement membranes [44-49], and as scaffolds [50-55] .

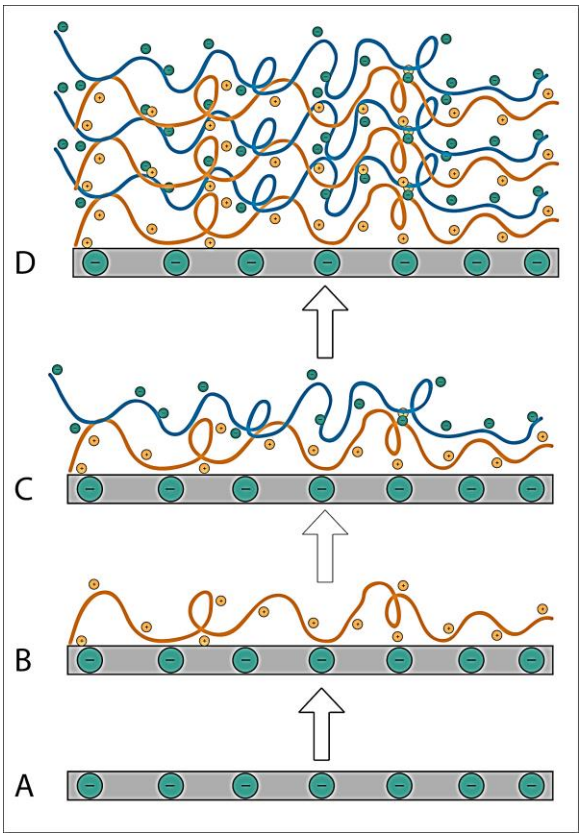

Figure 1: Schematic of LbL deposition for the assembly of PEMs. Cassin, M.E. and P. Rajagopalan, Polyelectrolyte Multilayers for Applications in Hepatic Tissue Engineering, in Layer-by-Layer Films for Biomedical Applications, C. Picart, F. Caruso, and J.C. Voegel, Editors. 2015, Wiley-VCH. p. 487-506. Used with permission of John Wiley and Sons, 2015.

PEMs can be assembled using a range of PE combinations [5, 54, 56-58]. The choice of PEs and the resulting range of properties lead to a wide range of applications. For example, thicker, more hydrated films can be used as hydrogel scaffolds [59-63], while thinner, more rigid multilayers can be used to emulate narrow tissue architectures such as membranes [35, 47, 64, 65]. Porous PEMs can be fabricated through salt- or pH-induced structural changes [11, 65] and enable the exchange of nutrients between cell types in a co-culture. In contrast, non-porous multilayers can function as barriers [66, 67].

PEMs composed of synthetic polymers typically exhibit a linear correlation between thickness and the number of bilayers, while their biological counterparts show an exponential relationship

[8, 13, 28, 56, 68, 69]. The height of a PEM can be controlled by varying the ionic strengths and pH of individual PE solutions [5, 7, 33, 69-73]. The presence of salts increases the mobility of the polymer chains, allowing them to attain a more thermodynamically favorable structure [69, 71-73]. The arrangement of the available protonated and deprotonated groups, resulting from changes in pH, can result in linear or “loopy” chain configurations, contributing to differences in thickness [5, 7, 33, 70].

Synthetic PEs used in biomedical applications include poly(acrylic acid) (PAA), poly(allylamine hydrochloride) (PAH), poly(diallyldimethylammonium) (PDAC) and sulfonated polystyrene (SPS) [5, 28, 33, 34, 39, 74, 75]. Some biologically-derived PEs are poly(glycolic acid) (PGA), poly(lactic acid) (PLA), their copolymer poly(lactic-glycolic acid) (PLGA), poly(caprolactone) (PCL), poly(ethylene oxide) (PEO), poly(ethylene glycol) (PEG) and poly-β-hydroxybutyrate (PHB) [35, 50, 57, 62, 67, 76-82].

Due to the wide-ranging biological applications of PEMs, different approaches have been utilized to modify their mechanical and chemical properties during or subsequent to their assembly [35, 57, 67, 80, 83]. Chemical modifications conducted post-assembly include conjugation of functional groups, peptide sequences or other small molecules that can promote cellular adhesion, proliferation and function [19, 28, 29, 37, 38, 84, 85]. Physical properties are usually varied through the use of naturally-occurring or synthetic cross-linkers [19, 21, 33, 43, 45, 86, 87]. Such processes assist in matching the mechanical properties to native tissues [88-90].

The combination of the ease of assembling PEMs and the ability to modify them post-assembly has led to their uses in drug delivery [40, 58, 75, 91], tissue engineering [47, 54, 57, 67, 84, 86, 92, 93], nano- and microfluidic devices [66, 94], and cellular adhesion studies [30, 33, 35, 37,

39, 49, 95]. In subsequent sections, we outline how these versatile PEMs are being modified and utilized for hepatic tissue engineering.

1.1.1 The Liver

The liver is a highly vascularized organ and is involved in several metabolic functions [96] (**Figure 2**). This organ plays a critical role in the biotransformation of drugs and pharmaceuticals, cholesterol metabolism, glucose homeostasis and in the synthesis of blood plasma proteins [80, 96-98]. Hepatocytes are the principal or parenchymal cells (PCs) of the liver, comprising over 80% of its mass [96]. These cells are involved in the synthesis of cholesterol, bile, salts, and phospholipids, protein synthesis and storage, transformation of carbohydrates, and the modification and excretion of substances such as alcohol and drugs from the body [57, 80, 96, 99]. The liver is divided into hexagonal lobules; these lobules contain the microcirculatory units known as liver sinusoids [96, 100]. In a liver sinusoid, PCs are separated from the non-parenchymal cells (NPCs) by an interfacial region called the Space of Disse [96] (**Figure 3A)**. The Space of Disse is a protein-enriched region (0.5-1μm in height) that facilitates the transfer of nutrients and signaling molecules between the hepatocytes and the NPCs [47, 96, 98, 101]. This interfacial region is composed of fibrillar and network collagens (I-IV), adhesion proteins, such as laminin and fibronectin, as well as proteoglycans, such as heparan sulfate, heparin, chondroitin sulfate, and dermatan sulfate [96, 102, 103]. The chemical and mechanical properties of the Space of Disse are altered during certain liver diseases due to increased production of extracellular matrix (ECM) components by hepatic cells [99, 101, 104] (**Figure 3B**). NPCs are comprised of Kupffer cells (KCs), liver sinusoidal endothelial cells (LSECs), and hepatic stellate cells (HSCs). KCs are specialized macrophages that initiate and contain inflammation, and are responsible for mounting the immune response [96]. LSECs are highly metabolic in nature and participate in the scavenging of lipid and fat molecules [96, 101,

105]. These cells exhibit fenestrae or pores that range from approximately 90-150nm in diameter depending on the species. These fenestrae can expand or contract resulting in the promotion or prevention of the transport of small molecules or pathogens to the hepatocytes below [106-108]. HSCs store vitamin A droplets and secrete ECM proteins during liver fibrosis [57, 96, 109-113]. Together, these four cell types perform several metabolic functions and maintain organ-level homeostasis.

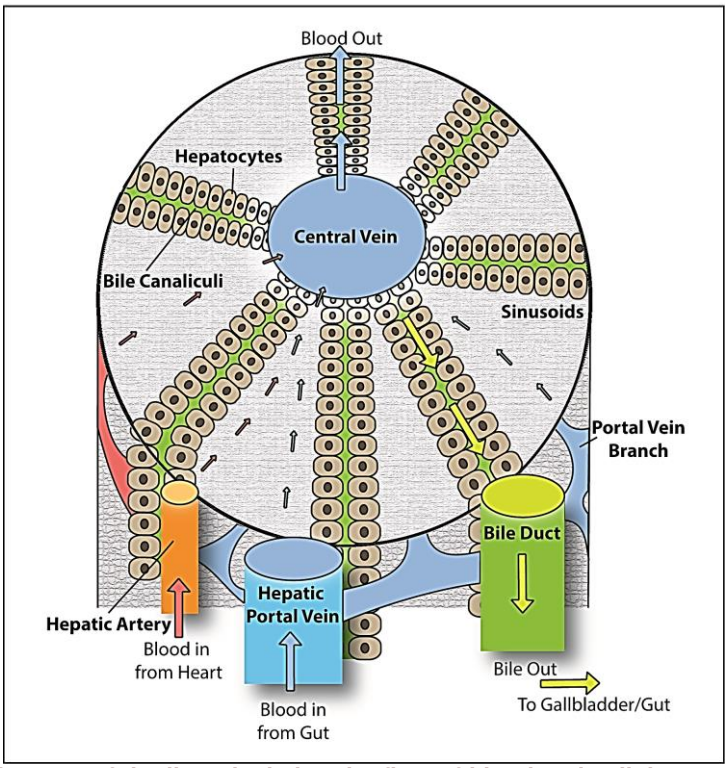

Figure 2: Cellular architecture of the liver depicting the flow of blood and cellular arrangement. Cassin, M.E. and P. Rajagopalan, Polyelectrolyte Multilayers for Applications in Hepatic Tissue Engineering, in Layer-by-Layer Films for Biomedical Applications, C. Picart, F. Caruso, and J.C. Voegel, Editors. 2015, Wiley-VCH. p. 487-506. Used with permission of John Wiley and Sons, 2015.

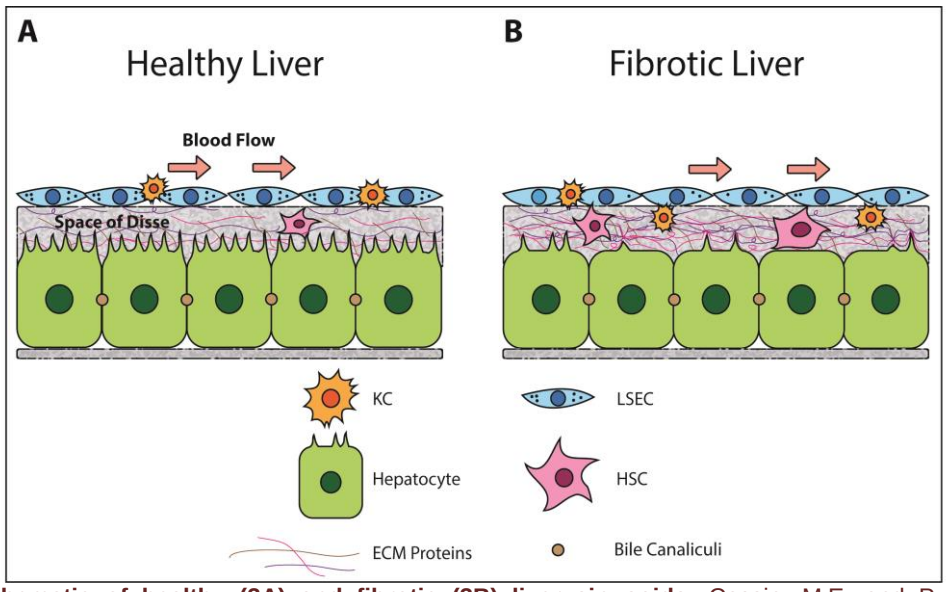

Figure 3: Schematic of healthy (3A) and fibrotic (3B) liver sinusoids. Cassin, M.E. and P. Rajagopalan, Polyelectrolyte Multilayers for Applications in Hepatic Tissue Engineering, in Layer-by-Layer Films for Biomedical Applications, C. Picart, F. Caruso, and J.C. Voegel, Editors. 2015, Wiley-VCH. p. 487-506. **Used with permission of John Wiley and Sons, 2015.**

1.1.2 PEMs and Hepatic Tissue Engineering

The biocompatibility and inert properties of PEMs render them highly suitable for tissue engineering applications. Furthermore, the ability to incorporate biological molecules and the high degree of molecular control over film properties are critical to match their properties with those of native tissues [39, 57]. In hepatic tissue engineering, PEMs have been incorporated as encapsulants [94, 114, 115], biomimetic membranes [47, 48, 78], cell-adhesive regions [19, 33-35, 37, 38, 116], and in drug delivery [58, 75, 91, 117, 118].

PEMs used in biological applications often include ECM proteins or peptides. This has arisen from the popularity of ECM-based proteins such as collagen, used as scaffolds in tissue engineering, [57, 92, 93], wound healing devices [36, 40, 119], and films [45, 49, 83, 95]. Three commonly used biologically-derived PEs are collagen (COL), chitosan, and hyaluronic acid (HA) [45-49, 78, 86, 87, 95, 120]. COL is increasingly used in PEMs since it is cationic [43, 45, 76, 121]. Specifically, in the context of the liver, COL (type I) is found in the Space of Disse [45, 46,

49, 83, 121] and is likely to improve hepatic functions *in vitro* [86, 99]. Chitosan is derived from the shells of crustaceans, and has been repeatedly shown to be a PE compatible with hepatic cells [78, 122, 123]. HA, an anionic PE, found in the basal membrane of connective tissues has been used in combination with both COL and chitosan to produce biologically compatible multilayers [46, 78, 83, 95, 121, 122, 124]. Other biological PEs such as polysaccharides [125, 126], polypeptides [54, 127], and DNA [35, 54, 128, 129] have also been used in the fabrication of biocompatible PEMs. Synthetic and naturally derived PEs can elicit differing adhesive and functional behaviors when placed in contact with hepatic cells [57]. Whether a PE is naturally-occurring or synthetic in its origin, the mechanical and chemical properties of the resulting self-assembly must often be changed in order to recapitulate the tissue microenvironment.

1.1.3 Tuning Mechanical and Chemical Properties of PEMs

The ability to alter the mechanical properties of PEMs enables a broad range of cell-based studies [22, 33, 35, 43, 116, 126, 130-132]. Chemical crosslinking agents are often introduced to modify the modulus of the resulting multilayer after the assembly is completed [24, 45, 83, 116, 133]. In addition, several factors during the assembly process such as pH and ionic strength can influence the stiffness of the PEM [28, 33, 69, 134]. Other forms of altering mechanical properties have been investigated, such as, temperature and pH responsive materials [135, 136], biochemical functionalization of the film [35, 137], as well as electrochemically responsive films [133].

Chemical crosslinking is one approach to enhance PEM stability and alter its moduli [21, 43, 45, 86]. Biological PEMs assembled with COL (cationic) and HA (anionic) or chitosan (cationic) and HA are not stable in aqueous environments and thus require crosslinking to prevent their dissolution once placed in an *in vitro* culture. Un-crosslinked PEMs have been reported to

dissociate within minutes of being placed in an aqueous environment [9, 46, 47, 122]. Cross-linking can also improve cellular responsiveness. However, some of the issues that arise using any cross-linking reagent are loss in optical transparency of the PEM and reorganization of polymer chains [45, 138]. Additionally, the presence of unreacted cross-linkers can result in cytotoxicity.

Ionic crosslinking can also be employed to alter the stability and moduli of the multilayer during deposition by altering the pH of each PE [33, 69, 70]. In a study on the behavior of hepatocytes as a function of mechanical compliance, the pH of strong PEs, such as PAA and PAH were varied [28]. It was found that when the pH of the PE solutions was closer to neutral, a higher degree of ionic crosslinking was obtained. PEMs deposited at lower pH (pH=2.0) self-assembled in a linear fashion and had a lower compliance than those assembled at neutral pH. Primary hepatocytes cultured on PEM surfaces exhibited a higher degree of adhesion on stiffer substrates (elastic modulus ~140MPa), while hepatic functions, such as albumin and urea secretion and cytochrome P450 activity, were found to be higher on softer substrates (elastic modulus ~200kPa) over a 2 week period [24, 28]. It is therefore important to assemble PEMs with moduli which improve both hepatic function and adhesion.

Modulation of chemical properties can also affect hepatic function and adhesion. Since ECM proteins are a ubiquitous component of the liver, hepatic cells are commonly cultured on COL or fibronectin-coated substrates. Studies show that hepatic functional and phenotypic markers are maintained when cultured in contact with ECM proteins [57, 80, 84, 92]. Since ECM proteins contain integrins, such as the arginine-glycine-aspartic acid (RGD) sequence which aid in cellular adhesion, these peptide sequences have been incorporated to promote adhesion [19, 23, 139]. Synthetic PEs can be limited for hepatic tissue engineering applications due to their lack of naturally occurring cell recognition motifs [19, 57, 140].

1.1.4 PEMs for 3D Hepatic Cell Cultures

Mechanical and chemical modifications have been used extensively in 2D cell cultures for adhesive, migratory, and functional studies. However, commonly used 2D culture architectures such as hepatocyte monolayers (HM), collagen sandwiches (CS) and co-cultures cannot mimic the intricate interactions between cells in a tissue system. The ability to tune the physical properties of PEMs using LbL deposition has expanded their use from 2D cultures to 3D systems. These 3D models can provide environments more suitable for long-term hepatic tissue engineering studies.

3D hepatic tissues cultured in microenvironments that recapitulate the liver *in vivo*, exhibit significant potential as *in vitro* models of the liver [47, 54, 141-143]. However, designing such *in vitro* constructs necessitates recreating the physical, chemical and cellular composition found in the organ [54, 57, 80, 141, 142].

1.1.4.1 PEMs that Mimic the Space of Disse

The assembly of liver tissue models is challenging since hepatic cells exhibit reduced functional capabilities *in vitro*. One approach to enhance cellular functions is to use PEMs as substitutes for the Space of Disse [47, 48, 54, 78, 98]. Using the LbL technique, Rajagopalan *et al.* assembled nano-scale chitosan/DNA polyelectrolyte scaffolds above a confluent layer of primary hepatocytes [54]. Chitosan and DNA solutions were sequentially deposited directly above live cells. PEMs were composed of DNA and chitosan since these PEs are ionic at values of pH compatible with cell-culture [52, 144-146]. A second layer of cells was subsequently cultured above the PEM. Through this approach, multicellular 3D tissue mimics (hepatocytes-PEM-hepatocytes, hepatocytes-PEM-endothelial cells, and hepatocytes-PEM-

fibroblasts) were designed. Over a seven-day culture period, 3D liver models exhibited significantly higher albumin secretion than HM cultures. Hepatocytes also maintained their polygonal morphology when in contact with the multilayer.

Using this approach, Kim *et al.* designed liver sinusoidal structures using primary hepatocytes and either human or rat LSECs. Instead of DNA, HA was used as the anionic PE in the assembly of the multilayer [48, 98] since this biopolymer is found in the Space of Disse [147, 148]. The height of the PEMs ranged from 30 to 55nm and exhibited a shear modulus of approximately 100kPa. In the hepatocyte–PEM–LSEC liver-mimetic cellular constructs, LSEC phenotype was maintained, and these cultures exhibited stable urea and albumin production. Cytochrome P450 1A1/2 (CYP1A1/2) enzymatic activities activity was significantly higher in the hepatocyte–PEM–LSEC constructs than in 2D cultures. A 16-fold increase in CYP1A1/2 activity was observed for hepatocyte–PEM–LSEC models, demonstrating that inter-cellular communications between cell types promoted important hepatic functions. A rat LSEC-specific marker, the sinusoidal endothelial 1 antibody (SE-1) was only exhibited over 12 days in the 3D models. In addition, the hepatocyte-PEM-rat LSEC cultures exhibited increasing CYP1A1/2 and CYP3A activity, as well as well-defined bile canaliculi. When these liver models were monitored for their ability to maintain bile acid homeostasis, only the 3D liver models exhibited ratios similar to those obtained *in vivo* [149].

Although, these studies exhibited the potential of PEMs in the design of liver-mimetic tissues, the deposition of the PEs directly above cells limited their capacity for assembly and post-deposition modifications. Therefore, Larkin *et al.* designed detachable PEMs for use in 3D hepatic cultures [47, 78]. Detachable, free standing chitosan/HA PEMs were assembled on hydrophobic poly-(tetrafluoroethylene) (PTFE) substrates [47, 78]. The hydrophobicity of PTFE enabled easy detachment of the chitosan/HA PEMs. Using primary rat hepatocytes, KCs and

LSECs, a liver model was developed to mimic closely the *in vivo* architecture [48, 54, 96, 98]. The hydrated thickness for a 12.5 bilayer (BL) (chitosan/HA) PEM was 751± 29 nm which is close to the height of the Space of Disse (0.5-1μm). A BL was designated as one anionic and one cationic PE layer. PEMs were cross-linked to increase their stability in aqueous media as well as to match the Young's modulus to mimic that of bulk liver tissue [150, 151]. The PEMs exhibited a modulus of 41.79 ± 3.65kPa, were optically transparent, and exhibited smooth surfaces [47, 98].

Liver-mimetic models composed of primary hepatocytes, KCs and LSECs were assembled and investigated. Markers of hepatic function, such albumin secretion and urea production were higher in the 3D tissues in comparison to 2D cultures and co-cultures [67, 98, 99]. Hepatocytes, KCs and LSECs proliferated in the 3D liver model, and maintained cellular ratios at the end of the culture, that were very close to those observed *in vivo* [152]. LSECs and KCs maintained their characteristic phenotypic markers, SE-1 and CD163, respectively, throughout the culture period.

The versatility of PEMs has been utilized in different ways to design engineered liver tissues. We have discussed an innovative way that researchers incorporate LbL methods in efforts to recreate the hepatic microenvironment. We anticipate that through ongoing and future efforts, additional novel applications will emerge. For example, PEMs are already being studied in the realm of regenerative medicine, specifically, in stem cell differentiation [93]. In the future, we envision that the synergy between PEMs and liver tissue engineering will continue to grow. Here, we strive to investigate the potential for PEMs in liver hepatic tissue engineering in contact with pathogens.

Text in this section was used with permission from John Wiley and Sons, 2015 in Cassin, M.E. and P. Rajagopalan, Polyelectrolyte Multilayers for Applications in Hepatic Tissue Engineering, in Layer-by-Layer Films for Biomedical Applications, C. Picart, F. Caruso, and J.C. Voegel, Editors. 2015, Wiley-VCH. p. 487-506.

1.2 Bacteria

While there are many pathogens, in this review we will focus on bacteria. Bacteria can be categorized as Gram-positive or Gram-negative based on the composition of their cell walls and membranes. The Gram stain was invented in 1884 by Christian Gram; this stain allowed for the visualization of bacteria in a tissue sample. Gram-positive bacteria retain a deep purple color when stained versus the light pink color of gram-negative bacteria. This difference arises due to the thickness of the peptidoglycan layer in bacteria [153]. Some common examples of gram-positive bacteria are in the *Staphylococcus*, *Enterococcus* and *Lactobacillus* genus [154, 155]. Common gram-negative bacteria fall in the geneses of *Escherichia*, *Enterobacter*, and *Pseudomonas* [153, 156].

The internal cytoplasm can create substantial turgor pressure; therefore, to prevent the cell from bursting, both gram-positive and gram-negative bacteria possess rigid cell walls and membranes [153]. The plasma membrane is comprised of a lipid bilayer. Unlike eukaryotic cells, bacteria do not possess organelles. Therefore, all DNA synthesis and biological processes occur within the cell's cytoplasm or along the cellular membrane. The inner plasma membrane is where significant transport and energy functions occur [153]. Eukaryotic cell membranes contain a significant fraction of sterol molecules which give the membrane fluidity and permeability whereas bacterial membranes have far fewer of these molecules [157, 158]. The

higher fraction of phospholipids to sterols results in a greater negative potential on the bacterial surface as well as a more rigid membrane [159].

1.2.1 Gram-positive bacteria

Gram-positive bacteria have a thick cell wall comprised of peptidoglycan. Peptidoglycan is a molecule comprised of glycan which is a sugar backbone composed of N-acetylglucosamine and N-acetylmuramic acid. These moieties are crosslinked by peptides (**Figure 4**). Polymers such as teichoic acids, teichuronic acids, neutral polysaccharides, lipoteichoic acids, and glycolipids are linked to glycan chains [153-155]. These polymers are typically polyanionic in nature, giving the surface of a bacterial a negative charge. Additionally, these polymers provide additional strength and structure to the cell wall. Below the peptidoglycan layer of the gram-positive bacteria lies the plasma membrane.

1.2.2 Gram-negative bacteria

Gram-negative bacteria differ from gram-positive bacteria due to the presence of a secondary outer membrane. This outer membrane serves to protect the cell's thin peptidoglycan layer, periplasmic space, and inner plasma membrane (**Figure 4**). The outer membrane is a complex structure comprised of lipopolysaccharide (LPS), phospholipids and proteins. LPS is composed of 3 regions a) lipid A, b) the core, and c) the O-antigen [153, 156, 160]. LPS is responsible for much of the barrier function of the outer membrane but it also recognized by immune cells in the body as a foreign entity. Therefore, LPS is routinely used as a marker for bacterial presence [159]. The periplasm is a hydrated gel-like layer containing many enzymes and solubilizing factors. It also contains transport and chaperone proteins to enable the passage of nutrients and waste from the interior of the cell to the extracellular space. Within this periplasmic space is

the thin peptidoglycan layer of the gram-negative cell. Together the outer membrane and peptidoglycan layer add structural support to the cell [153].

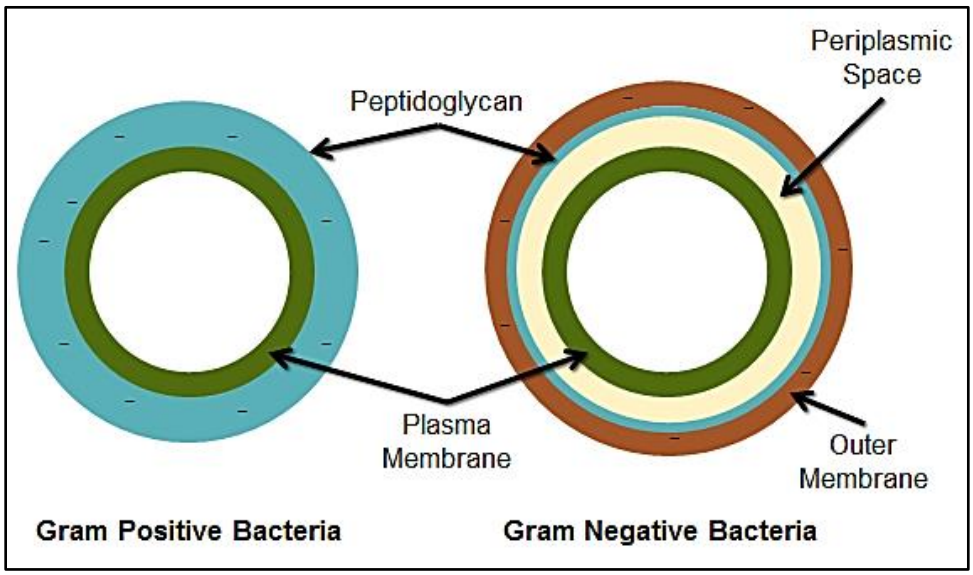

Figure 4: Membrane structures of Gram-negative and Gram-positive bacteria

1.2.3 Microbial Infections

Both gram-positive and gram-negative bacteria have developed resistance mechanisms against traditional antibiotics [161-165]. Antibiotics commonly target a specific component of the bacterial peptidoglycan layer or outer membrane since these entities are not present in eukaryotic cells. When a gram-negative bacterium develops resistance to an antibiotic treatment, it can often alter the makeup of its O-antigen, therefore, rendering the antibiotic ineffective [153, 156, 160]. Likewise, gram-positive bacteria can alter their peptidoglycan composition to have a lesser negative potential reducing the effect of charge dependent therapies [155]. Due to the overuse and misuse of antibiotics it is extremely important to identify and investigate new antimicrobial strategies that can be effective against resistant pathogens. Drug resistant pathogens are a global problem [166-172]. Infections caused by these “super bugs” can result in serious health risks and high health care costs [173-177]. In the United States alone antibiotic-resistant bacteria annually cause over 2 million infections and over

23,000 deaths [178]. Many products such as medical implants, surgical supplies, and food packaging are often contaminated by bacteria. Such contaminated products are often the cause of microbial infections [179-182].

Some non-antibiotic antimicrobial strategies currently being pursued are metal oxide nanoparticles, silver impregnated coatings, and cationic polymers and peptides. Metal oxide nanoparticles such as TiO_2, ZnO, CuO, and SiO_2, have been used to promote oxidative stress to kill pathogens [183, 184]. These nanoparticles can also alter the DNA replication in bacteria which leads to reduced microbial proliferation or complete annihilation. A second and commonly used strategy is impregnating coatings with silver [36, 185-188]. Silver ions, specifically in the form of nanoparticles can alter the conformation of enzymes such as dehydrogenases necessary for glycolysis. Silver can also increase permeability in bacterial membranes through binding with thiol groups, which results in bacterial death. Metallic antimicrobial strategies can be effective; however, they can also be toxic to eukaryotic hosts.

We have investigated antimicrobial strategies using cationic polymers and peptides. These polymers and peptides disrupt bacterial membranes through electrostatic interactions [36, 167, 189-194]. For this reason, such materials possess anti-bacterial properties against a broad spectrum of pathogens. For the remainder of this work, we will discuss a class of cationic peptides known as antimicrobial peptides (AMPs).

1.3 Antimicrobial Peptides

AMPs are an inherent component of the body's defense against invading pathogens [195-208]. They are short peptide sequences (<100 amino acids) that can exhibit broad-spectrum function against gram-positive and gram-negative bacteria, fungi, and certain enveloped viruses [189,

209]. AMPs can be found in plants, insects, and animals and act as a first line of defense more commonly known as the innate immune response [189]. Hundreds of AMPs have been identified and are present at constitutive levels in organisms [201, 203]. The concentration of these AMPs can increase at the site of infection or inflammation [190]. Some AMPs can also influence other physiological functions such as the promotion of angiogenesis, the recruitment of immune cells, and the acceleration of the wound healing process [189, 190, 200, 206, 210-212].

1.3.1 Membrane Disruption Mechanisms

AMPs function by disrupting the cell membrane through electrostatic interactions [201, 203]. AMPs typically carry a positive charge (ranging from +2 to +9) and have an amphipathic structure [190]. The separation of the charged groups from hydrophobic residues on the peptide promote the interaction of an AMP with the negatively charged bacterial membrane and subsequent penetration into the hydrophobic lipid bilayer [189]. Due to the differing charge and composition of bacterial and mammalian membranes, bacteria have a higher number of negatively charged lipids within their membranes. For this reason, AMPs preferentially target bacteria over their eukaryotic hosts, and therefore function as host defense peptides [203]. AMPs can disrupt microbial membranes through various mechanisms such as pore formation (barrel-stave or toroidal-pore model) or detergent-like solubilization (carpet or detergent model) [189, 190, 204, 205, 213, 214] (**Figure 5**). The increase in permeability can disrupt the potential within the bacterial cell as well as cause outflow of cellular contents into the extracellular space, ultimately killing the microbe. These methods of neutralization reduce the likelihood of bacteria becoming resistant to the AMP.

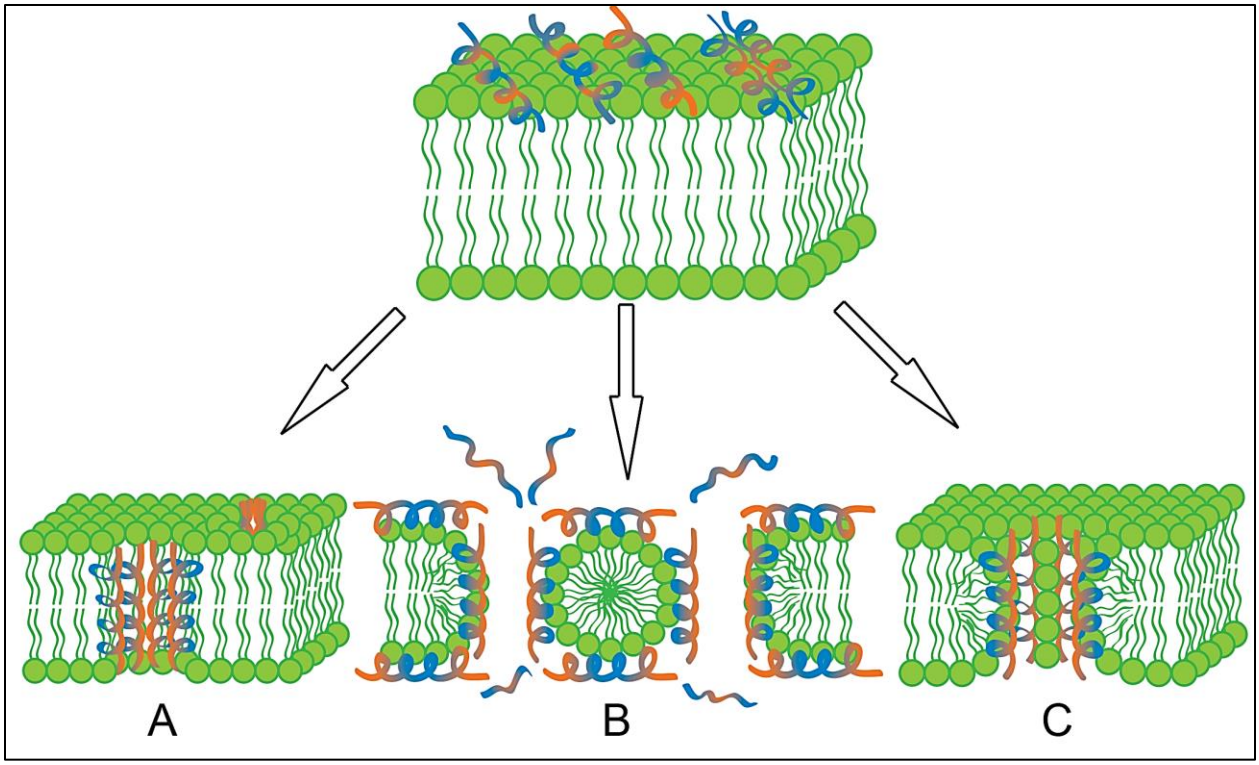

Figure 5: AMP membrane disruption models. (A) Barrel stave model: peptides aggregate and insert into the lipid bilayer. Hydrophilic regions of AMP form the interior of pore. (B) Carpet model: AMPs disrupt bilayer by orienting parallel to membrane surface to form a 'carpet' layer. (C) Toroidal pore model: peptides aggregate and induce lipids to bend throughout the pore. The core of the pore is lined with hydrophilic regions of the AMP and lipid heads groups. (Hydrophobic regions = blue, Hydrophilic regions = orange)

1.3.2 Defensins and Cathelicidins

The majority of AMPs can be categorized into two broad groups: defensins and cathelicidins [189, 209]. Defensins represent a diverse family of AMPs containing 6-8 cysteine residues which enable the formation of disulfide bridges. Based on the location of these disulfide bridges, defensins can form α- or β-defensin structures which alter their microbial activity. Humans possess six α-defensins which are typically expressed in neutrophils, the gastrointestinal (GI) tract and the female genitourinary tract [189]. Likewise, humans express four β-defensins found in many cells types, but predominantly epithelial cells and neutrophils. The majority of defensins function through pore forming mechanisms of microbial neutralization. The second major class of AMPs, cathelicidins, are defined by their conserved cathelin precursor domain with variable C-terminal positively charged peptide sequence. The cathelin domain mimics the cathelin

protein which inhibits cathepsin L. This is a lysosomal endopeptidase involved in the catabolism of ECM components during wound healing [189]. The N-terminal cathelin domain is proteolytically cleaved to form the mature, active peptide [190, 209]. This cleavage results in an increase in cathelicidin concentration at the site of infections, while keeping constitutively (or basal) levels low.

1.3.3 LL-37

The only human cathelicidin is LL-37, a 37-amino acid sequence beginning with two leucine residues (LLGDFFRKSKEKIGKEFKRIVQRIKDFLRNLVPRTES; MW 4.5kDa) [215-217]. LL-37 is the mature peptide expressed after the cleavage of the human cationic antimicrobial protein (hCAP18) encoded by the *CAMP* gene. It is produced by granulocytes and is naturally found in blood plasma at concentrations ranging from 1-2μg/mL (0.2-0.4μM) which can increase up to >25μM during infections [202, 206, 218]. LL-37 is commonly found in inflamed skin keratinocytes and is linked to inflammatory skin conditions, such as atopic dermatitis or psoriasis, when under or over expressed, respectively [189, 201, 209, 219].

The cationic (+6 charge) and amphipathic nature of LL-37 promotes interaction with bacteria cell membranes though the toroidal pore mechanism [204, 217, 220, 221]. In solution, LL-37 is found in a predominantly random coil formation, but upon contact with bacteria or in high salt environments such as sweat glands, this peptide forms an α-helical structure [204, 222]. The α-helices in LL-37 first cover the surface of the membrane. They then aggregate to penetrate the lipid bilayer which “bends” the lipid molecules. A resulting pore is formed, lined with the hydrophilic regions of the LL-37 peptide and the membrane’s polar head groups (**Figure 5**).

LL-37 exhibits antimicrobial activity against gram-positive and gram-negative bacteria. Studies have shown that this AMP performs best in environments with low ionic concentrations and at neutral pH [215, 218, 223]. LL-37 has also been shown to act as a chemoattractant for macrophages at concentrations ranging from 0.1-11μM. The chemoattraction occurs through the formyl peptide receptor-like 1 (FPRL1) on the surface of immune cells [206, 210, 211, 218, 223, 224]. In addition, LL-37 has been shown to aid in wound healing by promoting cell proliferation and angiogenesis at the site of injury [218, 225-227]. Incorporating AMP sequences, such as LL-37, in thin films, scaffolds, or basement membranes can prevent bacterial infections as well as aid in the wound healing process.

1.4 Combining PEMs and LL-37 to Study Hepatic Infections

1.4.1 Bacterial Infections in the Liver

The liver can be affected by a variety of infections. Some infections stem from the blood due to trauma, abscesses, or complications from liver disease such as cirrhosis [228]. While haematogenous infection of the liver is less frequent today due to the use of circulating intravenous antibiotics, it is still common for bacteria to infect the liver through the biliary or GI tracts. The majority of these infections are caused by trauma, such as disease or surgery, to an infected organ or tissue which then spreads to the liver [228, 229].

The GI tract contains numerous strains of beneficial and infectious microbes [230]. Since the liver receives approximately 70% of its blood supply from the GI tract, bacteria and bacterial components often come in contact with hepatic cells [229, 231]. In a healthy individual, the majority of these foreign organisms are cleared from the body by the liver. This role typically performed by the KCs as well as other smaller populations of immune cells in the liver sinusoid, such as neutrophils [229, 230, 232]. In addition, when liver cells, specifically KCs are exposed to

LPS, they release nitric oxide, a vasodilator to remove the pathogens from the liver sinusoids and recruit more neutrophils [233]. However, when the liver is not functioning properly due to disease, such as fibrosis or cirrhosis (resulting from alcoholic or nonalcoholic fatty live disease, ischemic liver injury or hepatocarcinoma), major complications can occur due to the presence and proliferation of bacteria in the liver [229].

Bacterial infections are a common complication associated with cirrhosis of the liver. They are responsible for up to 25% of liver disease related deaths [234]. While the use of broad-spectrum antibiotics has reduced the severity of infections, the ever-present risk of antibiotic resistant bacteria still results in high morbidity and mortality. As of 2013, patients with cirrhosis exhibited a ~30% bacterial infection rate. This percentage increased to approximately 45% in patients being treated for both cirrhosis and GI hemorrhage [234-236]. In comparison, the general population has only shown a 5-7% hepatic infection rate. The most common bacterial infections arise from *Escherichia coli* (*E. coli*) and *Klebsiella pneumoniae (K. pneumoniae)* due to the continuous interactions between the liver and the GI tract [228, 234, 237]. While the majority of *E. coli* strains can still be neutralized by conventional antibiotics, the antibiotic-resistant *K. pneumoniae*, *Pseudomonas aeruginosa*, methicillin-resistant *Staphylococcus aureus* (MRSA), and vancomycin-resistant *Enterococcus* (VRE) are all still major concerns [236]. The presence of a bacterial infection can then lead to renal failure, shock, sepsis, and ultimately full system organ failure if left untreated [234].

1.4.2 Antimicrobial PEMs

The Rajagopalan group has been designing 3D liver models to investigate hepatic function and signaling. In order to recreate the microbial hepatic environment it is critical to incorporate AMPs to the model. Although, soluble AMPs can be added, they may be rapidly metabolized by

hepatocytes. For this reason, we have designed PEMs that contain immobilized AMPs. When such antimicrobial PEMs are cultured with hepatic cells and bacteria, the microenvironment may begin to emulate what is found *in vivo*.

PEMs have been designed to promote microbial death as well as stimulate wound healing. Antimicrobial PEMs are traditionally impregnated with conventional antibiotics [36, 238-242] or silver nanoparticles [36, 179, 187, 243] which are released into the surrounding environment over time as the PEM degrades. Other studies use PEMs assembled with innately antimicrobial PEs such as chitosan, HA, and N-alkylated poly(ethylenimine) (PEI) [179, 244-247]. Many of these PEs mimic the cationic and hydrophobic charge and structure of native AMPs. Significant work has been done using antibacterial agents as well as AMPs in solution [194, 199, 215, 220, 221, 242, 248] or on materials, including non-detachable PEMs, as coatings [36, 175, 187, 239, 241, 247, 249-255].

Due to the cost and experimental challenges associated with AMPs, many studies have been conducted using synthetic AMPs which mimic the charge and structure of native peptides [169, 170, 179, 194, 245, 247]. While these synthetic peptides can interact with bacterial membranes and cause microbial death, they do not allow for further interaction with the host organism in terms of immune system communication or cell proliferation. Additionally, higher concentrations of synthetic AMPs are needed than their natural counterparts in order to kill bacteria. Therefore, incorporating natural AMP sequences, such as LL-37, in thin films has the potential to kill bacteria in addition to aiding in the immune response at physiologically relevant concentrations.

Our work focuses on the AMP LL-37 which is either physisorbed or immobilized on biocompatible, detachable, PEMs. While there are many known AMPs, LL-37 is the only human derived cathelicidin, reducing xenogeneic effects when in contact with infection and wounds. We

aim to investigate the interactions between hepatic cells and bacteria in a 3D liver model that contains an AMP-modified PEM. By harnessing the broad-spectrum antimicrobial capabilities of LL-37, as well as its' chemotactic properties, it is possible to design a thin film that can act as a Space of Disse mimic for hepatic models while also adding protection against bacterial infections.

1.5 Antimicrobial PEMs to Study Bacterial Infections in the Liver

The Rajagopalan research group has used detachable PEMs to design 3D hepatic models which mimic the stratified architecture of a liver sinusoid by incorporating a polymeric space of Disse [47, 48, 78, 98]. However, there have been no studies to date that utilize PEMs modified with AMPs to study bacterial infections in the liver.

We have designed novel thin films modified with LL-37. The polymeric membranes were assembled with Type 1 COL (polycation) and HA (polyanion) using the LbL deposition technique [6, 35, 45, 67, 256]. COL and HA were chosen to mimic the chemical composition of the ECM found *in vivo*, particularly the Space of Disse. The detachable nature of the PEMs enables mechanical and chemical modification of the films post-assembly.

LL-37 modified PEMs can be brought into contact with monocultures of bacteria and hepatic cells as well as co-cultures of the two. By combining cultures of bacteria and mammalian cells in contact with these LL-37 modified films, we can monitor the death or proliferation of both cell types to determine if LL-37 is preferentially neutralizing microbes while protecting hepatic cells. As mentioned earlier, LL-37 has been known to promote the proliferation of immune cells (macrophages) at the site of infection while simultaneously killing bacteria through electrostatic

interactions [257]. These films can be used as a biocompatible, space of Disse mimics for studying bacterial infections in hepatic models in addition to movable bandage inside or outside the body and coatings for medical equipment and implants.

There are five primary aims of my thesis.

1) **Assemble and characterize a PEM comprised of biocompatible COL and HA to be used as a Space of Disse mimic for *in vitro* liver model studies.**
2) **Incorporate LL-37 to the surface of PEMs via physisorption or immobilization.**
3) **Culture *E. coli* on LL-37 modified PEMs. We will vary the concentration of LL-37 to investigate "bacterial adhesion" and "contact killing".**
4) **Culture hepatic cells on LL-37 modified PEMs.**
5) **Co-culture hepatic cells and bacteria on LL-37 modified PEMs**

I seek to combine these five aims to design an *in vitro* hepatic model that can be utilized to study bacterial infections.

2 Assembly and Characterization of COL/HA PEMs Modified with LL-37

Research Aims:

1) **Assemble and characterize a PEM comprised of biocompatible COL and HA to be used as a Space of Disse mimic for *in vitro* liver model studies.**
2) **Incorporate LL-37 to the surface of PEMs via physisorption or immobilization.**

2.1 Introduction

From early reports on PEMs, they were assembled using synthetic PEs such as poly(vinyl sulfate) (PVS), PAH, PAA, and SPS [5, 9, 73, 258]. However, there has been recent interest in using more biologically derived or "natural" PEs to assembled PEMs for use in cellular adhesion studies [30, 33, 35, 37, 39, 49, 95], drug delivery [40, 58, 75, 91], and tissue engineering [47, 54, 57, 67, 84, 86, 92, 93].

Cationic COL is the most abundant protein in the body and is therefore suitable for many biological applications. COL has been used in combination with alginate, chondroitin sulfate and heparin to act as coatings to promote cellular attachment on implants [35, 45, 49, 259]. COL has also been used commonly with HA to design hydrated ECM scaffolds and coatings [35, 46, 83, 121]. HA, a common anionic PE, is naturally present in connective tissues. It has been used with poly(L-lysine) to design films to act as drug delivery systems [132, 259, 260], as well as with synthetic PEs like PEI to assemble adhesive coatings [261]. PEMs assembled from chitosan and HA exhibited anti-adhesive capabilities toward blood plasma proteins as well as cells [122]. The surfaces of these films could be modified with ECM components, such as COL or fibronectin, to allow for selective cell adhesion in cultures.

The Rajagopalan research group has assembled PEMs comprised of chitosan and HA to act as a Space of Disse mimic. Such a membrane enabled the exchange of nutrients and signaling molecules between cell types in 3D liver models [48, 98]. Chitosan/HA PEMs assembled by Larkin *et al.* [47, 78] were detachable from hydrophobic PTFE and mimicked the thickness of the space of Disse found *in vivo*.

It is of interest to modify the surfaces of PEMs with antimicrobial agents. Such multilayers have been used in different antimicrobial applications [179, 188, 238, 240, 245, 247, 262-264]. Significant work has been conducted using AMPs, specifically LL-37, however these studies have been performed *in vivo* or *in vitro* in solution [194, 199, 210, 212, 215, 220, 221, 224-226, 242, 248]. However, there are very few studies conducted with AMPs that have been immobilized on surfaces.

LL-37 is a cationic (+6 charge) 37 amino acid sequence and is the only human cathelicidin [215, 218, 222, 223, 265]. It is constitutively present in low concentrations in the blood in a random coil formation; however, at the site of infection or inflammation can alter its conformation to an α-helix and increase in concentration in order to interact with microbes and elicit an immune response [222, 266]. The conformational change allows for the separation of hydrophilic and hydrophobic residues to allow the AMP to interact with the bacterial lipid bilayer.

Depending on the concentration of the AMP and its' environment (e.g. ionic strength, pH), LL-37 can be used to elicit many different physiological responses. For example, LL-37 has been shown to be most beneficial for wound healing applications at concentrations ranging from 0.2μM to 1μM; whereas, antimicrobial potential has been observed at concentrations from

0.02μM to 16μM [223]. In contrast, studies conducted on individuals with skin lesions from psoriasis exhibit LL-37 concentration levels as high as 500μM [222, 267].

Significant work has been conducted utilizing the potential of LL-37 as an antimicrobial agent. LL-37 is known to act on a broad spectrum of pathogens including gram-positive and gram-negative bacteria, fungi, and some viruses [222, 223]. The antimicrobial capabilities of LL-37 rely heavily on the environment surrounding the AMP as well as the pathogen strain. The minimum inhibitory concentration (MIC) is defined as the lowest concentration of antimicrobial agent to inhibit bacterial growth. In a study conducted on gram-negative *Pseudomonas aeruginosa*, LL-37 could prevent biofilm formation at concentrations significantly lower (0.1μM) than the minimum inhibitory concentration (7.1μM to 14.2μM) [215, 223, 227]. In contrast, gram-positive *Staphylococcus aureus* showed much lower MIC values ranging from 0.4μM to 2.0μM [215]. Fungicidal effects were exhibited against the fungi, *Candida albicans* at LL-37 concentrations from 4.4μM to 6.6μM [268]. Depending on the strain, the MIC values for *E. coli* can range from 2μM to 25μM [220, 248, 269]. While higher concentrations can more effectively kill bacteria, at these higher concentrations, LL-37 can become less selective and target mammalian cells as well as microbes. Therefore, it is crucial to determine the optimal LL-37 concentration range that can kill pathogens without harming the host [223, 248].

A large fraction of studies dedicated to LL-37 focus on their antimicrobial capabilities [217, 223, 227, 248, 268]. However, LL-37 can also elicit a beneficial immune response. In an article by De Yang *et al.* [224], LL-37 induced chemotactic effects in human neutrophils, monocytes, and T-cells through FPRL1 indicating that this AMP can participate in the innate immune response as well. In a study by Koczulla *et al.* [226] LL-37 was shown to induce angiogenesis through FPRL1 in *in vivo* mouse and rabbit models. FPRL1 was initially thought to only affect immune

cells, but resulted in proliferation and the formation of vessel-like structures with endothelial cells.

In this work we assembled detachable PEMs comprised of HA and COL. The thickness, elastic modulus, optical transparency, stability and zeta potential of these PEMs were characterized. LL-37 was physisorbed and covalently immobilized on the PEMs at concentrations ranging from 0-16μM. Here we investigate the addition and release of LL-37 from these films to be used in future bacterial infection studies.

2.2 Materials and Methods

Glacial acetic acid and a Pierce® FITC antibody labeling kit were purchased from ThermoFisher Scientific. LL-37 (LLGDFFRKSKEKIGKEFKRIVQRIKDFLRNLVPRTES; MW 4.5kDa), was obtained from AnaSpec, Inc. (Fremont CA). Type I COL was isolated from rat tails. All other materials, unless otherwise noted, were received from Sigma Aldrich (St. Louis MO).

2.2.1 Extraction of COL

COL was extracted by dissecting tendons from rat tails [141, 270]. Tendons were dissolved in 3v/v% acetic acid and centrifuged at 13,000x*g*. A 30w/v% sodium chloride solution was dripped into the supernatant. The resulting gel was centrifuged at 8,500x*g*. The gelatinous pellet was collected, diluted in 0.6v/v% acetic acid for 48h and then dialyzed in 1mN hydrochloric acid. The final COL suspension (2.5-3.0mg/mL) was maintained at a pH of 3.1.

2.2.2 PEM Assembly

Detachable PEMs were assembled using type I COL and HA. COL (cationic) was dissolved in 1v/v% acetic acid to obtain a solution concentration of 1.5mg/mL. HA (anionic) was dissolved in

18MΩ·cm deionized water to obtain a concentration of 1.5mg/mL. The pH of the PEs and rinse solutions was maintained at 4.0. PEMs were assembled on PTFE (McMaster-Carr) substrates using a robotic deposition system (StratoSequence VI, nanoStrata Inc.). The PTFE substrates were cleaned prior to deposition by sonication in toluene for 1h. Water contact angle measurements were >110° for clean PTFE substrates. PEMs were assembled by depositing HA followed by COL for 30min each to assemble a PEM of 15BL. The PEM assemblies were rinsed for 10min between PE depositions with DI water. Dry, deposited PEMs were crosslinked with 8w/v% glutaraldehyde for 30s, rinsed and air-dried. After 24h of air-drying, films could be detached from the underlying hydrophobic substrate.

2.2.3 PEM Characterization

2.2.3.1 PEM Stability

Dry, detached COL/HA PEMs were weighed and placed in 1X PBS (37°C) over a 3, 7, or 14-day period. After the designated time period, the PEMs were dried under vacuum for 24h at 50°C. The mass of the PEM was recorded. Mass retention was calculated to determine the degree of degradation of the PEM in a hydrated state.

2.2.3.2 Profilometry

A DektakXT profiler (Bruker, Billerica MA) was used to determine the thickness of dry and hydrated detachable PEMs. A scan length of 1000μm was taken over 20s for each sample. Thickness values were measured at five different locations per sample. Hydrated thicknesses were obtained by submerging the PEMs in DI water for 20min and subsequently wicking off excess liquid.

2.2.3.3 Modulus and Surface Characterization

Young's moduli (YM) of dry and hydrated PEMs were obtained using a Veeco MultiMode Atomic Force Microscope (AFM; Veeco, Santa Barbara CA) in a liquid cell chamber. Pyramidal SiN cantilever tips (k=0.06Nm^{-1}; Bruker AFM Probes, Camarillo CA) were used for all measurements in contact mode. Force-distance curves were obtained using a Z-scan distance of 1um and 1Hz. The YM was obtained by fitting the force-distance curves to a modified Hertz-cone model (Eq 1,2) [116].

Eq. 1 $$F = k(d - d_o)$$

Eq. 2 $$F = \frac{2\tan\alpha}{\pi}\left[\frac{E}{1-\nu^2}\right]\delta^2$$

where F = applied force, α = half open tip angle; 18°, E = YM, k = spring constant of the cantilever, ν = Poisson's ratio (constant = 0.40) d = deflection of the cantilever, d_o = deflection point during contact, and δ = indentation. To eliminate substrate effects, indentations up to 10% of the overall PEM thickness were used when obtaining force-distance curves.

Surface images were also taken using the MultiMode AFM liquid cell in contact mode to determine the roughness and porosity of the resulting multilayer. ***All AFM work was performed by Andrew Ford, a graduate student in the Rajagopalan research group.***

2.2.3.4 Optical Transmission

The PEM optical transmission was measured on a SpectraMax M2 UV/vis spectrophotometer (Molecular Devices, Sunnyvale CA) over the range 400-900nm. Measurements were taken on dry and hydrated detached multilayers. Hydrated films were maintained in DI water for 20min before measurements were taken.

2.2.4 LL-37 Modification of PEMs

2.2.4.1 *Physisorption of* LL-37

The physisorption of LL-37 onto COL/HA PEMs was performed on both PTFE-adherent and detached PEMs. Detached PEMs were placed in 12-well plates with stainless steel washers placed above them to prevent folding of the PEMs. Films were hydrated with 1XPBS for 30min; 100µL of the desired LL-37 solution (2µM, 8µM, 16µM) was then added to the PEM and allowed to physisorb for 30min. The resulting PEM was then rinsed three times with 1XPBS.

2.2.4.2 *Immobilization of* LL-37

LL-37 was immobilized onto the surface of the PEMs using carbodiimide chemistry [271]. Briefly, PEMs were hydrated in 1XPBS for 30min. EDC (1-ethyl-3-[3-dimethylaminopropyl]carbodiimide) was added in 10-fold molar excess to LL-37 in 0.1M MES buffer (2-[morpholino]ethanesulfonic acid) at pH 6.0. NHS (N-hydroxysuccinimide) was added to the solution at 10-fold molar excess to LL-37. This solution was allowed to react for 15min. The LL-37 solution was then added to the hydrated PEMs (100µL/PEM) and allowed to react for 2h at room temperature. The PEMs were maintained in a hydrated state over the course of release studies for both physisorbed and immobilized films.

2.2.4.3 *Conjugation of FITC to* LL-37

FITC was conjugated to the LL-37 peptide using a Pierce® FITC antibody labeling kit. Unconjugated FITC dye was separated from conjugated dye by passing the LL-37/FITC solution through a resin-filled spin column. The resulting peptide+dye solution was passed through a 0.2µm syringe filter to remove excess resin beads. FITC-conjugated LL-37 was added to

hydrated PEMs and imaged using a green filter on a Nikon Eclipse TE2000-U microscope (Nikon, Linthicum MD) to detect LL-37 coverage on the surface of the PEM.

2.2.4.4 Zeta-potential

Zeta-potential measurements were conducted on unmodified and LL-37 modified PEMs using a SurPASS electrokinetic analyzer (Anton Paar, Ashland VA) equipped with a clamping cell; a minimum of eight measurements were taken per sample. Two PEMs attached to TCPS substrates were separated by a 100μm thick spacer with a 5mm wide channel (**Figure 6**). A solution of 0.05M NaCl was flowed in the channel between PEM samples in the clamping cell at a pressure of 200mbar to obtain pressure-potential curves. Zeta potential measurements were calculated using a modified Smoluchowski equation (Eq 3).

Eq. 3 $$\zeta = \frac{dU}{dp}\frac{\eta}{(\varepsilon * \varepsilon_0)} K_B$$

where ζ = zeta potential (mV), dU/dp = slope of streaming potential vs differential pressure, η = electrolyte viscosity, ε = dielectric coefficient of electrolyte solution, ε_0 = vacuum permittivity (8.854×10^{-12}F/m), and K_B = electrolyte conductivity [76, 272-274].

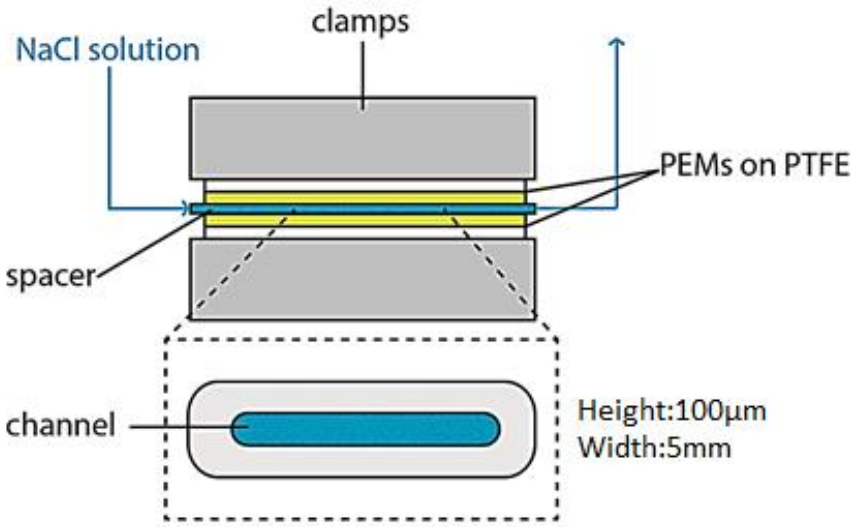

Figure 6: PEMs in clamping cell for zeta potential measurements

2.2.4.5 Release Profile

PEMs with FITC-conjugated LL-37 were maintained in 2mL of Lysogeny broth (LB). Sample aliquots were collected over a 96h period. The fluorescent intensity of aliquots was measured using a SpectraMax M2 UV/vis spectrophotometer (Molecular Devices, Sunnyvale CA) at 495nm. These values were compared to a standard curve to determine the release of LL-37 from PEMs.

2.2.5 Statistics

All PEM testing was conducted with a sample size $n \geq 3$. A two-tailed *t*-test ($\alpha=0.05$) assuming unequal variance was used to determine significance for zeta potential measurements between unmodified and LL-37-modified PEMs as well as zeta potential differences between the COL and HA terminating sides of the films.

2.3 Results

2.3.1 PEM Characterization

COL/HA PEMs were assembled using the LbL technique. The assembly process was optimized to obtain PEMs that were detachable and stable. The COL and HA concentrations, number of bilayers and crosslinking conditions were optimized to achieve these characteristics. For all PEM trials, the pH of PE and DI water solutions was maintained at 4.0. The deposition time was 30min and 10min for PE and DI water, respectively. The PEMs were all crosslinked with 8 w/v% glutaraldehyde. Our goal was to obtain hydrated PEMs that would be in the 2-3μm range in thickness.

Table 1: COL/HA PEM Optimization trials

Trial	[COL/HA] (mg/mL)	BL	Crosslink Time (s)	Detachable	Ease of Use	Hydrated Thickness (μm)
1	0.1/1.0	30	15	No	-	
2	1.0/1.0	30	15	No	-	
3	1.5/1.5	30	15	Yes	Good	15.2 ± 2.1
4	1.5/1.5	30	30	Yes	Good	14.4 ± 2.7
5	**1.5/1.5**	**15**	**30**	**Yes**	**Good**	**3.3 ± 0.6**
6	1.5/1.5	12	30	Yes	Poor	3.6 ± 0.8
7	1.5/1.5	10	30	Yes	Poor	3.5 ± 0.7
8	1.5/1.5	5	30	No	-	

The final PEM conditions that resulted in detachability were obtained by using 1.5mg/mL COL and HA, deposited for 15BL and crosslinked with glutaraldehyde for 30s (**Figure 7A**). These PEMs were then further characterized.

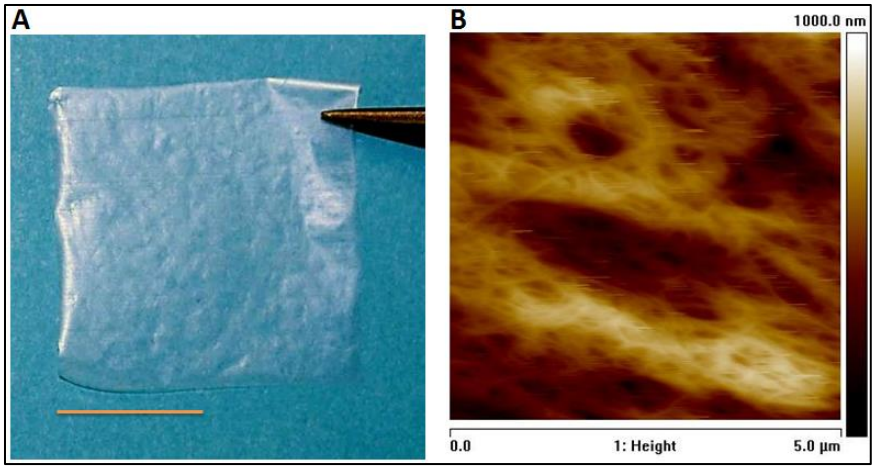

Figure 7: (A) COL/HA detached PEM (Scale = 1cm) (B) Surface AFM image of hydrated COL/HA film

The stability of these films was monitored over 14 days in an aqueous environment. The PEMs exhibited approximately 87% mass retention after 14 days, thereby, exhibiting stability in aqueous medium (**Table 2**).

Table 2: PEM stability in an aqueous environment as determined by mass retention

	Day 3	**Day 7**	**Day 14**
Mass Retention (%)	98.0 ± 0.9 (*n*=3)	94.6 ± 1.5 (*n*=9)	86.9 ± 0.1 (*n*=6)

Profilometry measurements were conducted using a DektakXT profiler on dry and hydrated PEMs. PEMs used in these studies exhibited dry and hydrated thicknesses of 2.1±0.6µm (*n*=38) and 3.3±0.6µm (*n*=62), respectively (**Table 3**). Hydrated film thickness was ~1.6-fold higher than dry films indicating swelling of the PEM. The observed increase in PEM thickness upon hydration is consistent with previous studies on multilayers [78, 275-277].

The Young's modulus of dry and hydrated PEMs was found to be 32.5±7.3MPa (*n*=9) and 128.6±24.4kPa (*n*=18), respectively (**Table 3**). The hydrated modulus of these films mimics the elastic modulus of several tissues found *in vivo* [278, 279]. Hydrated AFM surface images depict a highly porous film with an average roughness of 158.7±45.2nm (*n*=3 PEMs, 3

measurements/PEM) and a peak to valley ratio of 1.18±0.47μm (**Figure 7B**). The average pore diameter was found to be 161.0±43.2nm (*n*=90).

Table 3: PEM characterization of thickness and Young's modulus via profilometry and atomic force microscopy, respectively.

	Dry	Hydrated
Thickness (μm)	2.1 ± 0.6 (*n*=38)	3.3 ± 0.6 (*n*=62)
YM (kPa)	32503.9 ± 7296.0 (*n*=9)	128.6 ± 24.4 (*n*=18)

The optical transmittance over 400-900nm for these PEMs was found to range between 74.5-85.6% for dry multilayers (*n*=10) and 85.8-94.6% for hydrated films (*n*=10) (**Figure 8**). Optical transparency is one of the desired features of a PEM when assembling layered cellular architectures, since visual inspection and imaging of cellular layers above and below the PEM can be easily conducted.

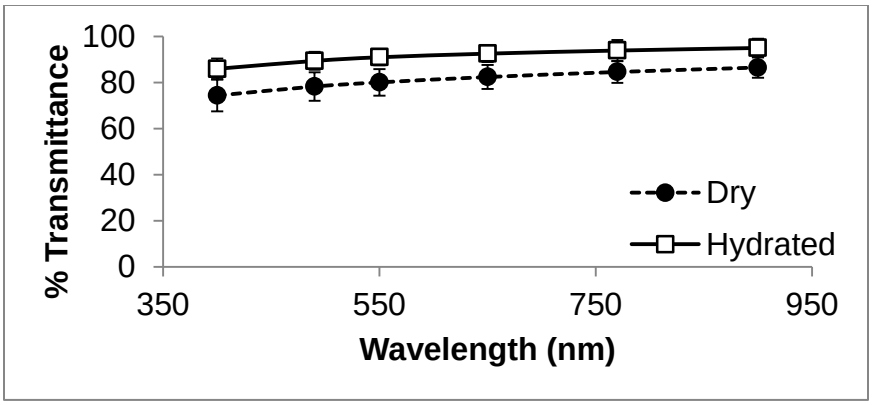

Figure 8: Percent transmission of light through dry and hydrated COL/HA PEMs between 400-900nm (*n*=10)

2.3.2 LL-37 Modification of PEMs

2.3.2.1 Zeta Potential

Zeta potential values were found to be significantly more negative on unmodified PEM surfaces compared to LL-37 modified films indicating the presence of cationic LL-37 on the surface of the PEM. COL/HA PEMs were assembled with the HA PE in contact with the PTFE substrate and

the COL PE as the last deposited layer in contact with air. The reverse assembly, (COL in contact with PTFE) was also deposited to determine the effect of PE chemistry and surface roughness on the zeta potential. The zeta potential was measured on both sides of the films and indicated that the HA side had a statistically less negative potential with the incorporation of cationic LL-37 compared to the COL counterpart for immobilized films. These values validated our choice to use the HA side of the PEM for future bacterial studies.

For physisorbed films, the zeta potential did not show a concentration dependence as a function of input LL-37 concentration from 2μM to 16μM (**Figure 9A**). The immobilized films (**Figure 9B**) however showed a marked decrease in zeta potential upon the addition of higher concentrations of LL-37.

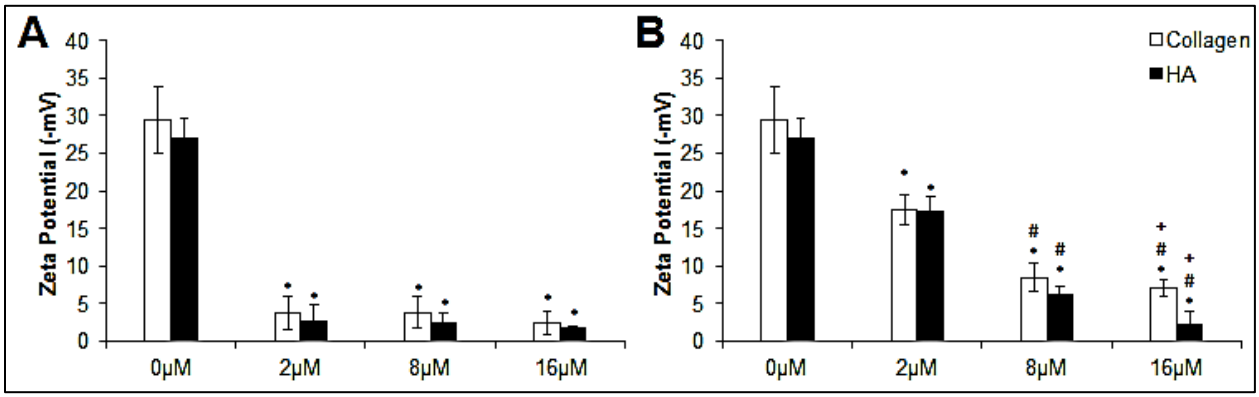

Figure 9: Zeta potential for A) physisorbed and B) immobilized LL-37 modified and unmodified COL/HA PEMs (*n*≥8) on COL and HA ending sides. Significance compared to 0μM (*), 2μM (#), 8μM (+) (*p*<0.05).

2.3.2.2 Release of LL-37 *from PEMs*

FITC-conjugated LL-37 was used to detect the presence of LL-37 on PEMs. The fluorescent signal from the FITC-conjugated LL-37 was observed across the entire surface area of the PEM (**Figure 10**). The release of LL-37 from physisorbed PEMs over a 96h period indicated sustained release of LL-37 into the media over time with approximately 20%, 60%, and 100% released after 24h, 48h and 96h, respectively (**Figure 11**). When LL-37 was chemically

conjugated to PEMs, there was virtually no release of this AMP into solution when monitored over 96h. These results indicate that the AMP continued to be covalently bound to the PEM over this time period.

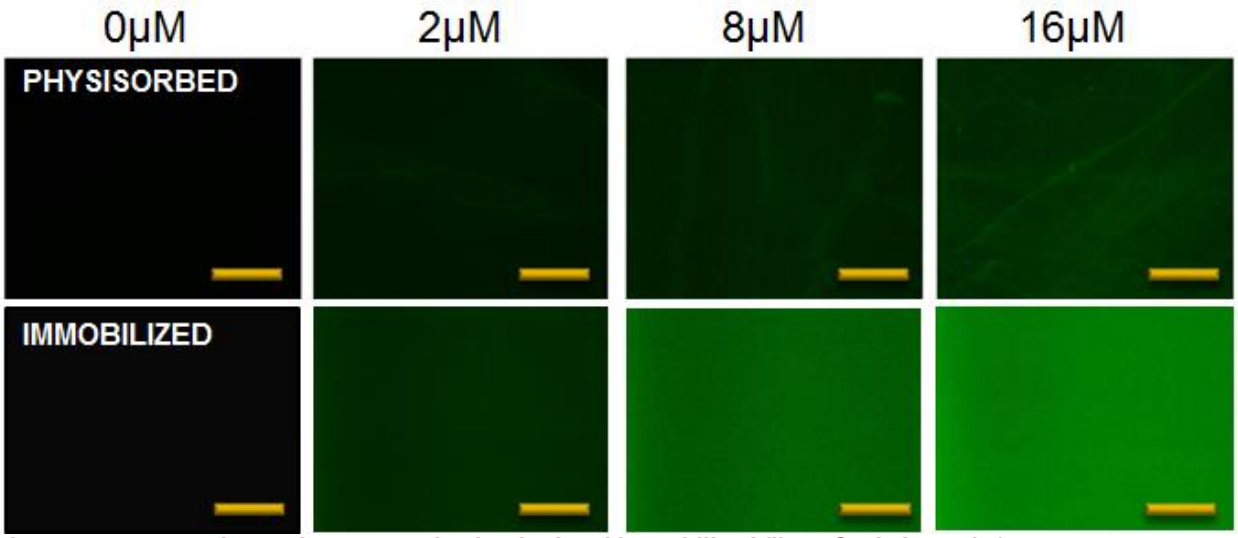

Figure 10: FITC-conjugated LL-37 on physisorbed and immobilized films. Scale bar = 150μm

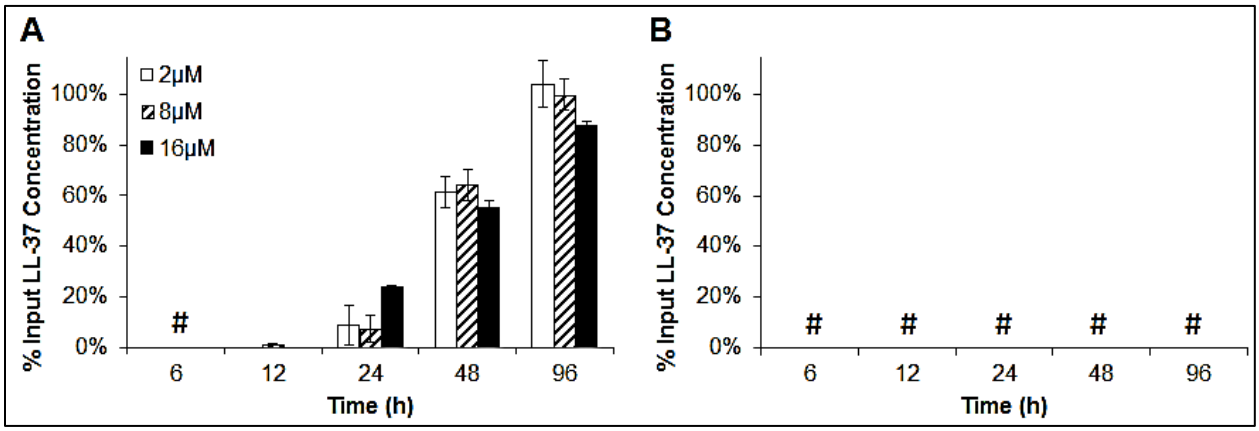

Figure 11: Release profile for (A) physisorbed and (B) immobilized FITC-conjugated LL-37 modified PEMs over 96h. No detectable LL-37 release indicated by #.

2.4 Discussion

COL and HA were used to assemble biocompatible, detachable PEMs. COL is the most abundant protein in the body while HA is naturally found in connective tissues. Together, the natural and biocompatible composition of these PEMs makes them ideal for studying biological systems. It is desirable to use these films in liver models. Therefore, the properties of the PEMs

such as thickness, stability, and elastic modulus were tuned to more closely mimic those of the Space of Disse found *in vivo*.

The properties of PEMs can be altered by modifying the number of bilayers, pH and concentration of PE solutions, crosslinking conditions, and deposition time [7]. By changing the crosslinking exposure time, a greater stability in aqueous solution was achieved. While uncrosslinked PEMs can deteriorate within minutes [78], the COL/HA PEMs crosslinked with 8 w/v% glutaraldehyde for 30s remained stable for up to two weeks. Increasing the concentration of COL and HA from 0.1 to 1.5mg/mL also allowed for more stable, easier to detach PEMs.

These PEMs were transparent over the 400-900nm range. Since these PEMs are to be used in biological systems, such as the aforementioned liver models, transparency is a desirable quality. The detachability of these PEMs is another important characteristic. The majority of PEMs are assembled on charged surfaces which limits their uses to coatings [8, 56]. Films that are detachable usually require the dissolution of a sacrificial layer [280, 281]. Due to the weak Van der Waals interactions between the first layers of PE and PTFE, these COL/HA PEMs can easily be peeled from their hydrophobic substrate.

In addition, by altering the number of deposited BLs from 30 to 15 we were able to decrease the thickness of the films from 14.4μm to 3.3μm when hydrated. Due to the biological nature of the chosen PEs, these PEMs grow in an exponential fashion [8, 9, 14, 29, 68, 69]. Therefore, dividing the number of BLs by two was sufficient to decrease the thickness of the PEMs 4-fold. Furthermore, the thickness of the hydrated films compared to their dry counterparts indicated significant swelling to a hydrogel-like state. Hydrogel materials, specifically those which model the native ECM are becoming more popular for use in 3D models to study cell migration and tissue physiology [282-286]. In addition to the PEM's hydrogel character, their hydrated YM

mimics the moduli of many tissues *in vivo* such as cartilage, ligament, and some connective tissues [278, 279].

Once a detachable, stable PEM was assembled the surface was modified with the AMP LL-37. While the majority of studies on LL-37 are conducted in solution [209, 214, 219, 220, 223, 247], here, we physisorbed and covalently linked the AMP to the surface of the COL/HA film. Zeta potential measurements of unmodified PEMs indicated a negatively charged surface even on the cationic COL ending side. This would suggest interdigitation of the anionic and cationic layers within the PEM [7, 287]. The addition of cationic LL-37 created a less negative potential with a concentration dependence observed on the immobilized films.

Based on the release profiles of LL-37 from these films it would be beneficial to use physisorbed PEMS for short-term studies in which sustained release of AMP is needed. In contrast, the immobilized films showed no detectable release of LL-37 over 4 days. These films could be used for longer studies as coating for medical equipment such as catheters or for sterile packaging.

2.5 Conclusion

We have shown the successful assembly of biocompatible, detachable COL/HA PEMs. These PEMs can be used in cellular studies due to their stability, optical transparency and ease of surface modification. Through the introduction of LL-37 to the film surface, these PEMs can be used to study bacterial infection.

3 LL-37 Modified PEMs in Contact with Bacteria

Research Aim:

3) **Culture *E. coli* on LL-37 modified PEMs. We will vary the concentration of LL-37 to investigate "bacterial adhesion" and "contact killing".**

3.1 Introduction

A wound is defined as any disruption in tissue. Common dermal wounds are a result of cuts, scraps or burns; however wounds can occur inside the body as well due to trauma or disease. Wounds leave the body open to attack by microbes which can proliferate and cause infections. The body defends itself through the activation of the immune response. Microbial infections can result in serious health risks [173, 177]. To date, microbial infections have led to close to $50 billion annually in health care costs in the United States alone [162, 163]. They are of concern in other applications such as medical implants, surgical equipment and in food packaging. These infections are traditionally treated by using either an oral or topical administration of antibiotics. However, bacteria such as *E. coli and Staphylococcus aureus* are common pathogens which are rapidly becoming antibiotic resistant (i.e. MRSA) [177]. Therefore there is emerging consensus that alternatives to conventional antibiotics must be identified.

One alternative approach to traditional antibiotics is the use of AMPs. AMPs are a key component of the body's natural defense mechanisms against invading pathogens. AMPs can exhibit broad-spectrum function against gram-positive and gram-negative bacteria, as well as other pathogens [205]. Some AMPs also have the ability to act as chemoattractants to direct the migration of white blood cells. By incorporating AMPs in a substrate, such as a PEM, a novel

multifunctional film can be designed which not only neutralizes invading microbes but also activates the organism's cellular immune response.

Research has recently been conducted using synthetic AMP or protein-impregnated PEMs as coatings for wound healing patches [247, 288]. However, these PEMs were permanently attached to a substrate and could not be peeled off, therefore, restricting their use only as coatings. Detachable, biocompatible PEMs composed of COL and HA have been assembled by the Rajagopalan research group which closely match the mechanical properties of tissues *in vivo* [47]. These robust PEMs are deposited on hydrophobic PTFE and can be easily detached due to weak van der Waal's interactions with the underlying substrate. In order to functionalize these PEMs, AMPs can be incorporated onto the surface to design a novel multifunctional patch which can elicit antimicrobial and immune responses. For this work, the human cathelicidin LL-37 was physisorbed and covalently linked to the surface of the PEM.

The bactericidal capabilities of these films were tested using two different models – "***bacterial adhesion***" and "***contact killing"***. Bacterial adhesion is a measure of the ability of an AMP-modified PEM to repel bacteria from the surface as well as kill any bacteria that do adhere. Contact killing is a measure of how an AMP-modified PEM functions when placed on a surface contaminated with bacterial growth. This is a measure of how such a film could potentially neutralize an existing infection.

LL-37 has been shown to have many effects on pathogen and hosts. For example, at concentrations 0.2-1μM, LL-37 has exhibited wound healing potential [223, 289, 290]. Below 1μM, this AMP has shown angiogenic and anti-biofilm capabilities [223, 227, 290]. From 0.2-16μM LL-37 has antibacterial properties against a number of gram-positive and gram-negative bacteria. Also in this range, chemotactic effects have been witnessed [224, 291]. However, with

increasing LL-37 concentrations, the host may also be negatively affected; cytotoxicity and apoptosis of mammalian cells can occur at concentrations >10μM [223, 289-291]. Therefore in this work, we study concentrations from 0-16μM to determine the optimal concentration of LL-37 on PEMs to elicit an antimicrobial response without harming mammalian cells.

This chapter studies the neutralization effects of detachable PEMs modified with LL-37 on the ubiquitous Gram-negative bacteria, *E. coli*.

3.2 Materials and Methods

Phosphate-buffered saline (PBS) and a LIVE/DEAD® BacLight™ bacterial viability kit were obtained from Invitrogen Life Technologies. The AMP LL-37 (LLGDFFRKSKEKIGKEFKRIVQRIKDFLRNLVPRTES; MW 4.5kDa), was obtained from AnaSpec, Inc. (Fremont CA). Type I COL was isolated from rat tails. *E. coli* strain DH10B was a gift from the Mukhopadhyay laboratory at Virginia Tech. All other materials, unless otherwise noted, were received from Sigma Aldrich (St. Louis MO).

3.2.1 *E. coli* Preparation

Gram negative *E. coli*, strain DH10B was used for all bacterial studies. *E. coli* was seeded on a LB agar plate and allowed to grow at 37°C overnight. The composition of LB was 10 g/L NaCl, 5 g/L yeast extract, and 10 g/L tryptone; 1.5% agar powder was added to the LB for agar plates. An inoculum was then prepared in 5mL LB and allowed to grow at 37°C with agitation for ~6h to late-log phase. The inoculum was diluted to OD_{600}=0.300 with fresh LB for bacterial studies; OD_{600} values were taken in a cuvette (1.5mL; 1cm path-length) using a SpectraMax M2 UV/vis spectrophotometer at 600nm. Bacterial measurements were taken at 24h and 48h after seeding.

3.2.2 Bacterial Growth Profile

For all bacterial studies, bacteria were seeded during the late-log phase of growth. Therefore it was necessary to first determine the growth profile for *E. coli* DH10B. This growth curve would provide information on the inoculation time associated with exponential growth. *E. coli* were plated on an LB agar plate and were allowed to incubate at 37°C overnight. A single colony was transferred from the agar plate to a test tube containing LB. The inoculated tubes were incubated at 35°C with agitation. OD_{600} measurements were taken from aliquots over 24h. A growth profile was plotted (Log OD_{600} vs time) and a best fit line using an S-curve function (Eq. 4) was calculated to match the data.

Eq. 4 $$X = \frac{1}{1+e^{-\propto(t-T_o)}}$$

where X=OD_{600} value (concentration scaled from 0 to 1), t=time, α and T_o are correction factors to fit data.

Once α and T_o were determined using a least squares approach, the derivative of the equation was taken. The minimum value was calculated which indicated the log/stationary transition point.

3.2.3 Minimum Inhibitory Concentration (MIC)

Bacteria were cultured on an LB agar plate overnight. An inoculum was prepared in LB broth and diluted to OD_{600}=0.050 according to the Clinical and Laboratory Standards Institute [292]. Equal parts LL-37 and bacteria inoculum (100μL each) were added to a 96 well plate in triplicate. LL-37 concentrations used in these studies, ranged from 0-16μM. Fresh broth acted

as a negative control and fresh inoculum (0μM LL-37) acted as a positive control. OD_{600} measurements were taken at time t=0 using a SpectraMax M2 UV/vis spectrophotometer. The samples were incubated at 37°C for 18h and then reread at 600nm. The MIC was determined to be the concentration of LL-37 which prevented bacterial growth – no change in OD_{600}.

3.2.4 Bacterial Adhesion Studies

Detached PEMs were placed in 12-well tissue culture polystyrene (TCPS; ThermoFisher Scientific) well plates. Sterile washers were placed above PEMs to hold multilayers in place when hydrated. PEMs were placed in wells with either the COL or HA ending side in contact with bacteria to determine if chemical and structural variations on the PEM surface could significantly alter bacterial adhesion. Desired concentrations of LL-37 were added to hydrated PEMs and allowed to physisorb for 30min. Bacteria were added to each well (0.5mL, OD_{600}=0.300) and incubated at 37°C. Bacteria seeded on TCPS and unmodified PEMs acted as controls. Spent broth was removed after 24 hours of incubation and PEMs were rinsed with fresh broth to remove non-adherent cells. Fresh LB was added to samples designated for 48h time points.

LIVE/DEAD staining was performed on the underlying PEMs (or TCPS control) using a LIVE/DEAD® BacLight™ bacterial viability kit; 100μL of dye solution (3μL live stain STYO9 + 3μL dead stain propidium iodide/1mL 1XPBS) was added to each well. The SYTO9 dye permeates both intact and membrane-altered cells, while the propidium iodide can only enter cells with a compromised membrane. The cultures were allowed to incubate in the dark for 15min at room temperature before being imaged on a Nikon Eclipse TE2000-U (Nikon, Melville NY) microscope using green and red filters for live and dead bacteria, respectively. Percent

area coverage measurements were taken for live and dead cells using NIS-Elements Advanced Research software (Nikon, Linthicum MD).

OD_{600} and LIVE/DEAD measurements were also conducted on the spent broth aliquots using a SpectraMax M2 UV/vis spectrophotometer. Aliquots were centrifuged at 10,000*xg* for 10min. The pellet was resuspended in 0.85% NaCl; 100µL of bacterial suspension was added to a 96-well plate in triplicate for OD_{600} measurements. LIVE/DEAD dye solution (100µL/well) was then added to determine percent viability. Live (SYTO9) and dead (propidium iodide) measurements were taken at 530nm and 630nm, respectively. A ratio of live:dead cells was calculated and compared to a standard curve to determine percent viability of the sample.

3.2.5 Contact Killing Studies

Contact killing studies were performed with PEMs adherent to PTFE substrates. Bacteria (0.5mL, OD_{600}=0.300) was seeded on empty 12-well TCPS plates and allowed to incubate at 37°C for 24h. PEMs, or clean PTFE (control), were added on top of the bacterial layer and incubated for 24h or 48h. At the designated time, the PEM was removed. LIVE/DEAD staining was performed on the underlying bacterial layer as described above.

3.2.6 Statistics

All bacteria testing was conducted with a sample size of $n \geq 3$. A two-tailed *t*-test ($\alpha < 0.05$) was used to determine significance between TCPS controls, unmodified PEMs and LL-37 modified PEMs. Bonferroni's correction was applied to adjust for multiple hypotheses testing.

3.3 Results

3.3.1 Bacterial Growth Profile

The growth profile for *E. coli* DH10B was constructed by monitoring OD_{600} values over time (**Figure 12**). The transition point between the log and stationary phases of growth was determined to be 6.53 ± 0.31h. Therefore an inoculation period of 5h was chosen to ensure that the bacteria would be in the log phase when seeded for further experiments.

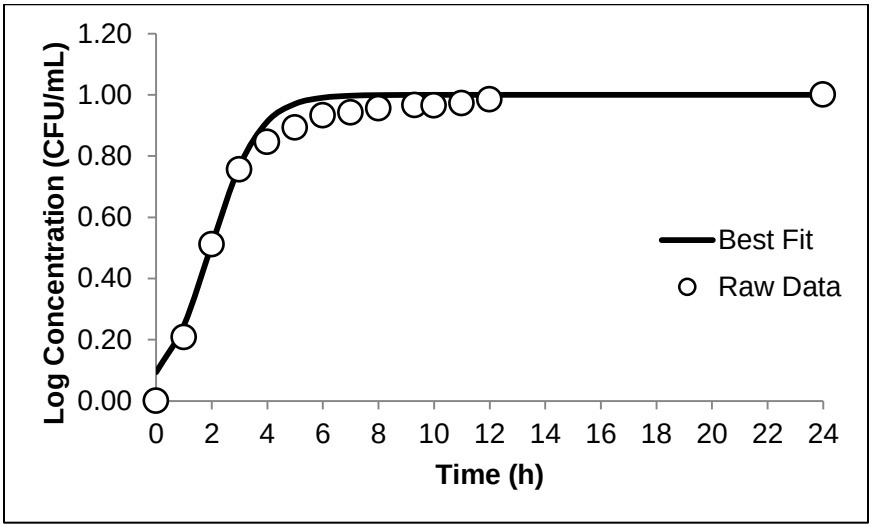

Figure 12: Growth profile for *E. coli* DH10B over 24h

3.3.2 Minimum Inhibitory Concentration

The MIC of LL-37 for the DH10B strain of *E. coli* was determined in LB. These studies were conducted by exposing bacteria to LL-37 in solution. The MIC for DH10B was found to be 8μM (**Figure 13**). Due to this MIC value, concentrations of 2μM (25% MIC), 8μM (MIC), and 16μM (200% MIC) were chosen to determine the effect LL-37 would have on *E. coli* when in contact with modified COL/HA PEMs.

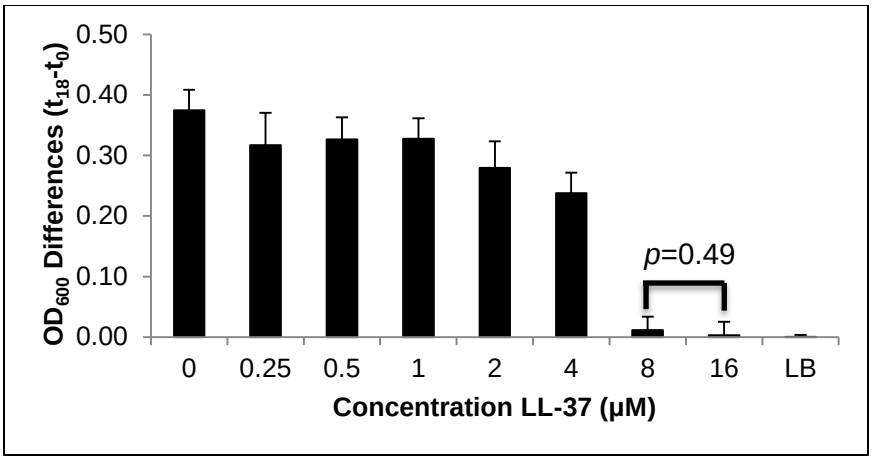

Figure 13: Difference in OD_{600} measurements for t=0h and t=18h to determine MIC of *E. coli* strain DH10B

3.3.3 Bacterial Adhesion Studies

LIVE/DEAD bacterial adhesion studies were performed in spent broth as well as on the surface of the PEM or TCPS control. Staining on the surface of the PEMs demonstrated a significant difference between the unmodified PEMs and TCPS; there was an approximate 2-fold decrease in live cell area coverage in the presence of unmodified PEMs (0μM) suggesting that these PEMs alone discourage bacterial adhesion (**Figure 14)**.

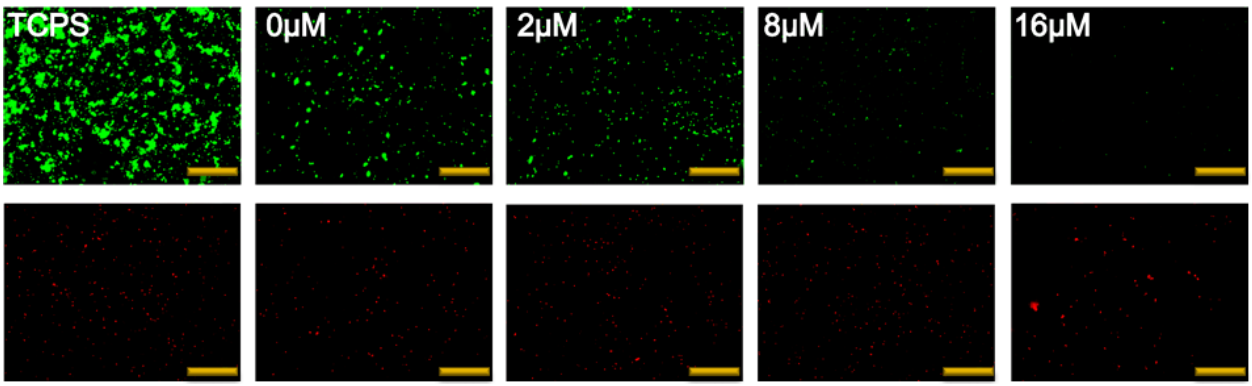

Figure 14: LIVE/DEAD staining of *E. coli* on physisorbed LL-37 modified PEMs for bacterial adhesion studies at 24h. (Magnification=20x, Scale bar=100μm, Green = live cells, Red = dead cells)

There was a decrease in the surface coverage of live bacteria between TCPS and unmodified PEMs. There was an additional decrease in the surface coverage of live bacteria coverage in contact with physisorbed LL-37 (**Figure 15A**). Interestingly, this decrease in live cell coverage

occurred at an LL-37 concentration of 2μM, a concentration that is significantly below that of the MIC (for *E. coli DH10B*). These results, suggest that the presence of the PEM can reduce the concentration of LL-37 required to prevent the adhesion of *E. coli*. Over a 48h period, the surface occupied by bacteria increased from 16% up to 23% in unmodified PEMs. In contrast, the LL-37 modified films exhibited no change (statistically insignificant) in bacterial coverage.

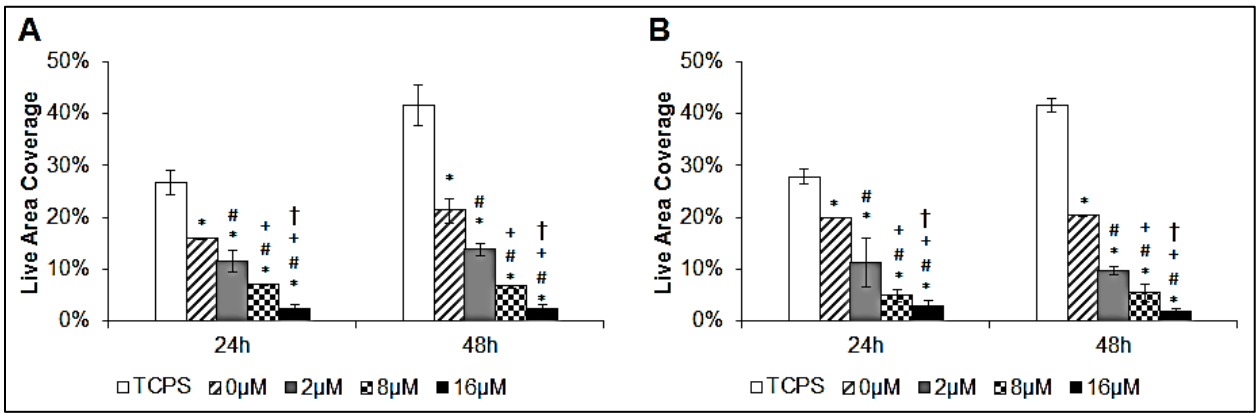

Figure 15: Live bacteria %area coverage over time on (A) physisorbed and (B) immobilized LL-37 modified and unmodified PEMs and TCPS controls for bacterial adhesion on HA ending side of PEM. (n≥6) Significance compared to TCPS controls (*), 0μM (#), 2μM (+), 8μM (†) (p<0.05).

Bacterial adhesion tests were conducted on the HA and COL ending sides of the PEMs. The HA side showed statistically lower adhesion compared to COL for all LL-37 concentrations at 24h (**Table 4**). These values, along with the previous zeta potential studies, influenced our choice to run the remainder of immobilized tests on the HA side of PEMs.

Table 4: Live %area coverage on HA and COL sides of physisorbed PEMs for bacterial adhesion at 24h and 48h (n≥6)

Condition	HA (24h)	COL(24h)	HA (48h)	COL (48h)
TCPS	26.7 ± 2.3	26.6 ± 10.4	41.7 ± 3.8	45.2 ± 10.4
0μM	15.9 ± 0.1	29.9 ± 6.9	21.3 ± 2.4	24.2 ± 11.5
2μM	11.5 ± 2.1	24.3 ± 4.3	13.8 ± 1.2	15.9 ± 4.9
8μM	6.9 ± 0.2	13.2 ± 4.2	6.5 ± 0.3	10.2 ± 7.1
16μM	2.3 ± 1.0	7.1 ± 3.2	2.3 ± 0.9	3.3 ± 0.3

Similar to the trends seen in the physisorbed films, the surface occupied by bacteria on immobilized PEMs was lower compared to TCPS and unmodified controls (**Table 5, Figure**

15B, 16). LL-37 modified PEMs showed a concentration dependent decrease in live cell coverage with 16μM films exhibiting approximately 2% live bacteria coverage. There was no significant increase in bacterial coverage between 24h and 48h on the modified films.

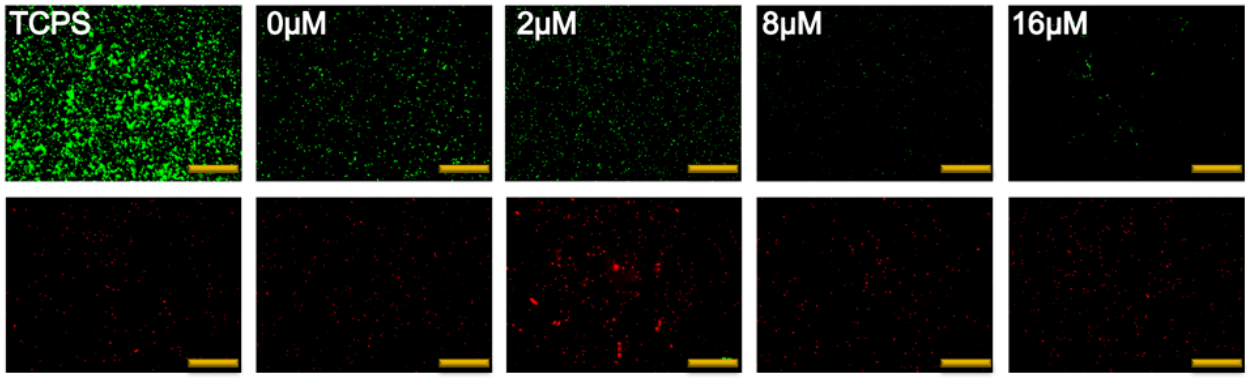

Figure 16: LIVE/DEAD staining of *E. coli* on immobilized LL-37 modified PEMs for bacterial adhesion studies at 24h. (Magnification=20x, Scale bar=100μm, Green = live cells, Red = dead cells)

Table 5: Live %area coverage on HA side of immobilized PEMs for bacterial adhesion at 24h and 48h (n≥6)

Condition	24h	48h
TCPS	27.8 ± 1.4	41.6 ± 1.4
0μM	19.8 ± 0.0	20.2 ± 0.0
2μM	11.2 ± 4.7	9.7 ± 0.8
8μM	4.8 ± 1.2	5.4 ± 1.8
16μM	2.9 ± 1.0	1.8 ± 0.5

There was no significant difference between the LL-37 concentrations on immobilized and physisorbed PEMS for bacterial adhesion. While the absolute average values for the immobilized films are consistently lower than the physisorbed, the standard deviations for all conditions result in non-significant p-values (p>0.05).

The surface area covered by dead bacteria (measured as a percentage) remained relatively constant over all conditions on the surface of the PEM/TCPS (<5%, **Table 6**). Dead cells lift off of the PEM/TCPS surface and enter the surrounding media. Therefore we investigated the number and viability of bacterial cells in the spent medium.

Table 6: Dead cell area coverage (%) for physisorbed and immobilized PEM bacterial adhesion studies at 24h and 48h (*n*≥6)

Condition	24h		48h	
	Physisorbed	*Immobilized*	*Physisorbed*	*Immobilized*
TCPS	2.5 ± 0.8	1.3 ± 0.1	5.4 ± 0.7	2.4 ± 0.7
0μM	1.6 ± 0.4	1.2 ± 0.7	3.7 ± 1.4	1.6 ± 0.8
2μM	3.1 ± 1.4	0.6 ± 0.4	2.3 ± 0.9	0.6 ± 0.1
8μM	1.1 ± 0.4	0.4 ± 0.0	1.5 ± 0.8	0.9 ± 0.4
16μM	0.5 ± 0.3	0.4 ± 0.1	1.2 ± 0.6	0.5 ± 0.0

The number of live cells in the broth was calculated based on OD_{600} and LIVE/DEAD staining (**Figure 17A**). At 24h, all PEM-based cultures exhibited fewer live cells in solution than TCPS controls. There was no significant change in live cells based on LL-37 concentration. Based on our release profile, for physisorbed PEMs <20% of the LL-37 is released into the broth by 24h; therefore, the dilute LL-37 concentration may not have a significant effect on bacterial viability in the broth.

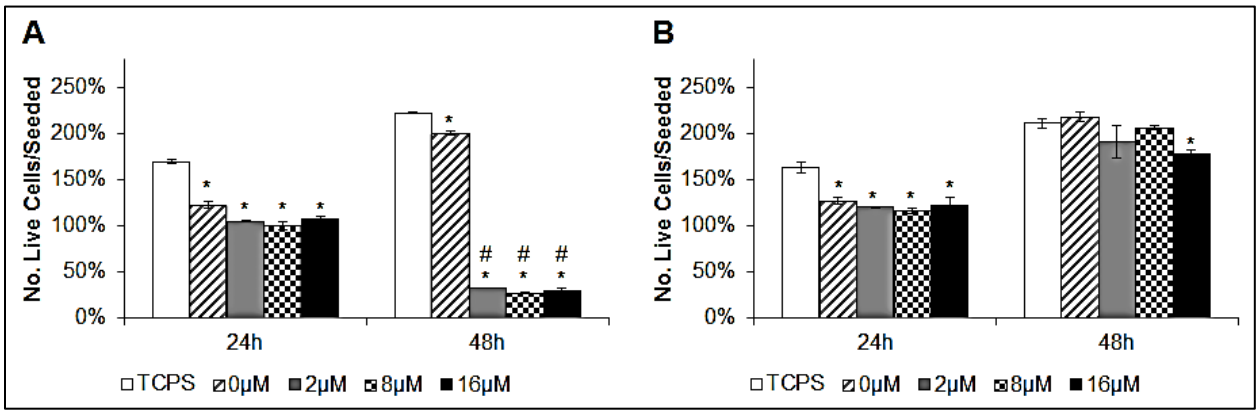

Figure 17: Live *E. coli*initial seeded density over time in broth from (A) physisorbed and (B) immobilized LL-37 modified and unmodified PEMs and TCPS controls for bacterial adhesion on HA ending side of PEM. (*n*≥3) Significance compared to TCPS controls (*), 0μM (#), 2μM (+), 8μM (†) (*p*<0.05)

At the end of 24h the PEMs were rinsed and the spent broth was replaced with fresh LB. In this manner, bacteria present in solution were removed leaving only the cells on the surface of the PEMs or the TCPS to repopulate the media. At 48h we saw a decrease from 100% live/seeded bacteria to approximately 30% for all physisorbed LL-37 modified conditions while the TCPS and unmodified films exhibited a 50% increase in live bacteria.

Broth values for bacteria in contact with immobilized films mimicked the values obtained at 24h for physisorbed PEMs (**Figure 17B**). In contrast, the number of live cells doubled by 48h. Based

on the release profile, LL-37 is not being released into the surrounding media to kill planktonic bacteria. Thus, any live planktonic cells would have the time to proliferate.

3.3.4 Contact Killing Studies

PEMs were modified with LL-37. These films were placed above a culture of *E. coli*. After 24h and 48h, the PEMs were removed and the underlying cultures were stained with LIVE/DEAD solutions and imaged. Unlike the bacterial adhesion studies, the unmodified PEMs did not exhibit a significant decrease in the surface coverage of live bacteria when compared to the TCPS samples (**Figure 18**).

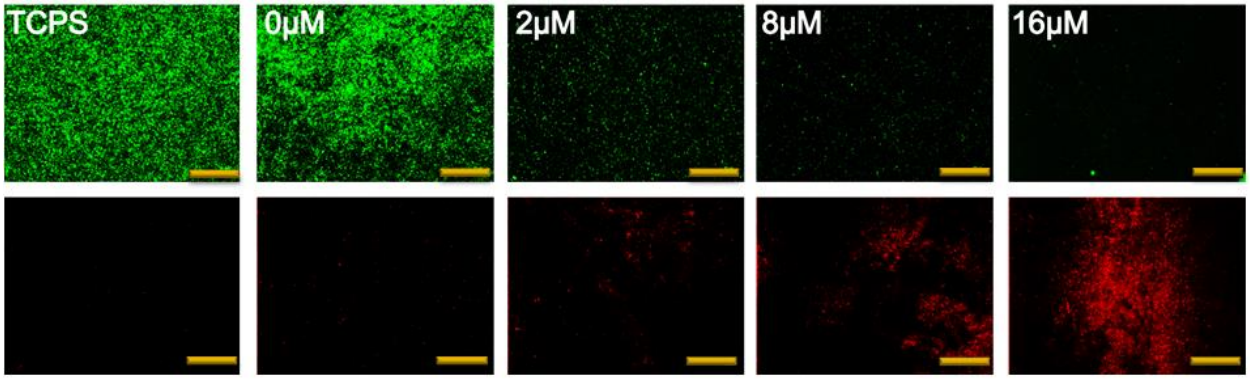

Figure 18: LIVE/DEAD staining of *E. coli* on physisorbed LL-37 modified PEMs for contact killing studies at 24h. (Magnification=20x, Scale bar=100μm, Green = live cells, Red = dead cells)

For the physisorbed films, the 8μM and 16μM modified films showed significant decreases in the surface coverage by bacteria compared to the TCPS and unmodified controls (**Figure 18A**). The 16μM films also exhibited statistically lower live cell coverage than the 2μM and 8μM PEMs. These findings indicate that the concentration of the LL-37 is an important factor for contact killing especially over time a 48h time period.

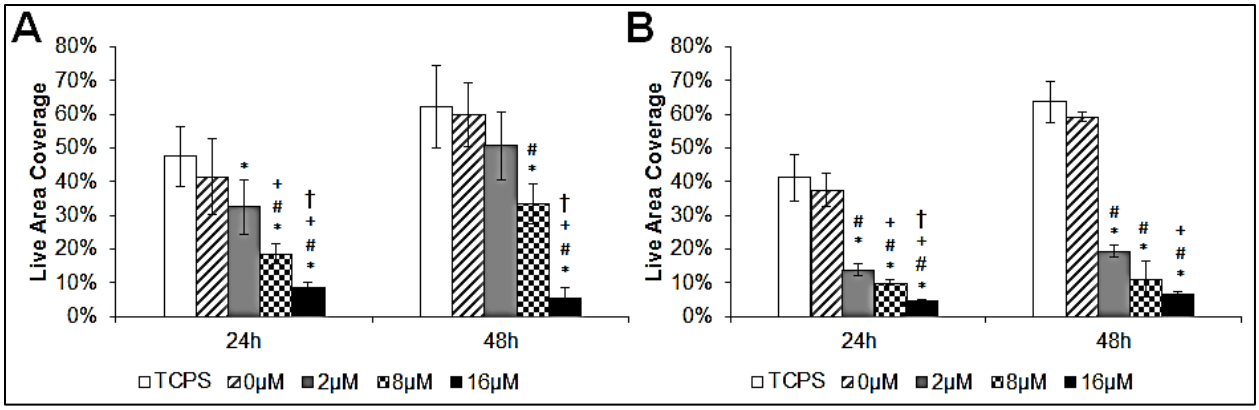

Figure 19: Live bacteria %area coverage over time on (A) physisorbed and (B) immobilized LL-37 modified and unmodified PEMs and TCPS controls for contact killing on HA ending side of PEM. ($n \geq 3$) Significance compared to TCPS controls (*), 0μM (#), 2μM (+), 8μM (†) ($p<0.05$).

Immobilized LL-37-PEMs exhibited bacterial areas that were statistically lower than the TCPS and unmodified controls (**Figure 19B, 20**). All modified PEMs exhibited live bacteria coverage <20% over 48h. The 16μM films exhibited the lowest coverage at approximately 5%.

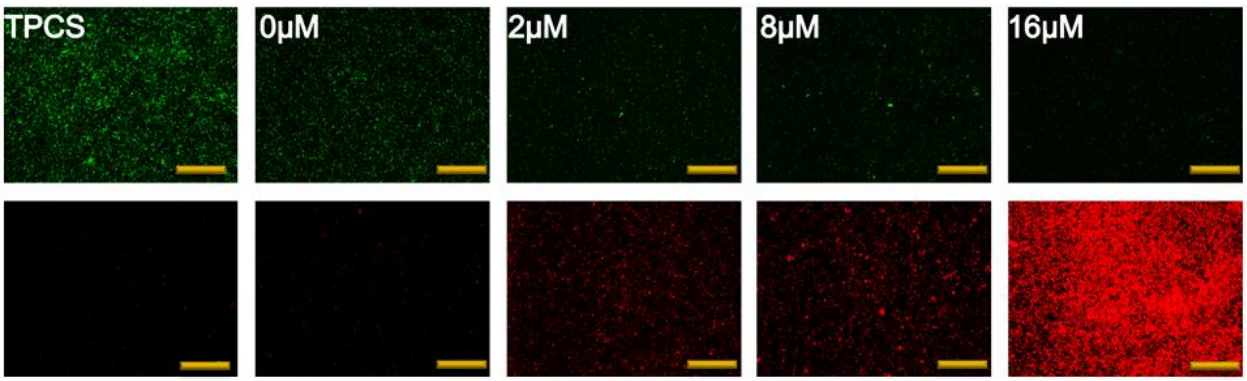

Figure 20: LIVE/DEAD staining of *E. coli* on immobilized LL-37 modified PEMs for contact killing studies at 24h. (Magnification=20x, Scale bar=100μm, Green = live cells, Red = dead cells)

The LL-37 immobilized films show much lower coverage than their physisorbed counterparts. The values of surface coverage by live bacteria are significantly less on the 2μM and 8μM films when immobilized compared to physisorbed. The presence of LL-37 on the surface of the PEM can be contributing to this effect. The release of LL-37 into the surrounding medium over time from the physisorbed films is likely contributing to their lower performance, however, such PEMs appear to better control the numbers of live bacteria in the surrounding environment. The 16μM

physisorbed films exhibit the same percent of surface-adherent bacteria. We attribute this result to the higher concentration of the input LL-37 solution.

3.4 Discussion

E. coli strain DH10B was placed in contact with LL-37 modified PEMs. These PEMs were modified through physisorption or covalent linking of 2μM, 8μM and 16μM LL-37. The range of LL-37 was based on corresponding values for MIC. While the MIC for DH10B was found to be 8μM in solution, we wanted to determine if the presence of LL-37 on a PEM could deter bacterial adhesion and growth. PEMs were tested in the presence of bacteria in two ways: a) bacterial adhesion and b) contact killing. Bacterial adhesion tests were used to determine the ability of an AMP-modified PEM to prevent bacterial adhesion and subsequent growth. In contrast, contact killing studies were used to establish the modified PEM's ability to neutralize an existing culture.

Bacterial adhesion tests demonstrated that even in the absence of an AMP, COL/HA PEMs were able to inhibit bacterial adhesion. This antimicrobial effect can be attributed to the negative zeta potential on the surface of the COL/HA PEM which could deter the adhesion of negatively charged bacteria. In addition, the hydrated state of the films can result in a thermodynamically unfavorable environment for cell attachment and spreading [293-295]. Lastly, the components of the films, COL and HA, result in a similar cationic and amphipathic makeup as an AMP [296, 297]. The cationic and hydrophobic components could interact with bacterial membranes and further discourage adhesion on the PEM surface. Additional studies in the future will provide deeper insights into the mechanisms by which COL/HA PEMs exhibit antimicrobial properties.

The negative charge of the unmodified PEMs themselves can repel some bacteria from adhering. However, with an increase in zeta potential through the addition of LL-37, we still see a decrease in adhesion. This would indicate that the addition of LL-37 can deter adhesion even without significant negative potential. Instead, the less negative character of the LL-37 modified PEM is attractive to the negatively charged bacteria. The LL-37 on the PEMs can then interact with the membrane surface.

LL-37 functions through the toroidal pore mechanism. Groups of LL-37 α-helices come together on the surface of bacteria to form pores. This would indicate that higher concentrations of LL-37 could form more pores killing more bacteria. However, anti-biofilm activity has been seen at concentrations below the MIC (25% MIC; [223, 227]) indicating that 2μM can still deter adhesion. We observed this result with the COL/HA PEM cultures.

The MIC by definition is the minimum *inhibitory* concentration, not bactericidal concentration. While 8μM may deter the growth of more bacteria, it is not as potent in killing as many bacteria as an AMP concentration of 16μM. Since 16μM is 200% of the MIC, there is a greater concentration of LL-37 to simultaneously reduce adhesion and promote bacterial death.

We also investigated the concentrations of live bacteria in the spent broth. There were significant differences between the bacterial broth from LL-37 physisorbed and immobilized film cultures. We observed that when LL-37 was physisorbed to PEMs, the resulting bacterial concentration was 160% percent lower than their corresponding immobilized counterparts. This difference can be attributed to the LL-37 release from the surface of the PEMs. By 48h approximately 60% of the input LL-37 concentration is released into the surrounding broth from physisorbed PEMs whereas there was no detectable LL-37 released from the immobilized films. This lack of release resulted in uninhibited planktonic bacterial growth.

Results obtained from contact killing demonstrated that AMP-modified PEMs can neutralize bacteria that are adherent on a plastic surface. Under these experimental conditions, immobilized LL-37 PEMs exhibited consistently lower cell coverage over the 48h period. This is attributed to the lack of release of the AMP when it is covalently linked to a COL/HA PEM. These data would suggest that to neutralize adherent bacteria a covalently linked LL-37 modified PEM would result in lower live cell coverage over time.

3.5 Conclusion

We have demonstrated that COL/HA PEMs alone exhibit some antimicrobial properties. Although, the exact mechanisms are not known, we hypothesize that a combination of protein charge, hydration and surface properties play a role. Our results indicate that when LL-37 is physisorbed on a COL/HA PEM it serves to prevent bacterial adhesion on the substrate as well as to kill pathogens in the surrounding environment. In contrast, immobilizing LL-37 resulted in better results when placed in contact with bacteria that had been growing on a plastic surface. In the future, incorporating LL-37 in PEMs via simultaneous physisorption and covalent linking may result in completely neutralizing bacteria on surfaces as well as in the surrounding aqueous environment.

4 LL-37 Modified Films in Contact with Hepatic Cells

Research Aims:

4) Culture hepatic cells on LL-37 modified PEMs.

5) Co-culture hepatic cells and bacteria on LL-37 modified PEMs

4.1 Introduction

The liver is continuously exposed to toxins and pathogens due to its connection with the GI tract and its detoxification and metabolic functionalities [227, 228]. The presence of immune cells in the liver sinusoid as well as the flow of blood through the liver work together to prevent hepatic infection [230, 231]. However, when the liver is damaged due to trauma or disease, infections can become more severe. Therefore, it is crucial to study hepatic infections.

The Rajagopalan research group has designed a liver model which combines hepatic cells separated by a polymeric Space of Disse [47, 48, 98]. It would be beneficial to modify this polymeric interface, comprised of a COL/HA PEM with an antimicrobial agent, such as LL-37, to study hepatic cells in an infected environment. While it is necessary to determine the bactericidal capabilities of LL-37, it is also important to determine the selectivity of the peptide so that this peptide does not kill or reduce the phenotypic functions of hepatic cells.

LL-37 is naturally present in the human body at constitutively expressed low levels 0.2-1μM in serum. Increasing concentrations of LL-37 aids in microbial neutralization and wound healing, but excessive LL-37 concentrations can do damage to host cells [222]. LL-37 has been shown

to promote apoptosis of epithelial cells, smooth muscle cells, and T-cells at concentrations between 6-11μM and has been shown to be cytotoxic above 13μM [223, 290]. LL-37 has also been found at elevated levels in patients with skin disorders such as psoriasis (200-500μM) [175, 187, 195, 205] as well as individuals with liver disease like hepatitis C (2-fold higher serum levels than healthy individuals) [298, 299].

In an article by Park *et al*., the AMP melittin, a component of bee venom, was used to deter the effect of LPS on hepatic cells [300]. Mice were administered LPS in the presence and absence of melittin. Mice treated with melittin exhibited lower levels of inflammatory cytokines in serum, a decrease in hepatocyte apoptosis, and an inhibition in the expression of caspase-3 than untreated mice. These results indicated that melittin had a protective effect against hepatic infection [300, 301]. While this AMP functioned against LPS, this xenogeneic peptide could cause adverse health effects in humans, especially at high concentrations. Therefore, an AMP of human origin was desired for experiments which would be used to study hepatic infection. The human cathelicidin LL-37 was chosen.

Similar to Park *et al*., Suzuki *et al.* performed an *in vivo* study wherein they injected mice with LPS and then studied the response of this toxin in the presence and absence of LL-37 (50μg LL-37/mouse) [174]. LPS alone showed significant hepatocyte and LSEC apoptosis while injections coupled with LL-37 exhibited 3-fold less hepatic death. Likewise, in Cirioni *et al.*, rats were injected with LPS or *E. coli* along with various antibiotics such as polymyxin B, imipenem, and piperacillin. LL-37 was also administered at a dose of 1mg/kg [302]. Levels of inflammatory cytokines (such as IL-6 and TNF-α) and bacterial counts in the blood, spleen and liver were measured. Rats treated with LL-37 showed the lowest lethality (25% verses 100%) when infected with *E. coli* and a significant reduction in bacterial counts in the liver compared to

controls (10^5 CFU/mL compared to 10^7 CFU/mL). These studies investigated *in vivo* effects of LL-37 on bacteria in the liver.

There has been significant research conducted using hepatic cells in contact with PEMs. The adhesion and function of hepatic cells could be modified by altering PE chemistry, assembly pH, or modification of the PEM surface [24, 28, 30]. The Rajagopalan group has previously shown enhanced hepatic function when PEMs were utilized to imitate the Space of Disse to mimic the 3D stratified structure of a liver sinusoid [47, 48, 54, 98]. Nonetheless, none of these PEM based hepatic studies focused on liver function in the presence of an infection.

As mentioned in **Chapter 1**, there has been significant work using PEMs impregnated or coated with antibiotics and AMPs to deter microbial infections. However, the majority of these studies are tested *in vitro* against fibroblasts, cancer cells, or in whole animal *in vivo* models [178, 186, 237, 240, 254]. Hepatic infections are a serious problem, especially in those patients already suffering from liver disease. To the best of our knowledge, there have been no studies that have combined AMPs and PEMs to study hepatic infections.

In this work we investigated *in vitro* cultures of primary hepatocytes in contact with physisorbed and immobilized LL-37 modified PEMs at concentrations between 0-16μM. We also studied the response of hepatocyte and *E. coli* co-cultures when in contact with these thin films to determine the selectivity and protective effects of LL-37 in contact with mammalian and bacterial cells.

4.2 Materials and Methods

Dulbecco's modified Eagle medium (DMEM), PBS, and penicillin-streptomycin were purchased from Invitrogen Life Technologies (Carlsbad, CA). Glucagon, calcium chloride, hydrocortisone, sodium dodecyl sulfate (SDS), glutaraldehyde, calf thymus DNA, Hoechst 33258 pentahydrate-bis-benzimide dye, and collagenase type IV were obtained from Sigma-Aldrich (St. Louis, MO). All other chemicals were ordered from Fisher Scientific (Pittsburgh, PA) unless otherwise stated.

4.2.1 Isolation and Culture of Rat Hepatocytes

Primary hepatocytes were isolated from female Lewis rats (175-200g; Harlan Laboratories, Indianapolis, IN) using a two-step *in situ* collagenase perfusion technique [48, 270]. Surgical protocols and animal care practices followed Virginia Tech's Institutional Animal Care and Use Committee requirements. After surgery and isolation, viabilities (typically ≥97%) were determined via trypan blue exclusion. A typical surgery resulted in 150-200 million hepatocytes.

For HM controls, cells were cultured on collagen gels. COL (0.25mL, 1.1mg/mL) was added to each well and gelation was induced by incubating the collagen solution at 37°C for approximately 45min. For LL-37 modified PEM samples (physisorbed and immobilized), detached PEMs were placed in wells and held down with stainless steel washers and hydrated. The PEMs were sterilized by exposure to germicidal UV for 60min. Hepatocytes were seeded at a density of 0.6×10^6 cells/well in 0.5mL hepatocyte-specific medium [48, 98].

Cultures were maintained in hepatocyte-specific media containing DMEM supplemented with 10% (v/v) heat-inactivated fetal bovine serum, 100 U/ml penicillin-streptomycin, 0.5 IU/ml insulin, 14.3 ng/ml glucagon, 20 ng/mL epidermal growth factor and 7.6 µg/ml hydrocortisone.

Spent medium was collected every 24h and stored at -80°C until analysis. Cultures were maintained in a 10% CO_2, 37°C humidified incubator.

4.2.2 Assaying for DNA

At the end of the culture period, COL gels and PEMs were digested with 0.1 w/v% collagenase and 2.5 v/v% trypsin, respectively, to allow for the release of hepatocytes. Released cells were lysed in a 0.1% SDS solution. Lysates were treated with a light sensitive DNA-binding dye (Hoechst 33258). Fluorescent intensities were measured using a SpectraMax M2 plate reader (Ex: 355nm, Em: 460nm). Absorbance values were converted to DNA concentrations via comparison to a calf thymus DNA standard curve.

4.2.3 Urea Secretion

Hepatocyte function was determined by measuring secreted urea in spent medium. Media samples were placed in a 96 well plate in triplicate along with standards generated from diluted urea in hepatocyte media. Urea Nitrogen (BUN) test kit solutions were used according to manufacturer's instructions (Stanbio Laboratory, Boerne TX). Plates were sealed with acetate plate sealers and incubated in a 60°C water bath for 90min. Plates were then removed from the water and placed on ice for 10min before reading on a SpectraMax M2 microplate reader with an absorbance dual endpoint ranging from 520-650nm.

4.2.4 Albumin Secretion

Albumin concentrations were determined from spent hepatocyte media. An enzyme-linked immunosorbent assay (ELISA) was conducted using a polyclonal anti-rat albumin antibody (Cappel Laboratories, Cochranville, PA) [54]. The albumin concentration was measured dual

endpoints from 490-650nm, using a SpectraMax M2 microplate reader. Standard curves were generated using purified rat albumin in hepatocyte culture medium.

4.2.5 Imaging Hepatocytes for Albumin by Immunostaining

Hepatocyte cultures were fixed with 2% (w/v) glutaraldehyde in 1XPBS. The cultures were then exposed to 0.1% (w/v) sodium borohydride to prevent auto-fluorescence. Cultures were sequentially exposed to 0.1% (v/v) Triton X-100 in 1XPBS and a 1% (w/v) bovine serum albumin (BSA/PBS) blocking suspension with rabbit serum to reduce non-specific binding. Cultures were incubated with a sheep-anti rat FITC-conjugated albumin antibody (ab53435; Abcam, MA). Cells were maintained in 25% (v/v) glycerol and stored at 4°C until imaging using a green filter on a Nikon Eclipse TE2000-U microscope (Nikon, Linthicum MD). Mean fluorescent intensities were used to determine the presence of albumin in the cultures.

4.2.6 Hepatocyte/*E. coli* Co-cultures

Hepatocytes were seeded on PEMs and COL gels as described above. They were maintained in hepatocyte medium without the antibiotics penicillin and streptomycin. Culture plates were incubated at 37°C with 10% CO_2. After 5h, *E. coli* were added to the cell cultures at 1:1 and 2:1 ratios of hepatocytes:bacteria. Bacteria were incubated with hepatocytes for 1h; the media was collected and 1mL fresh hepatocyte medium was added. Media was collected after an additional 6h and 12h (**Figure 21**). Phase images were taken between media collections to determine morphological changes in the co-cultures. Secreted albumin and urea concentrations in spent medium were quantified as described above. OD_{600} values from the spent medium were also determined using a SpectraMax M2 plate reader.

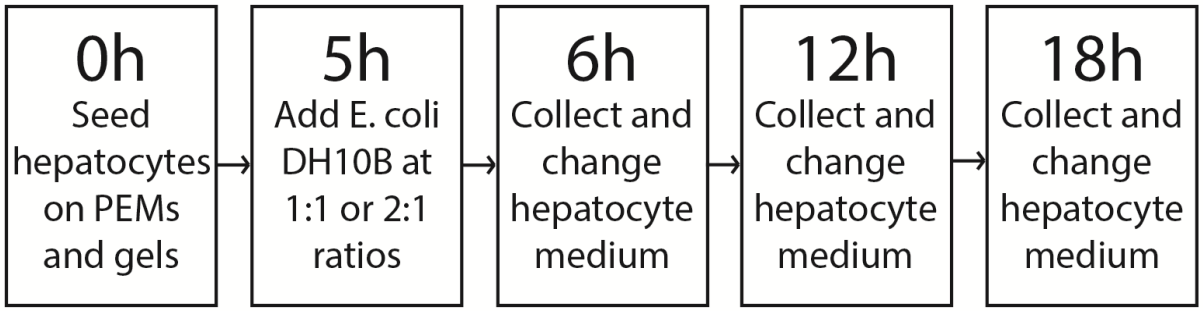

Figure 21: Timeline for hepatocyte/bacteria co-cultures

For the hepatocyte/bacteria co-culture conditions, we have used the following notation. An "**HM**" and "**P**" refer to hepatocytes seeded on a COL gel and a PEM, respectively. LL-37 concentrations of 0μM and 16μM are denoted "**0**" or "**16**". Physisorbed or covalently immobilized LL-37 on the PEM surface are abbreviated as "**Phys**" and "**Imm**", respectively. Ratios of hepatocytes:bacteria are denoted as "**1:1**" or "**2:1**". Therefore, a PEM with 16μM physisorbed LL-37 with a 2:1 hepatocyte:bacteria ratio is represented as **P/Phys/16/2:1**.

4.2.7 Statistics

All hepatocyte and co-culture testing was conducted with a sample size of n=3. A two-tailed t-test ($\alpha<0.05$) was used to determine significance between 2:1 and 1:1 hepatocyte:bacteria ratios.

4.3 Results

4.3.1 Hepatocyte Monolayers

Hepatocyte monocultures on COL gels and LL-37 modified PEMs were monitored over 5 days. Phase images were taken every 24h. On day 1 (24h after seeding), there were no significant morphological differences between culture conditions. By day 5 in contact with physisorbed and immobilized films, approximately 50% of the hepatocytes showed a rounded morphology on

0μM, 2μM and 8μM films compared to the >90% hepatocytes on the 16μM PEMs that exhibited an elongated fibroblast-like morphology (**Figure 22A,B**).

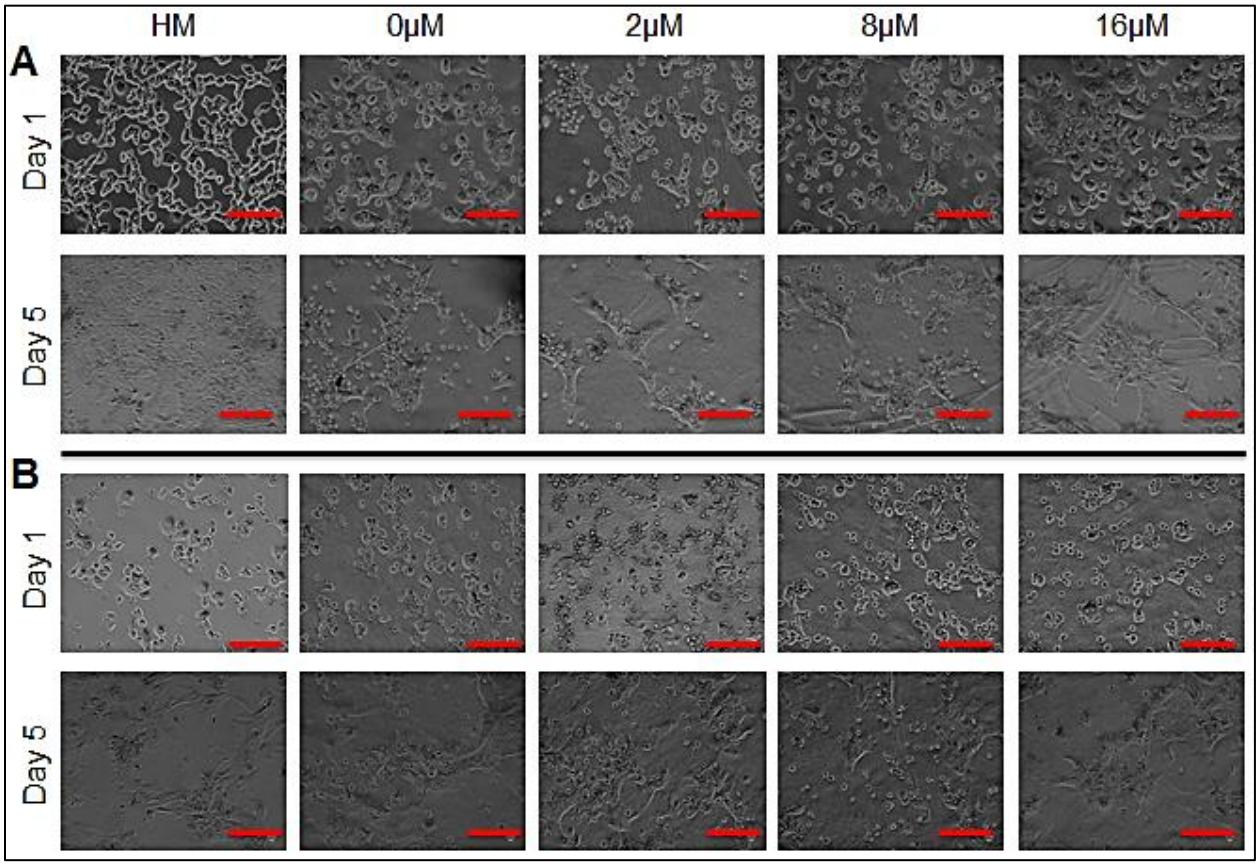

Figure 22: Phase images for hepatocytes on HM gel or (A) physisorbed and (B) immobilized LL-37 modified PEMs at day 1 and day 5 of culture. (Magnification = 10X, Scale bar = 200μm, *n*=3)

DNA content from hepatocytes was quantified after 5 days of culture (**Table 7**). All PEM samples exhibited similar DNA content. HM DNA values were suspect and will require future analysis.

Urea and albumin values were measured using spent medium samples (**Figure 23A,B**); these values were normalized to the number of hepatocytes seeded ($6x10^5$ cells). All urea values for physisorbed and immobilized PEM samples were within ±20% indicating that concentrations of LL-37 up to 16μM did not have a significant impact of urea levels on Day 2 (48h). A Day 2 time point was chosen to match the 48h bacterial culture periods in contact with LL-37 modified films.

Table 7: DNA content (µg DNA/mL) from hepatocytes on LL-37 physisorbed and immobilized films (*n*=3)

Condition	Physisorbed	Immobilized
HM	12.82 ± 1.27	6.59 ± 0.50
0µM	5.52 ± 2.19	5.23 ± 2.33
2µM	4.35 ± 2.51	5.46 ± 1.11
8µM	5.59 ± 1.62	5.20 ± 2.04
16µM	5.91 ± 1.58	5.30 ± 0.75

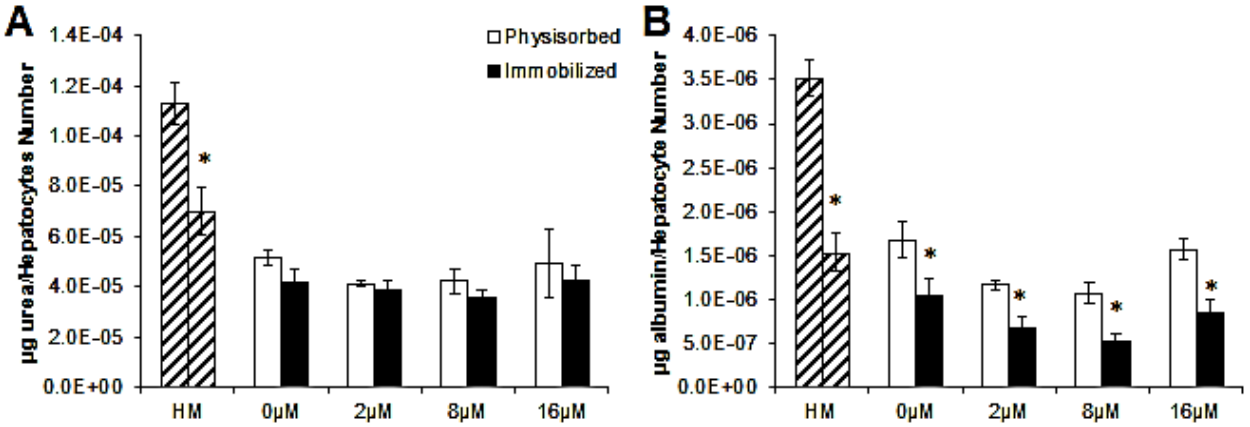

Figure 23: Secreted (A) urea and (B) albumin levels from hepatocyte monocultures after 48h for HM controls (striped) and physisorbed and immobilized PEMs normalized by the number of seeded hepatocytes. (*n*=3) Significance between physisorbed and immobilized films (*, *p*<0.05).

Albumin levels were measured using an ELISA assay as well as immunostaining. Albumin levels from the ELISA were consistently lower for LL-37 immobilized on PEMs compared to physisorbed. However, there was no significant difference between 2µM, 8µM or 16µM LL-37 indicating that the immobilization process and not the LL-37 alone may be the cause for the lower albumin secretion. Hepatocytes seeded on immobilized PEMs exhibited lower fluorescent intensities at 8µM and 16µM compared the physisorbed films when albumin immunostaining was performed (**Figure 24**). These differences in albumin quantification could be due to the technique used. An ELISA assay measures the total albumin secreted into the media from live and dead cells. Concentrations are determined by a color change in samples. In contrast, immunostaining detects cytoplasmic albumin.

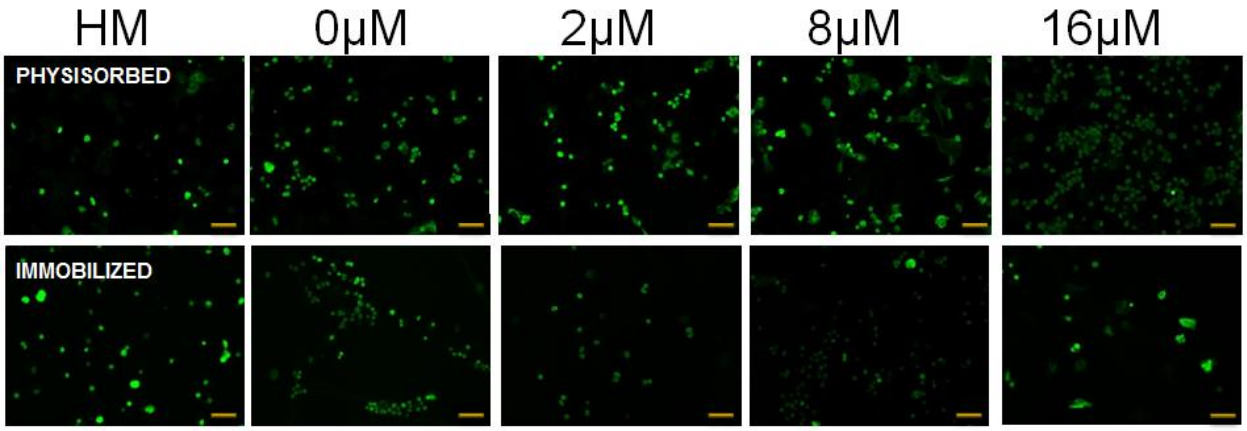

Figure 24: Albumin Immunostaining on LL-37 (A) physisorbed and (B) immobilized PEMs. (Magnification = 10x, Scale bar = 100μm, *n*=3)

Since the presence of LL-37 at concentrations up to 16μM did not cause any cytotoxic effects to the hepatocytes, we then investigated the addition of bacteria to these cultures.

4.3.2 Hepatocyte/*E. coli* Co-cultures

Hepatocyte/*E. coli* co-cultures were monitored over 18h. In this study, our goal was to determine the effect of LL-37 modified PEMs on the death or survival of bacteria and hepatocytes when cultured together. This experiment represented a static infected hepatic environment and serves as the initial set of experiments toward gaining a deeper understanding on how AMPs, bacteria, and hepatic cells mutually interact with each other. Please refer to **Figure 21** for a detailed timeline on the sequence of steps in these experiments. Levels of secreted albumin and urea were measured as well as OD_{600} measurements in the spent medium to determine the function of the hepatocytes and the presence of bacteria.

Co-cultures at t=6h exhibited statistically similar urea secretion values for all conditions regardless of hepatocyte:*E. coli* ratios. At t=12h, the urea values for hepatocytes on PEMs at a 2:1 hepatocyte:bacteria were statistically higher than 1:1 co-cultures (**Table 8, Figure 25**). These results indicate that urea secretion is dependent on the number of hepatocytes relative to

bacteria as well as the time point at which aliquots are obtained. In addition, urea levels on PEMs modified with 16μM LL-37 were higher for the 2:1 hepatocyte:*E. coli* ratio than unmodified PEMs. These data indicate that the presence of LL-37 has a protective effect on hepatocytes which is reflected by higher urea secretion.

Table 8: Hepatocyte:Bacteria co-culture urea secretion (μg urea/mL) in spent medium over time (un-normalized) (*n*=3)

Condition	T=6h	T=12h	T=18h
HM	19.86 ± 2.81	12.81 ± 2.41	10.51 ± 1.17
HM/1:1	15.97 ± 1.72	7.78 ± 2.12	4.27 ± 0.87
HM/2:1	17.21 ± 0.85	8.12 ± 0.69	6.43 ± 0.51
P/0/1:1	16.77 ± 0.96	5.81 ± 1.13	5.89 ± 1.53
P/0/2:1	20.12 ± 3.20	8.17 ± 0.69	5.70 ± 0.99
P/Phys/16/1:1	16.09 ± 1.82	6.50 ± 2.38	4.76 ± 1.82
P/Phys/16/2:1	18.76 ± 0.97	10.60 ± 1.18	12.74 ± 0.85
P/Imm/16/1:1	21.01 ± 2.31	4.93 ± 2.45	6.49 ± 1.17
P/Imm/16/2:1	17.30 ± 2.86	12.15 ± 1.25	5.52 ± 3.15

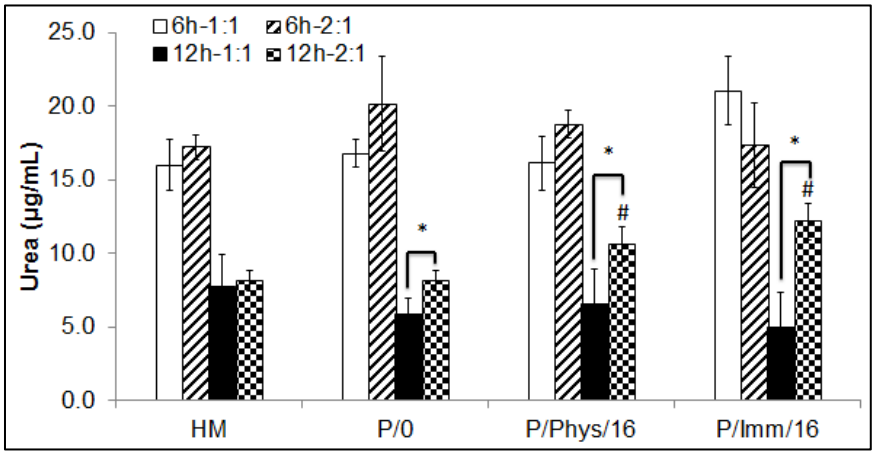

Figure 25: Secreted urea from hepatocyte/bacteria co-cultures with 1:1 and 2:1 hepatocyte:*E.coli* ratios at 12h. Significant difference between 1:1 and 2:1 ratios (*), compared to P/0 (#, *p*<0.05). (*n*=3)

These trends did not hold at the 18h time point. Unfortunately, by 18h, there was significant contamination of the hepatocyte media indicated by a color change from red to yellow. Visual inspection of the hepatocytes showed >95% cell death for all samples except control HMs without bacteria (**Figure 26**). However, the P/Phys/16/2:1 condition did exhibit statistically equivalent urea secretion to HM controls at 18h. This would indicate that urea function can be protected even at later time points in the presence of physisorbed LL-37 in less concentrated

bacterial cultures. Since LL-37 can be released from physisorbed films, the AMP can interact with the planktonic bacteria to decrease the impact of contamination on the hepatocytes.

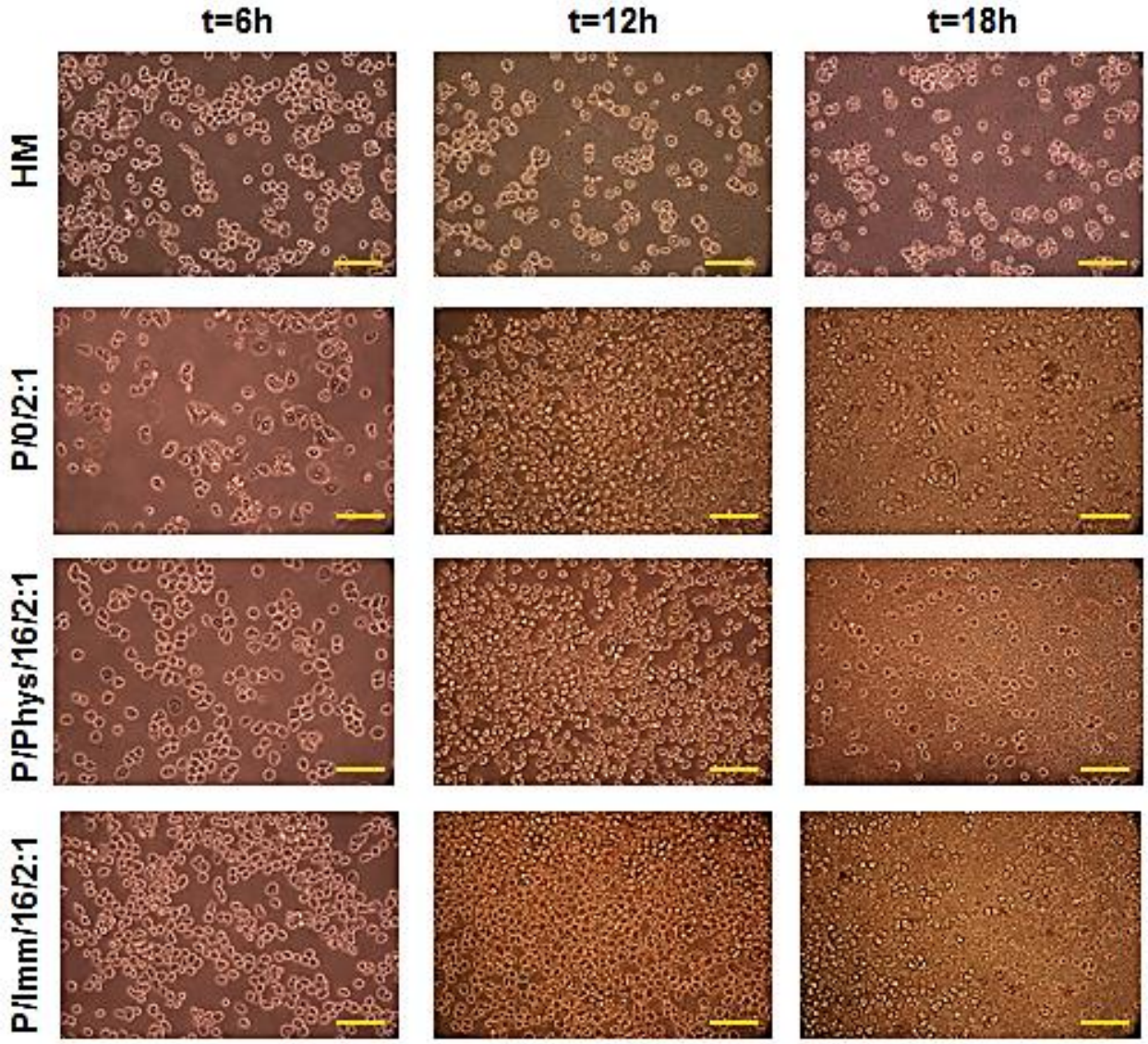

Figure 26: Images of hepatocyte/bacteria co-cultures at 6h, 12h, and 18h after hepatocyte seeding for 2:1 hepatocyte:*E. coli* ratio and HM controls. (Magnification = 20x, Scale bar = 200µm, *n*=3)

Albumin secretion was also monitored over the co-culture period. The albumin values at 6h and 18h were not significant from one another (**Table 9**). High albumin values at 6h can be attributed in part to the smaller volume of media in contact with cells for the first 6h (0.5mL) after seeding verses 1mL after every subsequent media change. While albumin concentrations

dropped at 12h there were significantly higher secretions for 2:1 ratios compared to 1:1, similar to the previous urea measurements (**Figure 27A**).

Table 9: Hepatocyte:Bacteria co-culture albumin secretion (µg urea/mL) in spent medium over time (un-normalized) (*n*=3)

Condition	T=6h	T=12h	T=18h
HM	0.79 ± 0.09	0.11 ± 0.02	0.08 ± 0.03
HM/1:1	0.88 ± 0.07	0.07 ± 0.01	0.04 ± 0.01
HM/2:1	0.78 ± 0.02	0.09 ± 0.02	0.05 ± 0.01
P/0/1:1	0.96 ± 0.02	0.12 ± 0.02	0.04 ± 0.01
P/0/2:1	0.68 ± 0.01	0.10 ± 0.03	0.03 ± 0.00
P/Phys/16/1:1	0.95 ± 0.08	0.08 ± 0.02	0.03 ± 0.00
P/Phys/16/2:1	0.91 ± 0.05	0.15 ± 0.02	0.03 ± 0.00
P/Imm/16/1:1	0.82 ± 0.04	0.06 ± 0.02	0.03 ± 0.00
P/Imm/16/2:1	0.77 ± 0.06	0.17 ± 0.03	0.02 ± 0.01

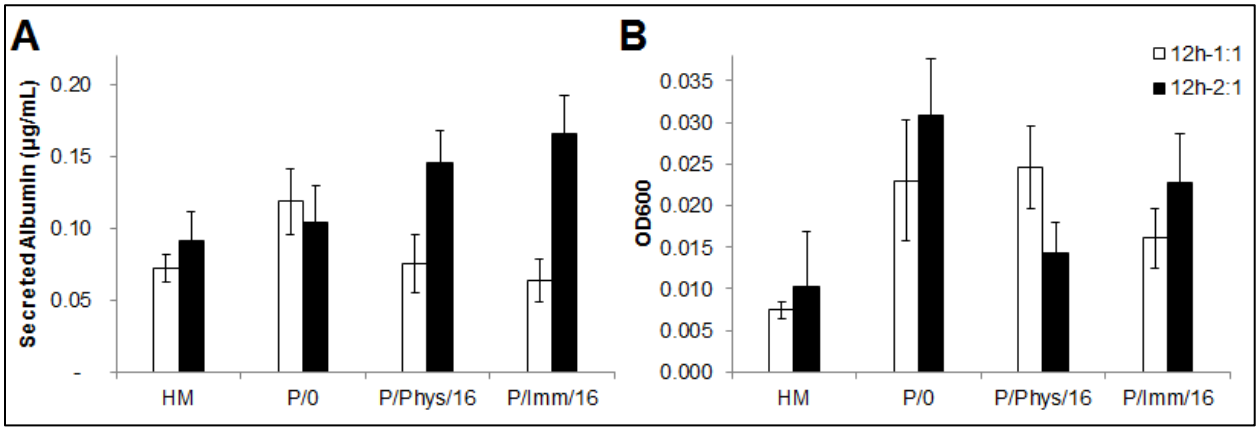

Figure 27: (A) Secreted albumin levels and (B) OD_{600} measurements from spent medium at 12h for 1:1 and 2:1 hepatocyte:bacteria ratios. (*n*=3)

OD_{600} measurements were also taken on the spent media to determine the number of cells in the medium. OD_{600} values were highest at t=6h. At this time point planktonic bacteria were removed from wells (after the 1h incubation with hepatocytes) (**Table 10**). From these measurements we cannot determine if the cells in the culture medium are hepatocytes or planktonic bacteria. Further studies will enable a precise identification of mammalian and bacterial cell populations in the culture medium. However, these data suggest that the number of cells floating in the medium from LL-37 modified PEM cultures resulted in lower OD_{600} values

(**Figure 27B**). The values were lowest for the physisorbed films at a 2:1 ratio compared to the immobilized PEMs which mimics the broth studies previously conducted on bacteria alone.

Table 10: Hepatocyte:Bacteria co-culture OD_{600} in spent medium over time (*n*=3)

Condition	T=6h	T=12h	T=18h
HM	0.33 ± 0.06	0.02 ± 0.00	0.01 ± 0.00
HM/1:1	0.28 ± 0.09	0.01 ± 0.00	0.07 ± 0.01
HM/2:1	0.34 ± 0.06	0.01 ± 0.01	0.05 ± 0.01
P/0/1:1	0.24 ± 0.07	0.02 ± 0.01	0.12 ± 0.01
P/0/2:1	0.22 ± 0.05	0.03 ± 0.01	0.11 ± 0.02
P/Phys/16/1:1	0.18 ± 0.00	0.02 ± 0.00	0.09 ± 0.01
P/Phys/16/2:1	0.25 ± 0.02	0.01 ± 0.01	0.12 ± 0.05
P/Imm/16/1:1	0.25 ± 0.05	0.02 ± 0.00	0.10 ± 0.01
P/Imm/16/2:1	0.19 ± 0.03	0.04 ± 0.02	0.10 ± 0.00

4.4 Discussion

Primary rat hepatocytes were cultured on LL-37 PEMs. In previous chapters, we have reported that AMP-modified PEMs can neutralize bacteria. Herein, we have demonstrated that up to an input concentration of 16μM, LL-37 does not exhibit cytotoxic effects on hepatocytes.

In hepatocyte monocultures, hepatocytes cultured on LL-37 physisorbed films exhibited higher albumin secretion than cells on immobilized PEMs. The immobilization process using carbodiimide chemistry may alter the surface of the PEM. If the covalent linking process can interact with the free HA and COL molecules in the PEM, the stiffness could be increased [271]. Stiffness of underlying substrates has been shown to affect hepatocyte function. Earlier reports in the literature have shown that hepatocytes on stiffer substrates exhibit better adhesion but lower functional capacilities such as albumin secretion [28].

Physisorbed films release LL-37 into the surrounding medium over time while immobilized films show no detectable release. For these hepatocyte specific studies, the physisorbed films represent a culture in which LL-37 is being slowly removed from the liver, as would be

representative of LL-37 or other AMPs circulating through this organ [174, 223]. In the immobilized LL-37 PEM cultures, hepatocytes are constantly exposed to LL-37. Such a culture may better emulate an injured or infected liver in which AMP levels would be highly expressed for longer periods of time [298, 299].

Once it was estabilished that the LL-37 concentrations tested were not harmful to the hepatocytes, co-cultures of primary hepatocytes and *E. coli* were investigated. In the liver, hepatocytes are separated from the blood by the Space of Disse and NPCs [96]. This would reduce their direct exposure to microbes and their metabolites. This work demonstrated that in the presence of LL-37 modified PEMs, even hepatocytes in direct contact with *E. coli* exhibited better function (albumin and urea secretion) than on PEMs alone. Hepatocytes in these experiments were seeded directly on top of LL-37 modified PEMs rather than on collagen gels and overlayed with multilayer films like the previously mentioned 3D liver models [47, 48]. For future studies it will be beneficial to introduce *E. coli* into a 3D construct to determine the hepatoprotective effects of the LL-37 modified PEMs when they are able to act not only as an antimicrobial film but also a barrier to the hepatocytes as would be seen *in vivo*.

NPCs have also been incorporaed in the 3D liver models in the Rajagopalan research group [47, 48]. In furture studies, since LL-37 is a known chemoattractant for macrophages, it is desirable to expand this hepatocyte/bacteria co-culture research to a tri-culture containing liver macrophages, KCs [206, 210, 211, 218, 223, 224]. The addition of more liver cells types can give a more holistic view of the liver microenvironment and will influence the bacterial infection potential.

4.5 Conclusions

In this study we have shown the effects of LL-37 in co-cultures of bacteria and hepatocytes. In hepatic monocultures, LL-37 concentrations up to 16μM did not exhibit any cytotoxic effects to the mammalian cells. In addition the LL-37 modified PEMs exhibited a hepatoprotective effect on albumin and urea secretion functions in co-cultures. These findings are encouraging that AMP-modified PEMs can be introduced into 3D liver models to study hepatic infections.

References

1. Morawetz, H., *Macromolecules in solution*. 2d ed. High polymers : a series of monographs on the chemistry, physics, and technology of high polymeric substances v 21. 1975, New York: Wiley. xvii, 549 p.
2. Anderson, C.F. and H. Morawetz, *Polyelectrolytes*, in *Kirk-Othmer Encyclopedia of Chemical Technology*, M. Grayson, Editor 1982, Wiley-Interscience: New York. p. 495-530.
3. Billmeyer, F.W., *Textbook of polymer science*. 3rd ed. 1984, New York: Wiley. xviii, 578 p.
4. Armstrong, R.W. and U.P. Strauss, *Polyelectrolytes*, in *Encyclopedia of Polymer Science and Technology*, H.F. Mark, N.G. Gaylord, and N.M. Bikales, Editors. 1969, Wiley-Interscience: New York. p. 781-861.
5. Decher, G., *Fuzzy nanoassemblies: Toward layered polymeric multicomposites.* Science, 1997. **277**(5330): p. 1232-1237.
6. Decher, G., *Polyelectrolyte multilayers: An overview.* Abstracts of Papers of the American Chemical Society, 2002. **223**: p. U374-U374.
7. Decher, G. and J.B. Schlenoff, *Multilayer thin films : sequential assembly of nanocomposite materials*. 2nd, compl. rev. and enl. ed. 2012, Weinheim: Wiley-VCH.
8. Schlenoff, J.B. and S.T. Dubas, *Mechanism of Polyelectrolyte Multilayer Growth: Charge Overcompensation and Distribution.* Macromolecules, 2001. **34**: p. 592-598.
9. Lvov, Y., G. Decher, and H. Mohwald, *Assembly, Structural Characterization, and Thermal-Behavior of Layer-by-Layer Deposited Ultrathin Films of Poly(Vinyl Sulfate) and Poly(Allylamine).* Langmuir, 1993. **9**(2): p. 481-486.
10. Decher, G., J.D. Hong, and J. Schmitt, *Buildup of Ultrathin Multilayer Films by a Self-Assembly Process .3. Consecutively Alternating Adsorption of Anionic and Cationic Polyelectrolytes on Charged Surfaces.* Thin Solid Films, 1992. **210**(1-2): p. 831-835.
11. Fery, A., et al., *Nanoporous thin films formed by salt-induced structural changes in multilayers of poly(acrylic acid) and poly(allylamine).* Langmuir, 2001. **17**(13): p. 3779-3783.
12. Schlenoff, J.B., H. Ly, and M. Li, *Charge and mass balance in polyelectrolyte multilayers.* Journal of the American Chemical Society, 1998. **120**(30): p. 7626-7634.
13. Liu, X., et al., *Multilayers of weak polyelectrolytes of low and high molecular mass assembled on polypropylene and self-assembled hydrophobic surfaces.* Langmuir, 2011. **27**(8): p. 4541-50.
14. Joseph, N., et al., *Layer-by-layer preparation of polyelectrolyte multilayer membranes for separation.* Polymer Chemistry, 2014. **5**.
15. Boudou, T., et al., *Multiple Functionalities of Polyelectrolyte Multilayer Films: New Biomedical Applications.* Advanced Materials, 2010. **22**(4): p. 441-467.
16. Minnikanti, S., A. Gangopadhyay, and D.R. Reyes, *Polyelectrolyte Multilayers in Microfluidic Systems for Biological Applications.* Polymers, 2014. **6**: p. 2100-2115.
17. Lutkenhaus, J. and P.T. Hammond, *Electrochemically enabled polyelectrolyte multilayer devices: from fuel cells to sensors.* Soft Matter, 2007. **3**: p. 804-816.
18. Fadhillah, F., et al., *Development of polyelectrolyte multilayer thin film composite membrane for water desalination application.* Desalination, 2013. **318**: p. 19-24.
19. Picart, C., et al., *Primary cell adhesion on RGD-functionalized and covalently crosslinked thin polyelectrolyte multilayer films.* Advanced Functional Materials, 2005. **15**(1): p. 83-94.
20. Langer, R. and J.P. Vacanti, *Tissue engineering.* Science, 1993. **260**(5110): p. 920-6.
21. Richert, L., et al., *Improvement of stability and cell adhesion properties of polyelectrolyte multilayer films by chemical cross-linking.* Biomacromolecules, 2004. **5**(2): p. 284-294.

22. Boudou, T., et al., *Polyelectrolyte Multilayer Nanofilms Used as Thin Materials for Cell Mechano-Sensitivity Studies.* Macromolecular Bioscience, 2011. **11**(1): p. 77-89.
23. Berg, M.C., et al., *Controlling mammalian cell interactions on patterned polyelectrolyte multilayer surfaces.* Langmuir, 2004. **20**(4): p. 1362-8.
24. Wittmer, C.R., et al., *Multilayer nanofilms as substrates for hepatocellular applications.* Biomaterials, 2008. **29**(30): p. 4082-90.
25. Wood, K.C., et al., *Controlling interlayer diffusion to achieve sustained, multiagent delivery from layer-by-layer thin films.* Proc Natl Acad Sci U S A, 2006. **103**(27): p. 10207-10212.
26. Richert, L., et al., *Cell interactions with polyelectrolyte multilayer films.* Biomacromolecules, 2002. **3**(6): p. 1170-1178.
27. Boura, C., et al., *Endothelial cells grown on thin polyelectrolyte mutlilayered films: an evaluation of a new versatile surface modification.* Biomaterials, 2003. **24**(20): p. 3521-3530.
28. Chen, A.A., et al., *Modulation of hepatocyte phenotype in vitro via chemomechanical tuning of polyelectrolyte multilayers.* Biomaterials, 2009. **30**(6): p. 1113-20.
29. Jessel, N., et al., *Bioactive coatings based on a polyelectrolyte multilayer architecture functionalized by embedded proteins.* Advanced Materials, 2003. **15**(9): p. 692-695.
30. Huang, X., et al., *Modulating the behaviors of C3A cells via surface charges of polyelectrolyte multilayers.* Carbohydr Polym, 2013. **92**(2): p. 1064-70.
31. Hubbell, J.A., *Bioactive biomaterials.* Curr Opin Biotechnol, 1999. **10**(2): p. 123-9.
32. Brunot, C., et al., *Response of fibroblast activity and polyelectrolyte multilayer films coating titanium.* Dental Materials, 2008. **24**(8): p. 1025-1035.
33. Thompson, M.T., et al., *Tuning compliance of nanoscale polyelectrolyte multilayers to modulate cell adhesion.* Biomaterials, 2005. **26**(34): p. 6836-45.
34. Davila, J., et al., *Cyto-mechanoresponsive Polyelectrolyte Multilayer Films.* Journal of the American Chemical Society, 2012. **134**(1): p. 83-86.
35. Gribova, V., R. Auzely-Velty, and C. Picart, *Polyelectrolyte Multilayer Assemblies on Materials Surfaces: From Cell Adhesion to Tissue Engineering.* Chemistry of Materials, 2012. **24**(5): p. 854-869.
36. Lichter, J.A., K.J. Van Vliet, and M.F. Rubner, *Design of Antibacterial Surfaces and Interfaces: Polyelectrolyte Multilayers as a Multifunctional Platform.* Macromolecules, 2009. **42**(22): p. 8573-8586.
37. Wittmer, C.R., et al., *Fibronectin terminated multilayer films: protein adsorption and cell attachment studies.* Biomaterials, 2007. **28**(5): p. 851-60.
38. Shen, H., J. Watanabe, and M. Akashi, *Heterofunctional Interfaces Achieve Dual Protein Adsorption on Polyelectrolyte Multilayers.* Polymer Journal, 2009. **41**(6): p. 486-491.
39. Kidambi, S., I. Lee, and C. Chan, *Controlling primary hepatocyte adhesion and spreading on protein-free polyelectrolyte multilayer films.* Journal of the American Chemical Society, 2004. **126**(50): p. 16286-7.
40. DeMuth, P.C., et al., *Polymer multilayer tattooing for enhanced DNA vaccination.* Nat Mater, 2013. **12**(4): p. 367-76.
41. Tezcaner, A., et al., *Polyelectrolyte multilayer films as substrates for photoreceptor cells.* Biomacromolecules, 2006. **7**(1): p. 86-94.
42. Brunot, C., et al., *Cytotoxicity of polyethyleneimine (PEI), precursor base layer of polyelectrolyte multilayer films.* Biomaterials, 2007. **28**(4): p. 632-640.
43. Hwang, Y.J., et al., *Effect of genipin crosslinking on the optical spectral properties and structures of collagen hydrogels.* ACS Appl Mater Interfaces, 2011. **3**(7): p. 2579-84.
44. Mehrotra, S., et al., *Polyelectrolyte Multilayer Stamping in Aqueous Phase and Non-Contact Mode.* Industrial & Engineering Chemistry Research, 2011. **50**(15): p. 8851-8858.

45. Chaubaroux, C., et al., *Collagen-based fibrillar multilayer films cross-linked by a natural agent.* Biomacromolecules, 2012. **13**(7): p. 2128-35.
46. Zhang, J., et al., *Natural polyelectrolyte films based on layer-by layer deposition of collagen and hyaluronic acid.* Biomaterials, 2005. **26**(16): p. 3353-61.
47. Larkin, A.L., et al., *Designing a Multicellular Organotypic 3D Liver Model with a Detachable, Nanoscale Polymeric Space of Disse.* Tissue Eng Part C Methods, 2013.
48. Kim, Y., et al., *The design of in vitro liver sinusoid mimics using chitosan-hyaluronic acid polyelectrolyte multilayers.* Tissue Eng Part A, 2010. **16**(9): p. 2731-41.
49. Mhanna, R.F., J. Voros, and M. Zenobi-Wong, *Layer-by-layer films made from extracellular matrix macromolecules on silicone substrates.* Biomacromolecules, 2011. **12**(3): p. 609-16.
50. Atala, A. and D.J. Mooney, *Synthetic biodegradable polymer scaffolds*. Tissue Eng. 1997, Boston: Birkhäuser. xii, 258 p.
51. Boura, C., et al., *Behaviour of endothelial cells seeded on thin polyelectrolyte multilayered films: a new biological scaffold.* Clin Hemorheol Microcirc, 2005. **33**(3): p. 269-75.
52. Chung, T.W., et al., *Preparation of alginate/galactosylated chitosan scaffold for hepatocyte attachment.* Biomaterials, 2002. **23**(14): p. 2827-34.
53. Huang, Y., et al., *In vitro characterization of chitosan-gelatin scaffolds for tissue engineering.* Biomaterials, 2005. **26**(36): p. 7616-27.
54. Rajagopalan, P., et al., *Polyelectrolyte nano-scaffolds for the design of layered cellular architectures.* Tissue Eng, 2006. **12**(6): p. 1553-63.
55. Tai, B.C.U., et al., *Polyelectrolyte complex fibrous scaffold for liver tissue engineering.* Tissue Engineering Part A, 2008. **14**(5): p. 767-768.
56. Decher, G. and J.B. Schlenoff, *Multilayer thin films : sequential assembly of nanocomposite materials*. 2003, Weinheim: Wiley-VCH. xix, 524 p.
57. Vasanthan, K.S., et al., *Role of biomaterials, therapeutic molecules and cells for hepatic tissue engineering.* Biotechnol Adv, 2012. **30**(3): p. 742-52.
58. Ariga, K., et al., *Layer-by-layer assembly for drug delivery and related applications.* Expert Opin Drug Deliv, 2011. **8**(5): p. 633-44.
59. Jiankang, H., et al., *Preparation of chitosan-gelatin hybrid scaffolds with well-organized microstructures for hepatic tissue engineering.* Acta Biomaterialia, 2009. **5**(1): p. 453-61.
60. Jiankang, H., et al., *Fabrication and characterization of chitosan/gelatin porous scaffolds with predefined internal microstructures.* Polymer, 2007. **48**: p. 4578-4588.
61. Antipov, A.A., et al., *Polyelectrolyte multilayer capsule permeability control.* Colloids and Surfaces a-Physicochemical and Engineering Aspects, 2002. **198**: p. 535-541.
62. Underhill, G.H., et al., *Assessment of hepatocellular function within PEG hydrogels.* Biomaterials, 2007. **28**(2): p. 256-70.
63. Chia, S.M., et al., *Multi-layered microcapsules for cell encapsulation.* Biomaterials, 2002. **23**(3): p. 849-856.
64. Li, Q., J.F. Quinn, and F. Caruso, *Nanoporous Polymer Thin Films via Polyelectrolyte Templating.* Advanced Materials, 2005. **17**: p. 2058-2062.
65. Mendelsohn, J.D., et al., *Fabrication of microporous thin films from polyelectrolyte multilayers.* Langmuir, 2000. **16**(11): p. 5017-5023.
66. Hajicharalambous, C.S., et al., *Nano- and sub-micron porous polyelectrolyte multilayer assemblies: Biomimetic surfaces for human corneal epithelial cells.* Biomaterials, 2009. **30**(23-24): p. 4029-4036.
67. Detzel, C.J., A.L. Larkin, and P. Rajagopalan, *Polyelectrolyte multilayers in tissue engineering.* Tissue Eng Part B Rev, 2011. **17**(2): p. 101-13.
68. Xu, L., et al., *Linear versus Exponential Growth of Weak Polyelectrolyte Multilayers: Correlation with Polyelectrolyte Complexes.* Macromolecules, 2012. **45**: p. 3892-3901.

69. Wang, N.X., et al., *The salt-, pH- and oxidant-responsive pervaporation behaviors of weak polyelectrolyte multilayer membranes.* Journal of Membrane Science, 2010. **354**(1-2): p. 14-22.
70. Shiratori, S.S. and M.F. Rubner, *pH-dependent thickness behavior of sequentially adsorbed layers of weak polyelectrolytes.* Macromolecules, 2000. **33**(11): p. 4213-4219.
71. Decher, G. and J. Schmitt, *Fine-Tuning of the Film Thickness of Ultrathin Multilayer Films Composed of Consecutively Alternating Layers of Anionic and Cationic Polyelectrolytes.* Trends in Colloid and Interface Science Vi, 1992. **89**: p. 160-164.
72. Sun, Q.L., et al., *Charge density threshold for LbL self-assembly and small molecule diffusion in polyelectrolyte multilayer films.* Polymer, 2005. **46**(13): p. 4958-4966.
73. Decher, G., Y. Lvov, and J. Schmitt, *Proof of Multilayer Structural Organization in Self-Assembled Polycation Polyanion Molecular Films.* Thin Solid Films, 1994. **244**(1-2): p. 772-777.
74. Kidambi, S., et al., *Patterned co-culture of primary hepatocytes and fibroblasts using polyelectrolyte multilayer templates.* Macromolecular Bioscience, 2007. **7**(3): p. 344-53.
75. Sukhorukov, G.B., et al., *pH-controlled macromolecule encapsulation in and release from polyelectrolyte multilayer nanocapsules.* Macromolecular Rapid Communications, 2001. **22**(1): p. 44-46.
76. Grant, G.G., et al., *Layer-by-layer assembly of collagen thin films: controlled thickness and biocompatibility.* Biomedical Microdevices, 2001. **3**(4): p. 301-306.
77. Sinha, V.R. and A. Trehan, *Biodegradable microspheres for protein delivery.* J Control Release, 2003. **90**(3): p. 261-80.
78. Larkin, A.L., R.M. Davis, and P. Rajagopalan, *Biocompatible, detachable, and free-standing polyelectrolyte multilayer films.* Biomacromolecules, 2010. **11**(10): p. 2788-96.
79. Wong, H.A. and D.J. Mooney, *Synthesis and properties of biodegradable polymers used as synthetic matrices for tissue engineering*, in *Synthetic biodegradable polymer scaffolds*, A. Atala and D.J. Mooney, Editors. 1997, Birkhauser: Boston, MA. p. 235-251.
80. Kulig, K.M. and J.R. Vacanti, *Hepatic tissue engineering.* Transplant Immunology, 2004. **12**(3-4): p. 303-310.
81. Houchin, M.L., K. Heppert, and E.M. Topp, *Deamidation, acylation and proteolysis of a model peptide in PLGA films.* J Control Release, 2006. **112**(1): p. 111-9.
82. Kulkarni, A., J. Reiche, and A. Lendlein, *Hydrolytic degradation of poly(rac-lactide) and poly[(rac-lactide)-co-glycolide] at the air-water interface.* Surface and Interface Analysis, 2007. **39**(9): p. 740-746.
83. Johansson, J.A., et al., *Build-up of collagen and hyaluronic acid polyelectrolyte multilayers.* Biomacromolecules, 2005. **6**(3): p. 1353-9.
84. Janorkar, A.V., et al., *The use of elastin-like polypeptide-polyelectrolyte complexes to control hepatocyte morphology and function in vitro.* Biomaterials, 2008. **29**(6): p. 625-32.
85. Rajagopalan, P., et al., *Direct comparison of the spread area, contractility, and migration of balb/c 3T3 fibroblasts adhered to fibronectin- and RGD-modified substrata.* Biophysical Journal, 2004. **87**(4): p. 2818-27.
86. Wang, X.H., et al., *Crosslinked collagen/chitosan matrix for artificial livers.* Biomaterials, 2003. **24**(19): p. 3213-20.
87. Yan, L.P., et al., *Genipin-cross-linked collagen/chitosan biomimetic scaffolds for articular cartilage tissue engineering applications.* J Biomed Mater Res A, 2010. **95**(2): p. 465-75.
88. Silver, F.H., et al., *Analysis of mammalian connective tissue: relationship between hierarchical structures and mechanical properties.* J Long Term Eff Med Implants, 1992. **2**(2-3): p. 165-98.
89. Meyer, U., *Fundamentals of tissue engineering and regenerative medicine*. 2009, Berlin: Springer. xxvi, 1049 p.

90. Hutmacher, D.W., *Scaffold design and fabrication technologies for engineering tissues--state of the art and future perspectives.* J Biomater Sci Polym Ed, 2001. **12**(1): p. 107-24.
91. Zhang, F., et al., *Hepatic-targeting microcapsules construction by self-assembly of bioactive galactose-branched polyelectrolyte for controlled drug release system.* Journal of Colloid and Interface Science, 2008. **317**(2): p. 477-484.
92. Tai, B.C., A.C. Wan, and J.Y. Ying, *Modified polyelectrolyte complex fibrous scaffold as a matrix for 3D cell culture.* Biomaterials, 2010. **31**(23): p. 5927-35.
93. Tai, B.C.U., et al., *The use of a polyelectrolyte fibrous scaffold to deliver differentiated hMSCs to the liver.* Biomaterials, 2010. **31**(1): p. 48-57.
94. Bhatia, S.R., S.F. Khattak, and S.C. Roberts, *Polyelectrolytes for cell encapsulation.* Current Opinion in Colloid & Interface Science, 2005. **10**(1-2): p. 45-51.
95. Li, X., et al., *The responses of preosteoblasts to collagen/hyaluronic acid polyelectrolyte multilayer coating on titanium.* Polymer Advanced Technologies, 2012. **23**: p. 756-764.
96. Arias, I.M., et al., *The Liver: Biology and Pathobiology*. 4 ed. 2001, Philadelphia, PA: Lippincott Williams and Wilkins.
97. Lasher, C.D., P. Rajagopalan, and T.M. Murali, *Discovering networks of perturbed biological processes in hepatocyte cultures.* PLoS One, 2011. **6**(1): p. e15247.
98. Kim, Y. and P. Rajagopalan, *3D hepatic cultures simultaneously maintain primary hepatocyte and liver sinusoidal endothelial cell phenotypes.* PLoS One, 2010. **5**(11): p. e15456.
99. Lanza, R.P., R.S. Langer, and J. Vacanti, *Principles of tissue engineering*. 3rd ed. 2007, Amsterdam ; Boston: Elsevier / Academic Press. xxvii, 1307 p.
100. Godoy, P., et al., *Recent advances in 2D and 3D in vitro systems using primary hepatocytes, alternative hepatocyte sources and non-parenchymal liver cells and their use in investigating mechanisms of hepatotoxicity, cell signaling and ADME.* Arch Toxicol, 2013. **87**(8): p. 1315-530.
101. Rodés, J., *Textbook of hepatology : from basic science to clinical practice*. 3rd ed. 2007, Malden, Mass.: Blackwell.
102. Reid, L.M., et al., *Extracellular matrix gradients in the space of Disse: relevance to liver biology.* Hepatology, 1992. **15**(6): p. 1198-203.
103. Mecham, R.P., *Regulation of matrix accumulation*. Biology of extracellular matrix. 1986, Orlando: Academic Press. xiii, 461 p.
104. Bataller, R. and D.A. Brenner, *Liver fibrosis.* Journal of Clinical Investigation, 2005. **115**(2): p. 209-18.
105. Elvevold, K., et al., *Liver sinusoidal endothelial cells depend on mannose receptor-mediated recruitment of lysosomal enzymes for normal degradation capacity.* Hepatology, 2008. **48**(6): p. 2007-15.
106. Wisse, E., et al., *The liver sieve: considerations concerning the structure and function of endothelial fenestrae, the sinusoidal wall and the space of Disse.* Hepatology, 1985. **5**(4): p. 683-92.
107. Braet, F. and E. Wisse, *Structural and functional aspects of liver sinusoidal endothelial cell fenestrae: a review.* Comp Hepatol, 2002. **1**(1): p. 1.
108. Braet, F., et al., *Structure and dynamics of the fenestrae-associated cytoskeleton of rat liver sinusoidal endothelial cells.* Hepatology, 1995. **21**(1): p. 180-9.
109. Friedman, S.L., *Evolving challenges in hepatic fibrosis.* Nat Rev Gastroenterol Hepatol, 2010. **7**(8): p. 425-36.
110. Asselah, T., et al., *Gene expression and hepatitis C virus infection.* Gut, 2009. **58**(6): p. 846-58.

111. Chang, Y.Z., L. Yang, and C.Q. Yang, *Migration of hepatic stellate cells in fibrotic microenvironment of diseased liver model.* Hepatobiliary Pancreat Dis Int, 2008. **7**(4): p. 401-5.
112. Wang, F.P., et al., *High mobility group box-1 promotes the proliferation and migration of hepatic stellate cells via TLR4-dependent signal pathways of PI3K/Akt and JNK.* PLoS One, 2013. **8**(5): p. e64373.
113. Grigorescu, M., *Noninvasive biochemical markers of liver fibrosis.* J Gastrointestin Liver Dis, 2006. **15**(2): p. 149-59.
114. Shen, C., et al., *Acetaminophen-induced hepatotoxicity of gel entrapped rat hepatocytes in hollow fibers.* Chem Biol Interact, 2006. **162**(1): p. 53-61.
115. Chia, S.M., et al., *Hepatocyte encapsulation for enhanced cellular functions.* Tissue Eng, 2000. **6**(5): p. 481-495.
116. Hale, N.A., Y. Yang, and P. Rajagopalan, *Cell migration at the interface of a dual chemical-mechanical gradient.* ACS Appl Mater Interfaces, 2010. **2**(8): p. 2317-24.
117. Ariga, K., et al., *Forming nanomaterials as layered functional structures toward materials nanoarchitectonics.* NPG Asia Materials, 2012. **4**(17).
118. Caruso, F., et al., *Enzyme encapsulation in layer-by-layer engineered polymer multilayer capsules.* Langmuir, 2000. **16**(4): p. 1485-1488.
119. Hoshi, T., H. Saiki, and J. Anzai, *Preparation of spatially ordered multilayer thin films of antibody and their binding properties.* Biosens Bioelectron, 2000. **15**(11-12): p. 623-8.
120. Caridade, S.G., et al., *Free-Standing Polyelectrolyte Membranes Made of Chitosan and Alginate.* Biomacromolecules, 2013. **14**(5): p. 1653-1660.
121. Li, X., et al., *The responses of preosteoblasts to collagen/hyaluronic acid polyelectrolyte multilayer coating on titanium.* Polymers Advanced Technologies, 2011. **23**: p. 756-764.
122. Croll, T.I., et al., *A blank slate? Layer-by-layer deposition of hyaluronic acid and chitosan onto various surfaces.* Biomacromolecules, 2006. **7**(5): p. 1610-22.
123. Ge, H., et al., *From crabshell to chitosan-hydroxyapatite composite material via a biomorphic mineralization synthesis method.* J Mater Sci Mater Med, 2010. **21**(6): p. 1781-7.
124. Slaughter, B.V., et al., *Hydrogels in regenerative medicine.* Advanced Materials, 2009. **21**(32-33): p. 3307-29.
125. Lvov, Y., et al., *Ultrathin films of charged polysaccharides assembled alternately with linear polyions.* J Biomater Sci Polym Ed, 1998. **9**(4): p. 345-55.
126. Richert, L., et al., *Layer by layer buildup of polysaccharide films: physical chemistry and cellular adhesion aspects.* Langmuir, 2004. **20**(2): p. 448-58.
127. Gribova, V., et al., *Effect of RGD functionalization and stiffness modulation of polyelectrolyte multilayer films on muscle cell differentiation.* Acta Biomaterialia, 2013. **9**(5): p. 6468-6480.
128. Decher, G., et al., *Layer-by-Layer Adsorbed Films of Polyelectrolytes, Proteins or DNA.* Abstracts of Papers of the American Chemical Society, 1993. **205**: p. 334-POLY.
129. Sukhorukov, G.B., et al., *Assembly of polyelectrolyte multilayer films by consecutively alternating adsorption of polynucleotides and polycations.* Thin Solid Films, 1996. **284**: p. 220-223.
130. Nolte, A.J., et al., *Effect of relative humidity on the Young's modulus of polyelectrolyte multilayer films and related nonionic polymers.* Macromolecules, 2008. **41**(15): p. 5793-5798.
131. Discher, D.E., P. Janmey, and Y.L. Wang, *Tissue cells feel and respond to the stiffness of their substrate.* Science, 2005. **310**(5751): p. 1139-43.
132. Ren, K.F., et al., *Polyelectrolyte multilayer films of controlled stiffness modulate myoblast cell differentiation.* Advanced Functional Materials, 2008. **18**(9): p. 1378-1389.

133. Schmidt, D.J., et al., *Electrochemically controlled swelling and mechanical properties of a polymer nanocomposite.* ACS Nano, 2009. **3**(8): p. 2207-16.
134. Ko, H.H., et al., *High-resolution Raman microscopy of curled carbon nanotubes.* Applied Physics Letters, 2004. **85**(13): p. 2598-2600.
135. Sukhishvili, S.A., *Responsive polymer films and capsules via layer-by-layer assembly.* Current Opinion in Colloid & Interface Science, 2005. **10**: p. 37-44.
136. Nolte, A.J., et al., *Effect of Relative Humidity on the Young's Modulus of Polyelectrolyte Multilayer Films and Related Nonionic Polymers.* Macromolecules, 2008. **41**: p. 5793-5798.
137. Thompson, M.T., et al., *Biochemical functionalization of polymeric cell substrata can alter mechanical compliance.* Biomacromolecules, 2006. **7**(6): p. 1990-5.
138. Martins, G.V., et al., *Crosslink effect and albumin adsorption onto chitosan/alginate multilayered systems: an in situ QCM-D study.* Macromolecular Bioscience, 2010. **10**(12): p. 1444-55.
139. Chua, P.H., et al., *Surface functionalization of titanium with hyaluronic acid/chitosan polyelectrolyte multilayers and RGD for promoting osteoblast functions and inhibiting bacterial adhesion.* Biomaterials, 2008. **29**(10): p. 1412-21.
140. Park, K.H. and Y.H. Bae, *Phenotype of hepatocyte spheroids in Arg-GLY-Asp (RGD) containing a thermo-reversible extracellular matrix.* Biosci Biotechnol Biochem, 2002. **66**(7): p. 1473-8.
141. Dunn, J.C., R.G. Tompkins, and M.L. Yarmush, *Long-term in vitro function of adult hepatocytes in a collagen sandwich configuration.* Biotechnol Prog, 1991. **7**(3): p. 237-45.
142. Bhatia, S.N., et al., *Effect of cell-cell interactions in preservation of cellular phenotype: cocultivation of hepatocytes and nonparenchymal cells.* Faseb Journal, 1999. **13**(14): p. 1883-900.
143. Bhatia, S.N., et al., *Probing heterotypic cell interactions: hepatocyte function in microfabricated co-cultures.* J Biomater Sci Polym Ed, 1998. **9**(11): p. 1137-60.
144. Park, I.K., et al., *Galactosylated chitosan-graft-poly(ethylene glycol) as hepatocyte-targeting DNA carrier.* J Control Release, 2001. **76**(3): p. 349-62.
145. Park, I.K., et al., *Galactosylated chitosan as a synthetic extracellular matrix for hepatocytes attachment.* Biomaterials, 2003. **24**(13): p. 2331-7.
146. Serizawa, T., et al., *Alternating bioactivity of polymeric layer-by-layer assemblies: anti- vs procoagulation of human blood on chitosan and dextran sulfate layers.* Biomacromolecules, 2000. **1**(3): p. 306-9.
147. Joddar, B. and A. Ramamurthi, *Elastogenic effects of exogenous hyaluronan oligosaccharides on vascular smooth muscle cells.* Biomaterials, 2006. **27**(33): p. 5698-707.
148. Remuzzi, A., et al., *Vascular smooth muscle cells on hyaluronic acid: culture and mechanical characterization of an engineered vascular construct.* Tissue Eng, 2004. **10**(5-6): p. 699-710.
149. Detzel, C.J., Y. Kim, and P. Rajagopalan, *Engineered three-dimensional liver mimics recapitulate critical rat-specific bile acid pathways.* Tissue Eng Part A, 2011. **17**(5-6): p. 677-89.
150. Nava, A., et al., *In vivo mechanical characterization of human liver.* Med Image Anal, 2008. **12**(2): p. 203-16.
151. Khetani, S.R. and S.N. Bhatia, *Microscale culture of human liver cells for drug development.* Nat Biotechnol, 2008. **26**(1): p. 120-6.
152. Mehal, W.Z., F. Azzaroli, and I.N. Crispe, *Immunology of the healthy liver: old questions and new insights.* Gastroenterology, 2001. **120**(1): p. 250-60.

153. White, D., J. Drummond, and C. Fuqua, *The physiology and biochemistry of prokaryotes*. 4th ed. 2012, New York: Oxford University Press. xxii, 632 p.
154. Dunny, G.M. and B.A. Leonard, *Cell-cell communication in gram-positive bacteria.* Annu Rev Microbiol, 1997. **51**: p. 527-64.
155. Rice, L.B., *Antimicrobial resistance in gram-positive bacteria.* Am J Infect Control, 2006. **34**(5 Suppl 1): p. S11-9; discussion S64-73.
156. Paterson, D.L., *Resistance in gram-negative bacteria: Enterobacteriaceae.* Am J Infect Control, 2006. **34**(5 Suppl 1): p. S20-8; discussion S64-73.
157. Desmond, E. and S. Gribaldo, *Phylogenomics of sterol synthesis: insights into the origin, evolution, and diversity of a key eukaryotic feature.* Genome Biol Evol, 2009. **1**: p. 364-81.
158. Dufourc, E.J., *Sterols and membrane dynamics.* J Chem Biol, 2008. **1**(1-4): p. 63-77.
159. Silhavy, T.J., D. Kahne, and S. Walker, *The bacterial cell envelope.* Cold Spring Harb Perspect Biol, 2010. **2**(5): p. a000414.
160. Raetz, C.R., et al., *Lipid A modification systems in gram-negative bacteria.* Annu Rev Biochem, 2007. **76**: p. 295-329.
161. Davies, J. and D. Davies, *Origins and evolution of antibiotic resistance.* Microbiol Mol Biol Rev, 2010. **74**(3): p. 417-33.
162. *Antimicrobial resistance*, 2013, World Health Organization.
163. *About Antimicrobial Resistance: A Brief Overview*, 2013: Centers for Disease Control and Prevention.
164. Spellberg, B., et al., *The epidemic of antibiotic-resistant infections: a call to action for the medical community from the Infectious Diseases Society of America.* Clin Infect Dis, 2008. **46**(2): p. 155-64.
165. Walsh, C., *Molecular mechanisms that confer antibacterial drug resistance.* Nature, 2000. **406**(6797): p. 775-81.
166. Fischbach, M.A. and C.T. Walsh, *Antibiotics for emerging pathogens.* Science, 2009. **325**(5944): p. 1089-93.
167. Li, P., et al., *Cationic peptidopolysaccharides show excellent broad-spectrum antimicrobial activities and high selectivity.* Advanced Materials, 2012. **24**(30): p. 4130-7.
168. Palermo, E.F., S. Vemparala, and K. Kuroda, *Antimicrobial Polymers: Molecular Design as Synthetic Mimics of Host-Defense Peptides*, in *Tailored Polymer Architectures for Pharmaceutical and Biomedical Applications*, C. Scholz and J. Kressler, Editors. 2013, American Chemical Society: Washington DC.
169. Palermo, E.F., et al., *Role of cationic group structure in membrane binding and disruption by amphiphilic copolymers.* Journal of Physical Chemistry B, 2011. **115**(2): p. 366-75.
170. Takahashi, H., et al., *Molecular design, structures, and activity of antimicrobial peptide-mimetic polymers.* Macromolecular Bioscience, 2013. **13**(10): p. 1285-99.
171. Qiao, Y., et al., *Highly dynamic biodegradable micelles capable of lysing Gram-positive and Gram-negative bacterial membrane.* Biomaterials, 2012. **33**(4): p. 1146-53.
172. French, G.L., *The continuing crisis in antibiotic resistance.* Int J Antimicrob Agents, 2010. **36 Suppl 3**: p. S3-7.
173. Gaynes, R. and D. Monnet, *The contribution of antibiotic use on the frequency of antibiotic resistance in hospitals.* Ciba Found Symp, 1997. **207**: p. 47-56; discussion 56-60.
174. Suzuki, K., et al., *Human anti-microbial cathelicidin peptide LL-37 suppresses the LPS-induced apoptosis of endothelial cells.* Int Immunol, 2011. **23**(3): p. 185-93.
175. Wang, B.L., et al., *Construction of degradable multilayer films for enhanced antibacterial properties.* ACS Appl Mater Interfaces, 2013. **5**(10): p. 4136-43.

176. Hsu, B.B., et al., *On structural damage incurred by bacteria upon exposure to hydrophobic polycationic coatings.* Biotechnology Letters, 2011. **33**(2): p. 411-6.
177. Peleg, A.Y. and D.C. Hooper, *Hospital-acquired infections due to gram-negative bacteria.* N Engl J Med, 2010. **362**(19): p. 1804-13.
178. Obama, B., *Combating Antibiotic-Resistant Bacteria*, 2014, Office of the Press Secretary: The White House.
179. Wong, S.Y., et al., *Dual functional polyelectrolyte multilayer coatings for implants: permanent microbicidal base with controlled release of therapeutic agents.* Journal of the American Chemical Society, 2010. **132**(50): p. 17840-8.
180. Ratner, B.D. and S.J. Bryant, *Biomaterials: where we have been and where we are going.* Annu Rev Biomed Eng, 2004. **6**: p. 41-75.
181. Donlan, R.M., *Biofilms and device-associated infections.* Emerg Infect Dis, 2001. **7**(2): p. 277-81.
182. Pavithra, D. and M. Doble, *Biofilm formation, bacterial adhesion and host response on polymeric implants--issues and prevention.* Biomed Mater, 2008. **3**(3): p. 034003.
183. Li, Y., et al., *Mechanism of photogenerated reactive oxygen species and correlation with the antibacterial properties of engineered metal-oxide nanoparticles.* ACS Nano, 2012. **6**(6): p. 5164-73.
184. Ariga, K., et al., *Ultrathin films of inorganic materials (SiO2 nanoparticle, montmorillonite microplate, and molybdenum oxide) prepared by alternate layer-by-layer assembly with organic polyions.* Applied Clay Science, 1999. **15**(1-2): p. 137-152.
185. Egger, S., et al., *Antimicrobial properties of a novel silver-silica nanocomposite material.* Appl Environ Microbiol, 2009. **75**(9): p. 2973-6.
186. Agarwal, A., et al., *Antibacterial Molecular Coatings of Silver-Nanoparticles for Integration in Wound-Beds.* Wound Repair and Regeneration, 2011. **19**(2): p. A9-A9.
187. Agarwal, A., et al., *Surfaces modified with nanometer-thick silver-impregnated polymeric films that kill bacteria but support growth of mammalian cells.* Biomaterials, 2010. **31**(4): p. 680-690.
188. Kruk, T., et al., *Nanostructured multilayer polyelectrolyte films with silver nanoparticles as antibacterial coatings.* Colloids Surf B Biointerfaces, 2015.
189. Izadpanah, A. and R.L. Gallo, *Antimicrobial peptides.* J Am Acad Dermatol, 2005. **52**(3 Pt 1): p. 381-90; quiz 391-2.
190. Jenssen, H., P. Hamill, and R.E. Hancock, *Peptide antimicrobial agents.* Clin Microbiol Rev, 2006. **19**(3): p. 491-511.
191. Engler, A.C., et al., *Effects of side group functionality and molecular weight on the activity of synthetic antimicrobial polypeptides.* Biomacromolecules, 2011. **12**(5): p. 1666-74.
192. Gerrard, S.E., et al., *Reducing infectivity of HIV upon exposure to surfaces coated with N,N-dodecyl, methyl-polyethylenimine.* Biotechnol Bioeng, 2013. **110**(7): p. 2058-62.
193. Liu, S.Q., et al., *Antimicrobial and antifouling hydrogels formed in situ from polycarbonate and poly(ethylene glycol) via Michael addition.* Advanced Materials, 2012. **24**(48): p. 6484-9.
194. Mizutani, M., et al., *Design and synthesis of self-degradable antibacterial polymers by simultaneous chain- and step-growth radical copolymerization.* Biomacromolecules, 2012. **13**(5): p. 1554-63.
195. Boman, H.G., B. Agerberth, and A. Boman, *Mechanisms of action on Escherichia coli of cecropin P1 and PR-39, two antibacterial peptides from pig intestine.* Infect Immun, 1993. **61**(7): p. 2978-84.
196. Kokryakov, V.N., et al., *Protegrins: leukocyte antimicrobial peptides that combine features of corticostatic defensins and tachyplesins.* Febs Letters, 1993. **327**(2): p. 231-6.

197. Park, C.B., H.S. Kim, and S.C. Kim, *Mechanism of action of the antimicrobial peptide buforin II: buforin II kills microorganisms by penetrating the cell membrane and inhibiting cellular functions.* Biochem Biophys Res Commun, 1998. **244**(1): p. 253-7.
198. Krause, A., et al., *LEAP-1, a novel highly disulfide-bonded human peptide, exhibits antimicrobial activity.* Febs Letters, 2000. **480**(2-3): p. 147-50.
199. Schittek, B., et al., *Dermcidin: a novel human antibiotic peptide secreted by sweat glands.* Nat Immunol, 2001. **2**(12): p. 1133-7.
200. Yang, D., O. Chertov, and J.J. Oppenheim, *The role of mammalian antimicrobial peptides and proteins in awakening of innate host defenses and adaptive immunity.* Cell Mol Life Sci, 2001. **58**(7): p. 978-89.
201. Gallo, R.L., et al., *Biology and clinical relevance of naturally occurring antimicrobial peptides.* J Allergy Clin Immunol, 2002. **110**(6): p. 823-31.
202. Ramanathan, B., et al., *Cathelicidins: microbicidal activity, mechanisms of action, and roles in innate immunity.* Microbes Infect, 2002. **4**(3): p. 361-72.
203. Zasloff, M., *Antimicrobial peptides of multicellular organisms.* Nature, 2002. **415**(6870): p. 389-95.
204. Brogden, K.A., et al., *Antimicrobial peptides in animals and their role in host defences.* Int J Antimicrob Agents, 2003. **22**(5): p. 465-78.
205. Reddy, K.V.R., R.D. Yedery, and C. Aranha, *Antimicrobial peptides: premises and promises.* Int J Antimicrob Agents, 2004. **24**(6): p. 536-547.
206. Barak, O., J.R. Treat, and W.D. James, *Antimicrobial peptides: effectors of innate immunity in the skin.* Adv Dermatol, 2005. **21**: p. 357-74.
207. Sang, Y., et al., *Porcine liver-expressed antimicrobial peptides, hepcidin and LEAP-2: cloning and induction by bacterial infection.* Dev Comp Immunol, 2006. **30**(4): p. 357-66.
208. Barlow, P.G., et al., *Antiviral potential of cathelicidins.* Future Microbiol, 2014. **9**(1): p. 55-73.
209. Hiemstra, P.S. and S.A.J. Zaat, *Antimicrobial peptides and innate immunity*. Progress in inflammation research. xi, 384 pages.
210. Niyonsaba, F., et al., *A cathelicidin family of human antibacterial peptide LL-37 induces mast cell chemotaxis.* Immunology, 2002. **106**(1): p. 20-6.
211. Carretero, M., et al., *In vitro and in vivo wound healing-promoting activities of human cathelicidin LL-37.* J Invest Dermatol, 2008. **128**(1): p. 223-36.
212. Steinstraesser, L., et al., *Skin Electroporation of a Plasmid Encoding hCAP-18/LL-37 Host Defense Peptide Promotes Wound Healing.* Mol Ther, 2014. **22**(4): p. 734-42.
213. Zhang, M., J. Zhao, and J. Zheng, *Molecular understanding of a potential functional link between antimicrobial and amyloid peptides.* Soft Matter, 2014. **10**(38): p. 7425-7451.
214. Grage, S.L., S. Afonin, and A.S. Ulrich, *Dynamic Transitions of Membrane-Active Peptides*, in *Antimicrobial Peptides, Methods and Protocols*, A. Giuliani and A.C. Rinaldi, Editors. 2010, Springer Science+Business Media: Methods in Molecular Biology.
215. Turner, J., et al., *Activities of LL-37, a cathelin-associated antimicrobial peptide of human neutrophils.* Antimicrobial Agents and Chemotherapy, 1998. **42**(9): p. 2206-2214.
216. Zaiou, M., V. Nizet, and R.L. Gallo, *Antimicrobial and protease inhibitory functions of the human cathelicidin (hCAP18/LL-37) prosequence.* J Invest Dermatol, 2003. **120**(5): p. 810-6.
217. Wang, G., et al., *High-quality 3D structures shine light on antibacterial, anti-biofilm and antiviral activities of human cathelicidin LL-37 and its fragments.* Biochim Biophys Acta, 2014. **1838**(9): p. 2160-72.
218. Beaumont, P.E., L. Hsin-Ni, and D.J. Davidson, *LL-37: An Immunomodulatory Antimicrobial Host Defense Peptide*, in *Antimicrobial Peptides and Innate Immunity*, P.S. Heimstra and S.A.J. Zaat, Editors. 2013, Springer Basel: Progress in Inflammation Research.

219. Reinholz, M., T. Ruzicka, and J. Schauber, *Cathelicidin LL-37: an antimicrobial peptide with a role in inflammatory skin disease.* Ann Dermatol, 2012. **24**(2): p. 126-35.
220. Oren, Z., et al., *Structure and organization of the human antimicrobial peptide LL-37 in phospholipid membranes: relevance to the molecular basis for its non-cell-selective activity.* Biochem J, 1999. **341 (Pt 3)**: p. 501-13.
221. den Hertog, A.L., et al., *Candidacidal effects of two antimicrobial peptides: histatin 5 causes small membrane defects, but LL-37 causes massive disruption of the cell membrane.* Biochem J, 2005. **388**(Pt 2): p. 689-95.
222. Nijnik, A. and R.E. Hancock, *The roles of cathelicidin LL-37 in immune defences and novel clinical applications.* Curr Opin Hematol, 2009. **16**(1): p. 41-7.
223. Duplantier, A.J. and M.L. van Hoek, *The Human Cathelicidin Antimicrobial Peptide LL-37 as a Potential Treatment for Polymicrobial Infected Wounds.* Front Immunol, 2013. **4**: p. 143.
224. De, Y., et al., *LL-37, the neutrophil granule- and epithelial cell-derived cathelicidin, utilizes formyl peptide receptor-like 1 (FPRL1) as a receptor to chemoattract human peripheral blood neutrophils, monocytes, and T cells.* J Exp Med, 2000. **192**(7): p. 1069-74.
225. Heilborn, J.D., et al., *The cathelicidin anti-microbial peptide LL-37 is involved in re-epithelialization of human skin wounds and is lacking in chronic ulcer epithelium.* J Invest Dermatol, 2003. **120**(3): p. 379-89.
226. Koczulla, R., et al., *An angiogenic role for the human peptide antibiotic LL-37/hCAP-18.* Journal of Clinical Investigation, 2003. **111**(11): p. 1665-72.
227. Overhage, J., et al., *Human host defense peptide LL-37 prevents bacterial biofilm formation.* Infect Immun, 2008. **76**(9): p. 4176-82.
228. Wisplinghoff, H. and D. Appleton, *Bacterial infections of the liver*, in *Comparative Hepatitis*, O. Weber and U. Protzer, Editors. 2008: Switzerland. p. 143-160.
229. Son, G., M. Kremer, and I.N. Hines, *Contribution of gut bacteria to liver pathobiology.* Gastroenterol Res Pract, 2010. **2010**.
230. Gao, B., W.I. Jeong, and Z. Tian, *Liver: An organ with predominant innate immunity.* Hepatology, 2008. **47**(2): p. 729-36.
231. Liaskou, E., D.V. Wilson, and Y.H. Oo, *Innate immune cells in liver inflammation.* Mediators Inflamm, 2012. **2012**: p. 949157.
232. Gregory, S.H., A.J. Sagnimeni, and E.J. Wing, *Bacteria in the bloodstream are trapped in the liver and killed by immigrating neutrophils.* J Immunol, 1996. **157**(6): p. 2514-20.
233. Billiar, T.R., et al., *Kupffer cell:hepatocyte cocultures release nitric oxide in response to bacterial endotoxin.* J Surg Res, 1990. **48**(4): p. 349-53.
234. Taneja, S.K. and R.K. Dhiman, *Prevention and management of bacterial infections in cirrhosis.* Int J Hepatol, 2011. **2011**: p. 784540.
235. Borzio, M., et al., *Bacterial infection in patients with advanced cirrhosis: a multicentre prospective study.* Dig Liver Dis, 2001. **33**(1): p. 41-8.
236. Fernandez, J. and V. Arroyo, *Bacterial Infections in Cirrhosis: A Growing Problem with Significant Implications.* Clinical Liver Disease, 2013. **2**(3).
237. Lata, J., O. Stiburek, and M. Kopacova, *Spontaneous bacterial peritonitis: a severe complication of liver cirrhosis.* World J Gastroenterol, 2009. **15**(44): p. 5505-10.
238. Agarwal, A., et al., *Polymeric multilayers that localize the release of chlorhexidine from biologic wound dressings.* Biomaterials, 2012. **33**(28): p. 6783-6792.
239. Fujie, T., et al., *Dual therapeutic action of antibiotic-loaded nanosheets for the treatment of gastrointestinal tissue defects.* Biomaterials, 2010. **31**(24): p. 6269-78.
240. Lv, H., et al., *Layer-by-layer self-assembly of minocycline-loaded chitosan/alginate multilayer on titanium substrates to inhibit biofilm formation.* J Dent, 2014. **42**(11): p. 1464-72.

241. Saito, A., et al., *Therapeutic efficacy of an antibiotic-loaded nanosheet in a murine burn-wound infection model.* Acta Biomaterialia, 2012. **8**(8): p. 2932-2940.
242. Ng, V.W., et al., *Synergistic co-delivery of membrane-disrupting polymers with commercial antibiotics against highly opportunistic bacteria.* Advanced Materials, 2013. **25**(46): p. 6730-6.
243. Agarwal, A., et al., *Dissolvable Microfilm Dressing with Silver-Nanoparticles Expedites Healing of Contaminated Excisional Wounds in Mice.* Wound Repair and Regeneration, 2013. **21**(2): p. A13-A13.
244. Wang, B.L., et al., *Construction of Degradable Multilayer Films for Enhanced Antibacterial Properties.* ACS Appl Mater Interfaces, 2013. **5**(10): p. 4136-4143.
245. Wong, S.Y., et al., *Drastically lowered protein adsorption on microbicidal hydrophobic/hydrophilic polyelectrolyte multilayers.* Biomacromolecules, 2012. **13**(3): p. 719-26.
246. Zhou, B., et al., *Chitosan/phosvitin antibacterial films fabricated via layer-by-layer deposition.* Int J Biol Macromol, 2014. **64**: p. 402-8.
247. Wong, S.Y., et al., *Bactericidal and virucidal ultrathin films assembled layer by layer from polycationic N-alkylated polyethylenimines and polyanions.* Biomaterials, 2010. **31**(14): p. 4079-87.
248. Sochacki, K.A., et al., *Real-time attack on single Escherichia coli cells by the human antimicrobial peptide LL-37.* Proc Natl Acad Sci U S A, 2011. **108**(16): p. E77-81.
249. Gabriel, M., et al., *Preparation of LL-37-grafted titanium surfaces with bactericidal activity.* Bioconjug Chem, 2006. **17**(2): p. 548-50.
250. Lichter, J.A. and M.F. Rubner, *Polyelectrolyte multilayers with intrinsic antimicrobial functionality: the importance of mobile polycations.* Langmuir, 2009. **25**(13): p. 7686-94.
251. Etienne, O., et al., *Multilayer polyelectrolyte films functionalized by insertion of defensin: A new approach to protection of implants from bacterial colonization.* Antimicrobial Agents and Chemotherapy, 2004. **48**(10): p. 3662-3669.
252. Agarwal, A., et al., *Polymeric Multilayers that Contain Silver Nanoparticles can be Stamped onto Biological Tissues to Provide Antibacterial Activity.* Advanced Functional Materials, 2011. **21**(10): p. 1863-1873.
253. Huang, X., M.J. Bolen, and N.S. Zacharia, *Silver nanoparticle aided self-healing of polyelectrolyte multilayers.* Physical Chemistry Chemical Physics, 2014.
254. Liu, H., et al., *Aerosol-assisted plasma deposition of hydrophobic polycations makes surfaces highly antimicrobial.* Appl Biochem Biotechnol, 2014. **172**(3): p. 1254-64.
255. Etienne, O., et al., *Antifungal coating by biofunctionalized polyelectrolyte multilayered films.* Biomaterials, 2005. **26**(33): p. 6704-12.
256. Choi, J.Y. and M.F. Rubner, *Surface modification of weak polyelectrolyte multilayers via selectively directed adsorption of amphiphilic block copolymers.* Abstracts of Papers of the American Chemical Society, 2002. **223**: p. U385-U385.
257. Koczulla, A.R. and R. Bals, *Antimicrobial peptides: current status and therapeutic potential.* Drugs, 2003. **63**(4): p. 389-406.
258. Decher, G. and J.D. Hong, *Buildup of Ultrathin Multilayer Films by a Self-Assembly Process .2. Consecutive Adsorption of Anionic and Cationic Bipolar Amphiphiles and Polyelectrolytes on Charged Surfaces.* Berichte Der Bunsen-Gesellschaft-Physical Chemistry Chemical Physics, 1991. **95**(11): p. 1430-1434.
259. Elbert, D.L., C.B. Herbert, and J.A. Hubbell, *Thin polymer layers formed by polyelectrolyte multilayer techniques on biological surfaces.* Langmuir, 1999. **15**(5355).
260. Lavalle, P., et al., *Free standing membranes made of biocompatible polyelectrolytes using the layer by layer method.* Journal of Membrane Science, 2005: p. 49-56.
261. Lee, H., et al., *Substrate-Independent Layer-by-Layer Assembly by Using Mussel-Adhesive-Inspired Polymers.* Advanced Materials, 2008. **20**(9): p. 1619-1623.

262. Min, J., R.D. Braatz, and P.T. Hammond, *Tunable staged release of therapeutics from layer-by-layer coatings with clay interlayer barrier.* Biomaterials, 2014. **35**(8): p. 2507-17.
263. Guthrie, K.M., et al., *Antibacterial Efficacy of Silver-Impregnated Polyelectrolyte Multilayers Immobilized on a Biological Dressing in a Murine Wound Infection Model.* Annals of Surgery, 2012. **256**(2): p. 371-377.
264. Agarwal, A., et al., *Nanoscopically-thin polymer films with silver nanoparticles that kill bacteria but support growth of fibroblasts.* Abstracts of Papers of the American Chemical Society, 2009. **238**.
265. Wang, G., *Human antimicrobial peptides and proteins.* Pharmaceuticals (Basel), 2014. **7**(5): p. 545-94.
266. Brogden, K.A., *Antimicrobial peptides: pore formers or metabolic inhibitors in bacteria?* Nat Rev Microbiol, 2005. **3**(3): p. 238-50.
267. Ong, P.Y., et al., *Endogenous antimicrobial peptides and skin infections in atopic dermatitis.* N Engl J Med, 2002. **347**(15): p. 1151-60.
268. Tsai, P.W., et al., *Responses of Candida albicans to the human antimicrobial peptide LL-37.* J Microbiol, 2014. **52**(7): p. 581-9.
269. Johansson, J., et al., *Conformation-dependent antibacterial activity of the naturally occurring human peptide LL-37.* J Biol Chem, 1998. **273**(6): p. 3718-24.
270. Dunn, J.C., et al., *Hepatocyte function and extracellular matrix geometry: long-term culture in a sandwich configuration.* Faseb Journal, 1989. **3**(2): p. 174-7.
271. Hermanson, G.T., *Bioconjugate techniques*. 1996, San Diego: Academic Press. xxv, 785 p.
272. Gottenbos, B., et al., *Initial adhesion and surface growth of Pseudomonas aeruginosa on negatively and positively charged poly(methacrylates).* J Mater Sci Mater Med, 1999. **10**(12): p. 853-5.
273. Chan, Y.M., et al., *Electrokinetic characterization of oligo- and poly(ethylene glycol)-terminated self-assembled monolayers on gold and glass surfaces.* Langmuir, 2003. **19**: p. 7380-7385.
274. Buksek, H., T. Luxbacher, and I. Petrinic, *Zeta potential determination of polymeric materials using two differently designed measuring cells of an electrokinetic analyzer.* Acta Chim Slov, 2010. **57**(3): p. 700-6.
275. Yamanlar, S., et al., *Surface functionalization of hyaluronic acid hydrogels by polyelectrolyte multilayer films.* Biomaterials, 2011. **32**(24): p. 5590-9.
276. Such, G.K., A.P. Johnston, and F. Caruso, *Engineered hydrogen-bonded polymer multilayers: from assembly to biomedical applications.* Chem Soc Rev, 2011. **40**(1): p. 19-29.
277. Tong, W., X. Song, and C. Gao, *Layer-by-layer assembly of microcapsules and their biomedical applications.* Chem Soc Rev, 2012. **41**(18): p. 6103-24.
278. Cox, T.R. and J.T. Erler, *Remodeling and homeostasis of the extracellular matrix: implications for fibrotic diseases and cancer.* Dis Model Mech, 2011. **4**(2): p. 165-78.
279. Akhtar, R., et al., *Characterizing the elastic properties of tissues.* Mater Today (Kidlington), 2011. **14**(3): p. 96-105.
280. Gui, Z.L., et al., *Fabrication of free-standing polyelectrolyte multilayer films: A method using polysulfobetaine-containing films as sacrificial layers.* Journal of Colloid and Interface Science, 2009. **340**(1): p. 35-41.
281. Ono, S.S. and G. Decher, *Preparation of ultrathin self-standing polyelectrolyte multilayer membranes at physiological conditions using pH-responsive film segments as sacrificial layers.* Nano Lett, 2006. **6**(4): p. 592-598.
282. Wang, Y., et al., *A novel poly(amido amine)-dendrimer-based hydrogel as a mimic for the extracellular matrix.* Advanced Materials, 2014. **26**(24): p. 4163-7.

283. Vu, L.T., et al., *Cell migration on planar and three-dimensional matrices: a hydrogel-based perspective.* Tissue Eng Part B Rev, 2015. **21**(1): p. 67-74.
284. Missirlis, D. and J.P. Spatz, *Combined effects of PEG hydrogel elasticity and cell-adhesive coating on fibroblast adhesion and persistent migration.* Biomacromolecules, 2014. **15**(1): p. 195-205.
285. Lau, H.K. and K.L. Kiick, *Opportunities for multicomponent hybrid hydrogels in biomedical applications.* Biomacromolecules, 2015. **16**(1): p. 28-42.
286. Tibbitt, M.W. and K.S. Anseth, *Hydrogels as extracellular matrix mimics for 3D cell culture.* Biotechnol Bioeng, 2009. **103**(4): p. 655-63.
287. R, V.K., *Internal structure of polyelectrolyte multilayer assemblies.* Physical Chemistry Chemical Physics, 2006. **8**(43): p. 5012-33.
288. Castleberry, S., M. Wang, and P.T. Hammond, *Nanolayered siRNA dressing for sustained localized knockdown.* ACS Nano, 2013. **7**(6): p. 5251-61.
289. Oudhoff, M.J., et al., *The role of salivary histatin and the human cathelicidin LL-37 in wound healing and innate immunity.* Biol Chem, 2010. **391**(5): p. 541-8.
290. Kai-Larsen, Y. and B. Agerberth, *The role of the multifunctional peptide LL-37 in host defense.* Front Biosci, 2008. **13**: p. 3760-7.
291. Nagaoka, I., H. Tamura, and M. Hirata, *An antimicrobial cathelicidin peptide, human CAP18/LL-37, suppresses neutrophil apoptosis via the activation of formyl-peptide receptor-like 1 and P2X7.* J Immunol, 2006. **176**(5): p. 3044-52.
292. Coyle, M.B. and American Society for Microbiology., *Manual of antimicrobial susceptibility testing*, 2005, American Society for Microbiology,: Washington, DC. p. 1 CD-ROM.
293. Ratner, B.D., *Biomaterials science : an introduction to materials in medicine*. 3rd ed. 2013, Amsterdam ; Boston: Elsevier/Academic Press. liii, 1519 p.
294. Hoffman, A.S., *Hydrogels for biomedical applications.* Advanced drud delivery reviews, 2012. **64**: p. 18-23.
295. Schneider, G.B., et al., *The effect of hydrogel charge density on cell attachment.* Biomaterials, 2004. **25**(15): p. 3023-8.
296. Pitarresi, G., et al., *Self-assembled amphiphilic hyaluronic acid graft copolymers for targeted release of antitumoral drug.* J Drug Target, 2010. **18**(4): p. 264-76.
297. Drago, L., et al., *Antiadhesive and antibiofilm activity of hyaluronic acid against bacteria responsible for respiratory tract infections.* APMIS, 2014. **122**(10): p. 1013-9.
298. Wertenbruch, S., et al., *The Anti-Microbial Peptide LL-37/CRAMP Is Elevated in Patients with Liver Diseases and Acts as a Protective Factor during Mouse Liver Injury.* Digestion, 2015. **91**(4): p. 307-17.
299. Iacob, S.A., et al., *The human cathelicidin LL37 peptide has high plasma levels in B and C hepatitis related to viral activity but not to 25-hydroxyvitamin D plasma level.* Rom J Intern Med, 2012. **50**(3): p. 217-23.
300. Park, J.H., et al., *Protective effect of melittin on inflammation and apoptosis in acute liver failure.* Apoptosis, 2012. **17**(1): p. 61-9.
301. Lee, W.R., et al., *Protective effects of melittin on transforming growth factor-beta1 injury to hepatocytes via anti-apoptotic mechanism.* Toxicol Appl Pharmacol, 2011. **256**(2): p. 209-15.
302. Cirioni, O., et al., *LL-37 protects rats against lethal sepsis caused by gram-negative bacteria.* Antimicrob Agents Chemother, 2006. **50**(5): p. 1672-9.

Appendix A: Copyright Permission

Copyright permission for literature review pages 1-12.

This Agreement between Margaret E Cassin ("You") and John Wiley and Sons ("John Wiley and Sons") consists of your license details and the terms and conditions provided by John Wiley and Sons and Copyright Clearance Center.

License Number	3710201376597
License date	Sep 14, 2015
Licensed Content Publisher	John Wiley and Sons
Licensed Content Publication	Wiley Books
Licensed Content Title	Layer-by-Layer Films for Biomedical Applications
Licensed Content Author	Catherine Picart, Frank Caruso, Jean-Claude Voegel, Gero Decher (Foreword by)
Licensed Content Date	Feb 1, 2015
Pages	592
Type of use	Dissertation/Thesis
Requestor type	University/Academic
Format	Electronic
Portion	Text extract
Number of Pages	24
Will you be translating?	No
Title of your thesis / dissertation	The Design of Antimicrobial Detachable Thin Films for the Study of Hepatic Infections
Expected completion date	Sep 2015
Expected size (number of pages)	93
Requestor Location	Margaret E Cassin 2682 Blossom Trail E BLACKSBURG, VA 24060 United States Attn: Margaret E Cassin
Billing Type	Invoice
Billing Address	Margaret E Cassin 2682 Blossom Trail E BLACKSBURG, VA 24060 United States Attn: Margaret E Cassin
Total	0.00 USD

This Agreement between Margaret E Cassin ("You") and John Wiley and Sons ("John Wiley and Sons") consists of your license details and the terms and conditions provided by John Wiley and Sons and Copyright Clearance Center.

License Number	3727181138735
License date	Oct 13, 2015
Licensed Content Publisher	John Wiley and Sons
Licensed Content Publication	Wiley Books
Licensed Content Title	Layer-by-Layer Films for Biomedical Applications
Licensed Content Author	Catherine Picart, Frank Caruso, Jean-Claude Voegel, Gero Decher (Foreword by)
Licensed Content Date	Feb 1, 2015
Pages	592
Type of use	Dissertation/Thesis
Requestor type	University/Academic
Format	Electronic
Portion	Figure/table
Number of figures/tables	3
Original Wiley figure/table number(s)	Figures 22.1, 22.2, 22.3
Will you be translating?	No
Title of your thesis / dissertation	The Design of Antimicrobial Detachable Thin Films for the Study of Hepatic Infections
Expected completion date	Sep 2015
Expected size (number of pages)	93
Requestor Location	Margaret E Cassin 2682 Blossom Trail E BLACKSBURG, VA 24060 United States Attn: Margaret E Cassin
Billing Type	Invoice
Billing Address	Margaret E Cassin 2682 Blossom Trail E BLACKSBURG, VA 24060 United States Attn: Margaret E Cassin
Total	0.00 USD